

https://dspace.org/

Inference of charge transfer from lightning flashes in South Africa

Tasman, Jesse Dean; Tasman, Jesse Dean

2019

https://hdl.handle.net/10539/29157

Tasman, Jesse Dean, (2019). Inference of charge transfer from lightning flashes in South Africa, University of the Witwatersrand, https://hdl.handle.net/10539/29157

Downloaded from a DSpace repository. https://dspace.org/

University of the Witwatersrand

Masters Dissertation

Inference of charge transfer from lightning flashes in South Africa

Author:

Jesse Dean Tasman

A Dissertation submitted in fulfillment of the requirements for the degree of Master of Science

in the

School of Electrical and Information Engineering

June 2019



Declaration

I, **Jesse Dean Tasman**, declare that this Dissertation titled, "**Inference of charge transfer from lightning flashes in South Africa**" and the work presented in it are my own. I confirm that:

- This work was done wholly or mainly while in candidature for a research degree at this University.
- Where any part of this thesis has previously been submitted for a degree or any other qualification at this University or any other institution, has been clearly stated.
- Where I have consulted the published work of others, this is always clearly attributed.
- Where I have quoted from the work of others, the source is always given. With the exception of such quotations, this dissertation is entirely my own work.
- I have acknowledged all main sources of help.

Signed: 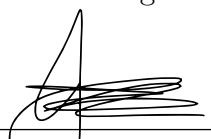

Date: 05/06/2019

UNIVERSITY OF THE WITWATERSRAND

Abstract

Engineering and the Built Environment
School of Electrical and Information Engineering

Master of Science

Inference of charge transfer from lightning flashes in South Africa

by Jesse Dean Tasman

Supervisors: Dr. Carina Schumann, Dr. Hugh Hunt, Prof. Ken Nixon

The objective of this study is to determine the quantity of charge transferred, in Coulombs, during the continuing current phase of natural cloud-to-ground (CG) lightning flashes over an area in Johannesburg, South Africa. Continuing current is responsible for most thermal related lightning damages such as destruction of property, electrical fires and physical human trauma. The mitigation of lightning-related risks can be better managed through improved measurement methods of naturally occurring lightning. The application of a point-charge model used to infer charge transfer from changing electric field measurements is detailed. A flat-plate antenna with an integrator is set up to record the changing electric fields from lightning flashes. These measurements, along with high-speed video footage to determine continuing current durations, are processed and charge transfer quantities are inferred. From 34 negative lightning strokes with long continuing current (i.e. $> 40\ ms$), the quantity of charge transfer ranges from $0.3\ C$ to $145.5\ C$ and has a mean quantity of $18.3\ C$. For the 5 recorded positive strokes, the quantity of charge transfer ranges from $3.7\ C$ to $66.6\ C$.

I dedicate this to my mom Sandy, dad Ian, sister Samantha and girlfriend Ariella

Your support and encouragement through this process has given me the motivation and confidence I needed to succeed. With this MSc and with life in general.

I love you all.

Acknowledgements

I would like to extend my sincerest thanks to Dr. Carina Schumann, Dr. Hugh Hunt and Prof. Ken Nixon for their unwavering support and assistance throughout this research process. They are incredibly passionate and knowledgeable about lightning research and I have thoroughly enjoyed my time spent working under them. I would also like to acknowledge and thank the South African Weather Service (SAWS) for their support and for providing the SALDN and radio sounding data used in this study. I would also like to thank Eskom for the support of the Lightning/EMCResearch Group through the TESP programme. Thanks are extended to the Department of Trade and Industry (DTI) for THRIP funding as well as to the National Research Foundation (NRF) for direct funding of the Research Group. Thank you to Tom Warner for providing the high-speed cameras and Marcelo Saba for the electric field measurement equipment that were both integral parts of this study. Thank you to Hannes Kohlmann for his support with the decay compensation algorithm design.

Contents

Declaration i

Abstract ii

Dedication iii

Acknowledgements iv

Contents v

List of Figures viii

List of Tables x

Abbreviations xi

Publications xii

1 Introduction 1
- 1.1 Problem statement . . . 1
- 1.2 Research question . . . 2
- 1.3 Dissertation structure . . . 2

2 Background 5
- 2.1 Relevant lightning fundamentals . . . 5
- 2.2 Lightning measurement instruments . . . 8
- 2.3 Flat-plate antenna measurements . . . 9
- 2.4 Charge inference . . . 13
- 2.5 Summary . . . 17

3 Equipment specifications and obtained data 18
- 3.1 The flat-plate antenna system . . . 19
  - 3.1.1 Specifications . . . 19
  - 3.1.2 Theoretical explanation . . . 21
  - 3.1.3 The recorded data . . . 22
- 3.2 High-speed cameras . . . 23
  - 3.2.1 Camera specifications . . . 23
  - 3.2.2 Measured continuing current data . . . 25
- 3.3 Auxiliary measurement equipment . . . 26

3.3.1 Lightning Location System . . . 27
3.3.1.1 Specifications . . . 27
3.3.1.2 Measured ground stike-point distance data . . . 28
3.3.2 Radio sounding measurement of charge centre height . . . 29
3.3.2.1 Data . . . 29
3.4 Summary . . . 30

4 The charge inference process 31
4.1 Methodology overview . . . 32
4.2 Electric field measurements . . . 33
4.3 Electronic decay compensation . . . 35
4.4 Continuing current duration . . . 39
4.4.1 Camera operation . . . 39
4.4.2 High-speed video analysis . . . 40
4.5 Auxiliary measurements . . . 42
4.5.1 Ground-strike point distance . . . 42
4.5.2 Charge centre height determination . . . 43
4.6 Inference of charge transfer . . . 44
4.7 Charge transfer computation algorithm . . . 45
4.8 Summary . . . 48

5 Results and discussion 49
5.1 Summary of records . . . 50
5.2 Charge transfer results . . . 51
5.3 Comparison of findings with similar studies . . . 54
5.4 Summary . . . 58

6 Conclusion and future work 59
6.1 Future work . . . 60

A Antenna calibration 66
A.1 Content discussion . . . 66
A.2 Relative antenna gain . . . 67
A.3 Overall building enhancement factor . . . 68

B The complete code used in the charge inference process 71
B.1 Content description . . . 71

C Characterisation of lightning flashes from changing electric field measurements in Johannesburg, South Africa 77
C.1 Paper description . . . 77

D Performance evaluation of the SALDN using high-speed camera footage of ground truth lightning events over Johannesburg, South Africa 83
D.1 Paper description . . . 83

E High-speed video observation of lightning flashes over Johannesburg, South Africa 2017 - 2018 **89**
E.1 Paper description 89

F High-speed video analysis of lightning flashes over Johannesburg, South Africa **97**
F.1 Paper description 97

List of Figures

2.1 Negative cloud-to-ground lightning over Johannesburg, South Africa [6]. 7
2.2 Impulse and continuing current phases of a lightning stroke on luminosity vs time axes. 7
2.3 Changing electric field waveform of a negative CG lightning flash. . 10
2.4 Flat-plate antenna and integrator measurement process. 11
2.5 Geometry configuration of an observer a distance d from the ground strike-point (adapted from [23]). 13
2.6 Tripolar model of charge separation in a cloud. Shown is the $-10°$ C isotherm and the estimated height of the positive charge centre. Adapted from [27]. 15

3.1 The flat-plate antenna measurement set-up used in this study. . . . 19
3.2 Operational amplifier configuration of integrator. Adapted from [22]. 20
3.3 Changing electric field waveform with individual strokes circled in red. 22
3.4 Field of view of the high-speed cameras. 24
3.5 The set-up of the Phantom v310 (far left) and the Phantom v7.1 (far right) high-speed cameras. 24
3.6 High-speed video frames of leader propagation (a), attachment (b) and continuing current (c) [6]. 26
3.7 The location of the 24 Vaisala LS7000 sensors distributed throughout South Africa, taken from 2014 [13]. 28

4.1 Methodology followed in the charge transfer inference process. . . . 32
4.2 Depiction of electric field gradient change with reference to leader propagation. 34
4.3 High-level structure of the offset correction and decay compensation algorithm. 36
4.4 The effect of offset correction on the final compensated output. . . . 38
4.5 Uncompensated changing electric field waveform (Efast) and corresponding compensated waveform (compensated Efast). 38
4.6 High-speed video frames and the corresponding changing electric field waveform and time stamps. 41

5.1 Average charge transfer in negative lightning strokes from this study and studies conducted in Brazil, Austria and the USA. 54

A.1 Scatter plot of the I_{wits} and $I_{calibration}$ amplification factor, α 68
A.2 The enhancement effect of a building on equipotential field lines . . 68

A.3 Scatter plot of the building enhancement factor after taking the amplification factor α into account 70

List of Tables

3.1 Data recorded using the flat-plate antenna measurement system. . . 22
3.2 Continuing current data obtained from high-speed camera footage. . 25
3.3 Ground strike-point distance data for a sample of 623 strokes. . . . 28
3.4 Summary of $-10\ ^{\circ}C$ isotherm heights. 29

4.1 An extract from the full radio sounding dataset for the hours of 24h00 - 12h00 on June 1 2018. 44
4.2 High-level code representation for the charge transfer inference algorithm. 46

5.1 The filtered data used in the charge transfer inference process. . . . 50
5.2 The final summarised results of the charge transfer inference process. 52
5.3 Results of this study (RSA) compared to similar studies conducted in Brazil, Austria and the United States [15]. 57

Abbreviations

CG	**C**loud-to-**G**round
CC	**C**ontinuing **C**urrent
CF	**C**alibration **F**actor
SALDN	**S**outh **A**frican **L**ightning **D**etection **N**etwork
SAWS	**S**outh **A**frican **W**eather **S**ervice
LLS	**L**ightning **L**ocation **S**ystem
GPS	**G**lobal **P**ositioning **S**ystem

Conferences and publications

[0.1] **J. D. Tasman**, C. Schumann, H. G. P. Hunt, H. G. Fensham, K. J. Nixon, M. M. F. Saba and T. A. Warner, "Characterisation of lightning flashes from changing electric field measurements in Johannesburg, South Africa", 34th *International Conference on Lightning Protection (ICLP)*, Rzeszow, Poland, 2018.

[0.2] **J. D. Tasman**, H. G. Fensham, C. Schumann, H. G. P. Hunt, K. J. Nixon and T. A. Warner, "High-speed video analysis of lightning flashes over Johannesburg, South Africa", 26th *Southern African Universities Power Engineering Conference (SAUPEC)*, Johannesburg, South Africa, 2018.

[0.3] C. Schumann, H. G. P. Hunt, **J. D. Tasman**, H. G. Fensham, K. J. Nixon, T. A. Warner and M. M. F. Saba, "High-speed video observation of lightning flashes over Johannesburg, South Africa 2017 - 2018", 34th *International Conference on Lightning Protection (ICLP)*, Rzeszow, Poland, 2018.

[0.4] H. G. Fensham, C. Schumann, H. G. P. Hunt, **J. D. Tasman**, K. J. Nixon, T. A. Warner and M. Gijben, "Performance evaluation of the SALDN using high-speed camera footage of ground truth lightning events over Johannesburg, South Africa", 34th *International Conference on Lightning Protection (ICLP)*, Rzeszow, Poland, 2018.

CHAPTER 1

Introduction

A cloud-to-ground (CG) lightning flash process consists of two phases; an impulse phase and a continuing current phase. Continuing current is classified by a persistent flow of charge in a lightning channel after the initial impulse phase. From the principle set by Ballarotti, et al., the study of continuing current is based only on charge flow persistence for durations greater than 3 ms [1]. These continuing currents are responsible for the thermal damages associated with lightning flashes. Measuring the charge transferred during the continuing current phase of a lightning flash is important for lightning protection design and for overall risk assessment and mitigation of lightning-related damages to property or physical human trauma.

1.1 Problem statement

Due to current being the cause of lightning-related damages, data on charge transfer is highly relevant. Rocket triggered lightning experiments along with instrumented structures provide the most accurate current measurements. Although these measurements are considered the most accurate, the lightning flashes recorded through these methods follow different physical processes to natural CG lightning [2]. These experiments have not been performed in South Africa and therefore, there is a scarcity of lightning current and charge transfer data in this country.

1.2 Research question

A research question was developed:

What is the average charge transferred during the continuing current phase of natural CG lightning over Johannesburg, South Africa?

To answer this research question, a point-charge model to infer charge transfer from changing electric field measurements is proposed. This model was originally developed and presented by Jacobson and Krider [3]. The primary measurement instrument is a flat-plate antenna with an integrator and amplifier. The integrator introduces an electronic decay that needs to be compensated for to reconstruct the slower-changing electric field waveforms associated with continuing current. From this reconstructed waveform, the proposed model can be applied and the total charge transferred can be calculated.

Through addressing the research question, the method of using changing electric field measurements allows for charge transfer quantities to be determined from lightning flashes without the need for instrumented structures. This provides a solution to the problem statement and enables charge transfer data to be attained for naturalal CG lightning over a specified region.

1.3 Dissertation structure

Chapter 2 of this paper provides a background on certain relevant lightning fundamentals and discusses different lightning measurement methods. Previous studies using flat-plate antennas and changing electric field measurements are consulted and are discussed. The model for inferring charge from these measurements is presented and explained.

Chapter 3 provides detail regarding the specifications of the measurement equipment used and presents the data that was obtained and recorded. The set-up

of the flat-plate antenna system and the high-speed cameras are detailed in this chapter. Also presented is the lightning location system (LLS) and radio-sounding technology that was used to attain necessary parametric quantities required for the charge transfer inference model.

Chapter 4 provides the methodology that was implemented to obtain charge transfer results. The methodology relating to the electric field measurements and the electronic decay compensation is discussed. The determination method for charge centre height, continuing current duration and ground strike-point distance is detailed.

Chapter 5 presents the final charge transfer results from this study. The results are compared to previous studies conducted in Brazil, USA and Austria and conclusions on the findings are drawn.

Chapter 6 consists of a conclusion on the outcome of this study, along with recommendations for relevant future work.

Appendix A presents the methodology and analysis results of the building enhancement factor determination process. Two antenna and integrator set-ups were used to collect and compare changing electric field magnitudes of lightning strokes. These measurements allowed for the enhancement effect of the building structure, on which the primary measurement antenna is placed, to be quantified.

Appendix B includes the code, in which the charge transfer inference algorithms were implemented. All main compensation and charge transfer inference files are included as well as all their subsequent functions. High-level explanations of this code are presented in the main body of this dissertation with reference to this appendix.

Appendix C consists of a paper that was submitted to and presented at the 34th International Conference on Lightning Protection (ICLP) in 2018. The conference was held in Rzeszow, Poland and the paper was published through the IEEE. The paper has the following title: **Characterisation of lightning flashes from changing electric field measurements in Johannesburg, South Africa.**

Appendix D consists of a paper that was submitted to and presented at the 34th International Conference on Lightning Protection (ICLP) in 2018. The conference was held in Rzeszow, Poland and the paper was published through the IEEE. The paper has the following title: **Performance evaluation of the SALDN using high-speed camera footage of ground truth lightning events over Johannesburg, South Africa.**

Appendix E consists of a paper that was submitted to and presented at the 34th International Conference on Lightning Protection (ICLP) in 2018. The conference was held in Rzeszow, Poland and the paper was published through the IEEE. The paper has the following title: **High-speed video observation of lightning flashes over Johannesburg, South Africa 2017 - 2018**

Appendix F consists of a paper that was submitted to and presented as a poster at the 26th Southern African Universities Power Engineering Conference, held in 2018 in Johannesburg, South Africa. The paper has the following title: **High-speed video analysis of lightning flashes over Johannesburg, South Africa**

CHAPTER 2

Background

A review of the relevant literature and a discussion on the background of lightning measurement methods and charge transfer inference is presented in this chapter. The difference between instrumented towers and electromagnetic measurements is explored and studies that used flat-plate antennas are discussed. An electromagnetic lightning model is presented and the inference of charge transfer from a changing electric field is examined.

2.1 Relevant lightning fundamentals

A lightning event in its entirety is referred to as a *flash*. For cloud-to-ground lightning, a flash can comprise of multiple *strokes* [4]. Each stroke consists of current flowing through a channel of ionised air that connects a charge centre in the cloud to a location or structure on the ground [4]. Depending on the direction of charge propagation and polarity of the charge transferred, a cloud-to-ground (CG) lightning discharge can be characterised as either upward positive, upward negative, downward positive or downward negative [4]. This study focusses solely on the downward lightning process and is referred to throughout as CG.

The CG process begins with preliminary breakdown of the charge distribution that is present within the cloud. In the case of negative CG, the preliminary breakdown in the cloud causes negative charge to propagate downwards from the cloud towards the ground. The charge propagates in a non-continuous fashion with discrete steps and hence, is referred to as *downward stepped leaders*. In the case of positive CG, the positively charged leader propagates downward in a slower, continuous manner. The leader propagation causes an enhancement of the electric field on the ground, which in turn, initiates *upward connecting leaders* from locations or structures on the ground. The downward leaders are attracted to these upward connecting leaders. The process of connection between a downward leader and an upward connecting leader is known as *attachment* and this is where a continuous ionised channel between the cloud and the ground is established [5].

After attachment, an initial *return stroke* occurs. This process comprises of charge that has accumulated from the atmosphere surrounding the leaders and travels through the ionised channel as a current impulse. Current impulses succeeding the return stroke are known as *subsequent return strokes*. These are initiated by a *dart leader* which follows the previously established ionised channel [5]. A dart leader is different to downward leaders in that it propagates in a continuous manner at a much higher speed. The attachment process succeeding subsequent return strokes is similar to the initial attachment process. Figure 2.1 shows a high-speed video frame of a negative CG over Johannesburg, South Africa, which is the type of lightning and region that is focussed on in this study [6].

The current profile of return and subsequent return strokes is made up of two distinct phases known as the impulse phase and the slower changing, lower magnitude, continuing current phase [4]. The impulse phase is in the order of microseconds and the continuing current phase is in the order of milliseconds. However, the continuing current can extend past a second in duration [7]. The continuing current following the initial return stroke, along with subsequent return strokes and continuing currents following them, are caused by a charge centre in the cloud being neutralised through the already established channel of ionised air [5]. The impulse

and continuing current phases are distinguished in Figure 2.2, which illustrates the relationship between their respective durations and current magnitudes.



FIGURE 2.1: Negative cloud-to-ground lightning over Johannesburg, South Africa [6].

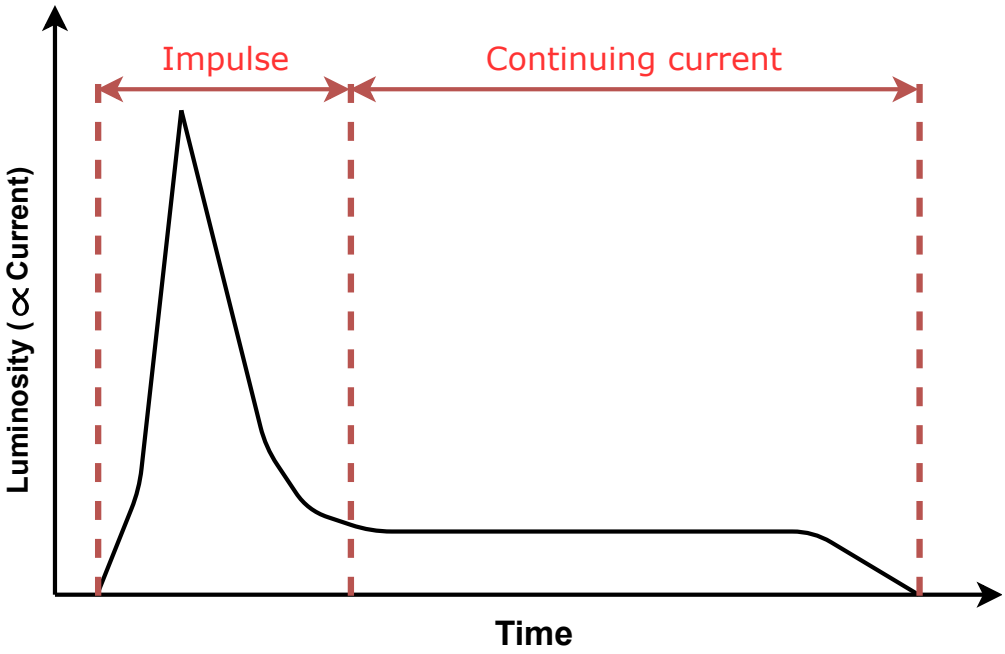

FIGURE 2.2: Impulse and continuing current phases of a lightning stroke on luminosity vs time axes.

2.2 Lightning measurement instruments

The peak current and charge transferred during a lightning stroke can be directly measured using shunt resistors or magnetic field integrator devices such as a Rogowski coil. The structures on which these devices are installed needs to be struck by lightning directly in order for measurements to be taken. The Gaisberg Tower in Austria, is a widely studied instrumented tower equipped with a current-viewing, 0.25 $M\Omega$, shunt resistor with a bandwidth of $0 - 3.2\ MHz$ [8]. This provides accurate data for a wide bandwidth. The tower is directly exposed to, on average, $40 - 50$ flashes annually [9]. The majority of these cases are upward flashes initiated by upward leaders from the tower. The lightning flash density in the vicinity of the tower is about 13 flashes/ km^2/year [10]. Considering electromagnetic measurements can be taken kilometers from the strike-point, instrumented structures only obtain data on a very small percentage of measureable flashes in their vicinity. Furthermore, the upward flashes initiated from the Gaisberg tower can account for up to 97 % of its total recorded per-annum lightning strikes [11]. The low amount of downward flashes on instrumented towers and the the fact that lightning flashes in the vicinity of the towers are not measured, highlights the importance of implementating a method to measure natural downward lightning.

Equipment has been developed that can measure the propagated electromagnetic fields from a lightning stroke. It is possible to obtain electric or magnetic measurements of lightning flashes without the need for a direct strike on a measurement instrument. Magnetic field measurements generally use loop antennas to integrate an induced voltage that is proportional to the changing magnetic field perpendicular to the loop. If multiple loops are used and oriented differently, magnetic fields from different directions can be measured. This method is commonly used to measure the magnetic field generated by lightning strokes, as discussed by Krider, et al. [12]. Lightning location systems are used as a means to determine characteristics of a lightning flash, such as the current magnitude, current polarity and

coordinates of the ground strike-point [13]. Many of these systems use magnetic field measurements to make these determinations.

Flat-plate antennas that make changing electric field measurements are used by lightning researchers as a method of inferring charge transfer from lightning flashes. These antennas can resolve high-frequency changes in electric fields. Post-processing can be introduced to further reconstruct waveforms that were distorted due to electronic bandwidth limitations and biased due to offset currents and voltages of the operational amplifier in the integrator circuit [14]. Schumann, et al. [15], used changing electric field measurements to infer charge transfer from the continuing current phase of natural CG lightning. The results obtained in this study are comparable to previous studies on natural CG lightning using electric field sensors. For positive flashes in Brazil, Schumann and Saba [7] found the charge transfer to range from $18 - 3070\ C$. For a study on negative flashes in Brazil, Ferraz [16] determined charge transfer ranged from $1 - 370\ C$. From studies conducted in New Mexico in the USA by Brook, et al. [17] and Kitagawa, et al. [18], the charge transferred by negative lightning was found to range from $3.4 - 29.2\ C$. All of the aforementioned studies made use of the same measurement equipment and the difference in charge transfer ranges can be attributed to differing geographical locations and atmospheric conditions. These studies provide strong benchmark charge transfer quantities against which future results can be compared.

Figure 2.3 shows the changing electric field waveform of a negative CG lightning flash used in this study, recorded on 14 November 2017 in Johannesburg. This figure illustrates the waveform produced by using a flat-plate antenna and integrator measurement system to record lightning flashes. From this waveform, post-processing is implemented and charge transfer quantities are obtained.

2.3 Flat-plate antenna measurements

The flat-plate antenna has been used as a measurement device in many studies around the world [7, 15–19]. In these studies, the antenna is cascaded with a

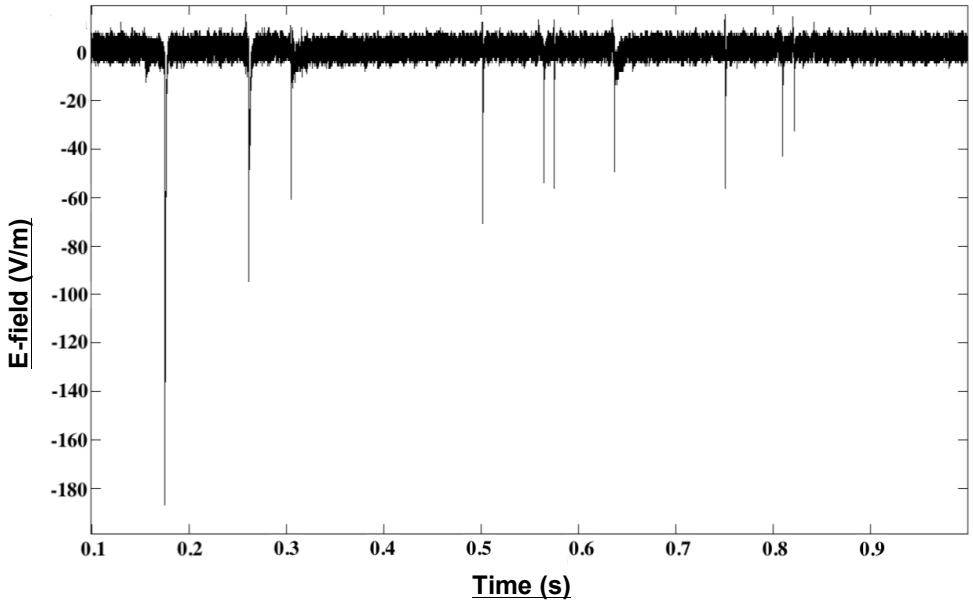

FIGURE 2.3: Changing electric field waveform of a negative CG lightning flash.

hardware integrator to produce a signal that is representative of a change in the local vertical electric field. Given that instrumented towers record very few downward flashes, the ability to infer charge quantities from natural downward flashes is of great importance. In the study conducted by Schumann, et al. [15], a flat-plate antenna and changing electric field measurements were used to study the charge transfer in natural negative and positive CG lightning. In the aforementioned study, a model developed by Jacobson and Krider [3], further explained in Section 2.4, was used. Through the implementation of this model, results were obtained that show that it is possible to use changing electric field measurements to infer the charge transferred during the continuing current phase of natural CG lightning flashes.

Figure 2.4 illustrates the process by which the flat-plate antenna and integrator produce a changing electric field waveform from the occurence of a lightning stroke. The impulse current from a lightning stroke causes a change in the vertical electric field measured by the antenna. The signal produced by the antenna due to this, is integrated and a resulting waveform is produced that represents the rate at which the electric field is changing.

According to research performed by Gill, 90.3 % of all downward lightning in

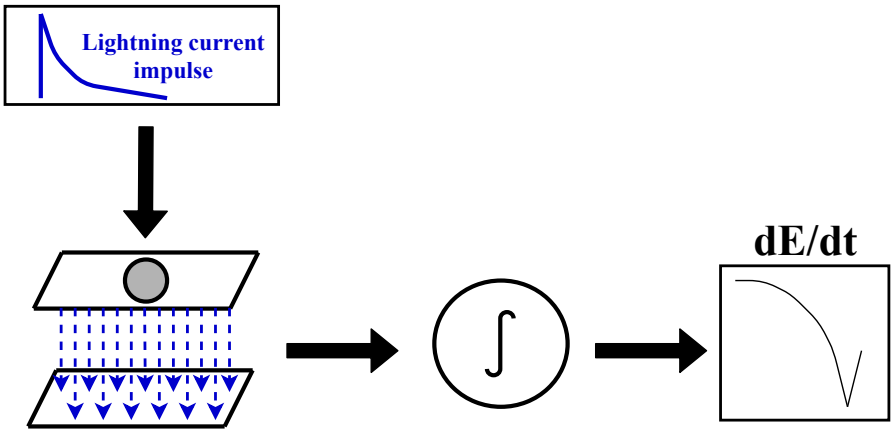

FIGURE 2.4: Flat-plate antenna and integrator measurement process.

South Africa has a negative current polarity [20]. Despite the large dominance of negative CG flashes over positive, the charge transfer inference methodology discussed in Chapter 4 allows for charge to be inferred from lightning flashes with either polarity. The analytical difference between the two polarities is the height at which the different charge centres are situated in the cloud [15]. In addition, using high-speed cameras in conjunction with changing electric field measurements, the luminosity persistence of the lightning channel in the video footage is used in determining the flash and continuing current durations. High-speed cameras have been used in previous studies as support for changing electric field measurements. In the study by Saba, et al. [19], high-speed cameras were used to confirm that the observed bipolar electric field changes in lightning flashes did, in fact, occur in a single channel. The use of high-speed cameras in Schumann and Saba [7], allowed for each flash recorded by the changing electric field sensor and video camera to be correlated with data from a lightning detection network. Schumann, et al. [15] used high-speed footage to determine continuing current durations by persistent luminosity of the channel. For the inference of charge, the duration of continuing currents is important and high-speed videos allow for more accurate determinations.

For the application of charge transfer inference using a flat-plate antenna and integrator measurement system, post-processing of the signal is required. An electronic decay of the signal is introduced in the flat-plate antenna measurement

system by the configuration of the integrator subsystem. If the integrator is set-up to monitor the fast-changing phase of a lightning flash, the slow-changing continuing current phase is distorted by the integrator decay. A technique to compensate for this decay was proposed by Rubinstein, et al. [21] and an algorithm based on this technique to reconstruct the previously distorted slow-changing electric field waveform, is presented by Kohlmann, et al. [22]. In this study, the compensation is implemented in software by cascading the output signal of the integrator with a first-order system defined by a transfer function introduced by Kohlmann [22]. This allows for the decay time-constant of the integrator to be compensated for and the application of this is discussed further in Chapter 4.

2.4 Charge inference

As presented by Jacobson and Krider [3], the charge distribution in a cloud can be modelled as a spherically symmetrical point-charge that is neutralised from a cloud-to-ground lightning discharge.

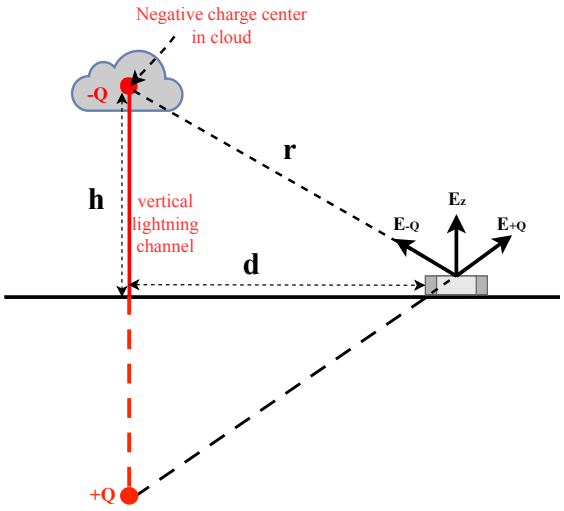

FIGURE 2.5: Geometry configuration of an observer a distance d from the ground strike-point (adapted from [23]).

Using the geometry in Figure 2.5, Equation 2.1 is used to determine the change in the electrostatic field observed at a point a distance d from the ground strike-point.

$$\Delta E_z = \frac{1}{2\pi\epsilon_0}\left[\frac{\Delta Q h}{r^3}\right] \tag{2.1}$$

This model produces more accurate results at larger distances from the strike-point as the deviations from ideal spherical symmetry in close-range make it an unreliable approximation. An infinitely conductive ground plane, discussed by Cooray [4] and used in many studies including Schumann, et al. [15], is assumed and allows for the horizontal components of the electric field to be neglected. In Equation 2.1, Q represents the net change in the overall cloud charge. A cloud with an overall negative charge $-Q$, will cause a negative change in the vertical component of the electric field, E_z, during a discharge stroke.

For the slow-changing continuing current phase of a lightning flash, the model based on the static component of the electric field is utilised and applied using Equation 2.1. In this mathematical representation of the model introduced by Jacobson and Krider, physics sign convention is used [3]. This regards a negative change in the electric field as a lightning stroke of current with a negative polarity. The model presented in this research corresponds to the model represented by Equation 2.1 and at large distances, has been determined to be a good approximation for modelling the continuing current phase of a lightning discharge [24–26].

This aforementioned model is accepted by lightning researchers as a means of inferring the charge transfer during the slow-changing, near DC, continuing current phase of a lightning stroke. This model was experimentally verified by Schumann, et al. [15]. This verification process consisted of the current measurement results of a subsequent stroke being taken from the instrumented Gaisberg Tower in Austria. This measurement was then compared to the result of the inference algorithm applied to a changing electric field measurement of the same subsequent stroke. The results of this comparison concluded that this method for charge transfer inference is sufficiently accurate and can be applied to strokes occurring within a $5 - 45$ km radius of the flat-plate antenna. This distance range was determined and justified by Schumann, et al. [15] after analysing the effect of charge centre height on charge transfer results. It was concluded that any error in the charge centre height approximation will result in significant errors in the charge transfer inference process for ground strike-point distances less than 5 km and greater than 45 km.

If changing electric field data is known and a change in charge is to be inferred using the previously defined Equation 2.1, the height of the charge centre is important. When a negative electric field change is measured, this is due to the charge neutralisation of a negative charge centre.

Using a tripolar cloud charge distribution model, presented in Figure 2.6, the height of the negative charge centre, $-Q$, is estimated to be at the $-10°$ C isotherm in the cloud [15]. The temperature and associated height differs for positive and negative CG flashes.

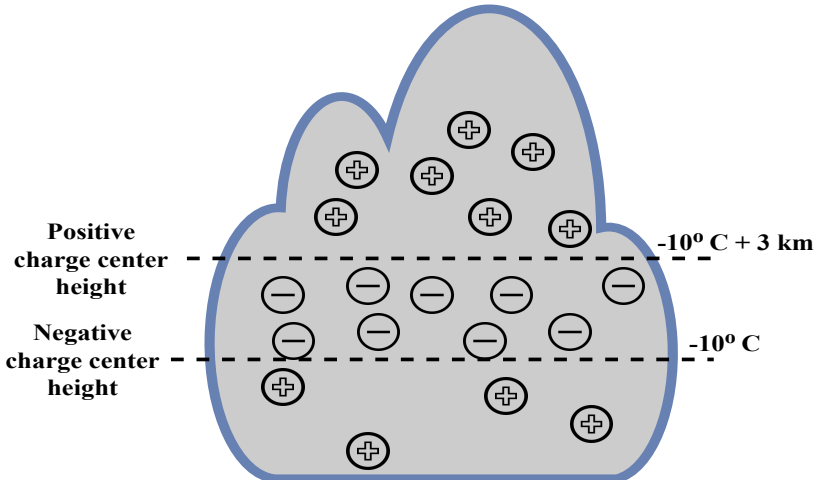

FIGURE 2.6: Tripolar model of charge separation in a cloud. Shown is the $-10°$ C isotherm and the estimated height of the positive charge centre. Adapted from [27].

Radio sounding is a technique that is used to determine the height of different thermal layers in the atmosphere. With satellites transmitting and receiving radio waves through the atmosphere, the occultation of the satellite transmitting the signal by the horizon of the earth causes the propagation speed of the radio waves to differ. Resulting from the relative motion of the transmitting and receiving satellites, this phenomenon yields information on atmospheric pressure, temperature and corresponding heights [28–32]. The United States GPS Global Navigation Satellite System (GNSS) is used to generate temperature *vs* height data for the local station in Irene, South Africa [33]. This station is the closest to Johannesburg and will provide the most accurate charge centre height data.

A method of charge transfer inference for both negative and positive CG flashes is presented by Schumann, et al. [15] and is used in this research. The different polarities of lightning discharges requires different height parameters to be used in the model. Apart from this difference in charge centre height and polarity of the

electric field change, the charge transfer inference methodology for both negative and positive cloud-to-ground flashes is fundamentally equivalent.

The radial distance r, from Equation 2.1, is represented by the corresponding h and d parameters seen in geometrical illustration in Figure 2.5. From this, Equation 2.1 can be simplified as shown below.

$$E_z = -\frac{Qh}{2\pi\epsilon_0}\frac{1}{(h^2+d^2)^{\frac{3}{2}}} \tag{2.2}$$

For the charge transfer to be inferred from changing electric field measurements, Equation 2.2 can be rewritten, as follows, in Equation 2.3.

$$\Delta Q = -\Delta E_z \frac{2\pi\epsilon_0(h^2+d^2)^{\frac{3}{2}}}{h} \tag{2.3}$$

The quantity of charge transferred during the continuing current phase of the lightning stroke can be determined using Equation 2.3 and the duration of continuing current present in the stroke. The use of high-speed videos in conjunction with changing electric field measurements assist in determining, more accurately, the duration of continuing current in a lightning flash. As illustrated in Figure 2.5 and applied in Equation 2.2 and 2.3, 'h' refers to the height of the charge centre above the ground and 'd' represents the distance from the ground strike-point of the lightning stroke to the flat-plate antenna.

2.5 Summary

A flat-plate antenna and integrator system allows for changing electric field measurements of lightning flashes to be recorded. This measurement can be processed in software, after the quantisation process, to correct offset biasing and compensate for the electronic decay introduced by the integrator. The resultant digital waveform corresponds to the continuous vertical electric field profile between the cloud and the ground during a lightning flash. Using a model introduced by Jacobson and Krider [3] and experimentally verified by Schumann, et al. [15], the quantity of charge transferred during the continuing current phase of a lightning stroke can be determined. Apart from the electric field waveform, this model requires the height of the relevant charge centre in the cloud, the distance between the antenna and the ground strike-point of the stroke and the duration of the continuing current.

The following chapter details all the measurement equipment used in this study and their corresponding specifications. All the raw data recorded by each measurement system is presented.

CHAPTER 3

Equipment specifications and obtained data

This chapter provides the detailed specifications of the measurement equipment used and presents the data that was obtained and recorded. The content in this chapter is with reference to the study that took place in South Africa over the period of two lightning seasons, between February 2017 and November 2018. The set-up of the flat-plate antenna system and the high-speed cameras is explained and the lightning location system (LLS) and radio-sounding technology that was used to attain necessary parametric quantities required for the charge transfer inference model is presented.

In order to infer charge transfer from the continuing current phase of lightning strokes, an electromagnetic model developed by Jacobson and Krider is used [3]. This model was introduced in Chapter 2. A flat-plate antenna is used to measure the changing electric field that is generated by a lightning flash. High-speed cameras are used to record the lightning flashes to determine the duration of the continuing current. The height of the charge centre above the ground and the distance from the ground strike-point to the antenna are parameters required for the model to be applied. The height parameter is obtained using radio-sounding technology and the distance parameter is obtained from lightning location system (LLS) data. Detail is provided on these in the 'Auxilliary measurements' section of this chapter.

3.1 The flat-plate antenna system

The flat-plate antenna is a passive, capacitive device that measures the local vertical electric field. The antenna is cascaded with an integrator that results in the measurement producing a waveform that is proportional to the change in the vertical electric field. From this, the electric field that propagates from a lightning stroke can be measured. This section provides detail regarding the specifications of the antenna system, including the set-up topology and physical characteristics. A brief explanation on the theory of how this device operates is also provided to give a mathematical basis of the functionality and to relate the device specifications to what is physically being measured. Furthermore, the raw data recorded using this measurement system is presented.

3.1.1 Specifications

A capacitive, flat-plate antenna is cascaded with an integrator and used in this study. This antenna is set up on the roof of a four storey building, 19 m above the ground, at a location in the central business district of Johannesburg, South Africa.

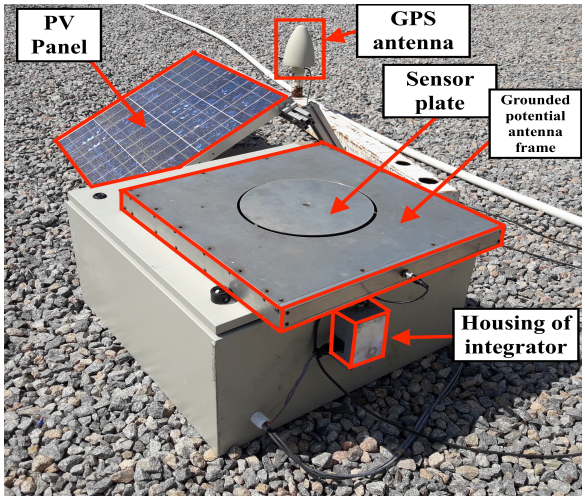

FIGURE 3.1: The flat-plate antenna measurement set-up used in this study.

Illustrated in Figure 3.1 is the set-up of the aforementioned antenna and integrator. The set-up consists of the antenna itself, which is a 500 mm X 500 mm X 50 mm

aluminium box that has a circular sensor plate with a diameter of 250 mm. The 5 mm air gap between the sensor plate and the box is to ensure there are no fringing effects around the circumference of the sensor plate. Connected to the antenna with a 250 mm, 50 Ω, RG223 co-axial cable is the integrator subsystem. Shown in Figure 3.1, the electronics that constitute the integrator are housed in a waterproof container next to the antenna. The output of the integrator is sampled by a PCI N-6110 National Instruments data acquisition unit at 5 MS/s with a $12 - bit$ resolution. The PV panel included in the set-up is used to ensure that the 12 V battery, which powers the operational amplifier in the integrator subsystem, always remains sufficiently charged. This measurement set-up allows for continuous recording of changing electric fields. To ensure that all recordings are accurately time-stamped, a Meinberg PCI-170GPS board is used. The external GPS antenna used by this board is shown in Figure 3.1. With the antenna placed on top of a building, an enhancement of the vertical electric field was observed. It was experimentally determined that the effect of the building caused the magnitude of the readings to be amplified by a factor of $BF = 1.55$. Appendix A contains the methodology and analysis results for determining this enhancement factor.

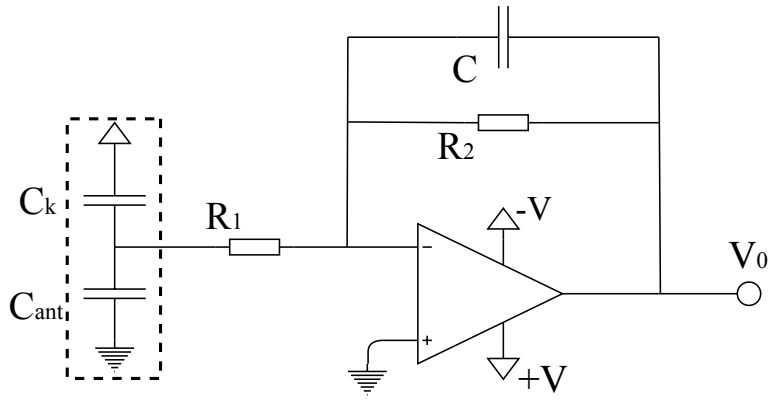

FIGURE 3.2: Operational amplifier configuration of integrator. Adapted from [22].

Figure 3.2 shows the electronic configuration of the integrator subsystem. The electronic decay introduced by the integrator, mentioned in Chapter 2, is due to the feedback combination of R_2 and C. The combination of C_k and C_{ant} represent the capacitance between the cloud and the ground. The bandwidth of integrator

is approximately 300 Hz $-$ 1.5 MHz with a decay time constant of $\tau = 0.47$ ms. This bandwidth ensures that the frequency components of the electromagnetic waves that propagate from a lightning stroke can pass through the integrator without irrevocable attenuation. The amplification calibration factor is $CF = 4.34$ $\frac{mV}{V/m}$.

3.1.2 Theoretical explanation

To further understand the performance of the operation of this system, Equation 3.1 is applied to explain the current waveform that is produced from the changing voltage on the antenna.

$$i_c = C\frac{dV_c}{dt} \tag{3.1}$$

The integration of the signal results in a waveform that tracks the voltage magnitude on the antenna, seen in Equation 3.2. This voltage level is directly proportional to the vertical electric field above the antenna developed between the cloud and the ground.

$$V_c' = k\int i_c dt \tag{3.2}$$

A fast change in voltage occurs when the antenna senses a fast change in the vertical electric field caused by a lightning flash. The integrator output can be represented by Equation 3.2, where k is an amplification factor determined by the capacitance of the antenna and the signal gain from the integrator.

3.1.3 The recorded data

The data provided in Table 3.1 shows the quantity of strokes and flashes that were recorded using the flat-plate antenna measurement system over two lightning seasons in the period between February 2017 and November 2018.

TABLE 3.1: Data recorded using the flat-plate antenna measurement system.

Description	Positive	Negative	Total
Number of flashes	7	165	172
Number of strokes	17	663	680

The numbers presented are raw and unfiltered and consist of some flashes that are not feasible for charge transfer inference analysis due to the $5 - 45\ km$ ground strike-point distance constraint, mentioned in Section 2.4 in Chapter 2. The filtering of the raw data and the constraint conditions are discussed further in the following chapters.

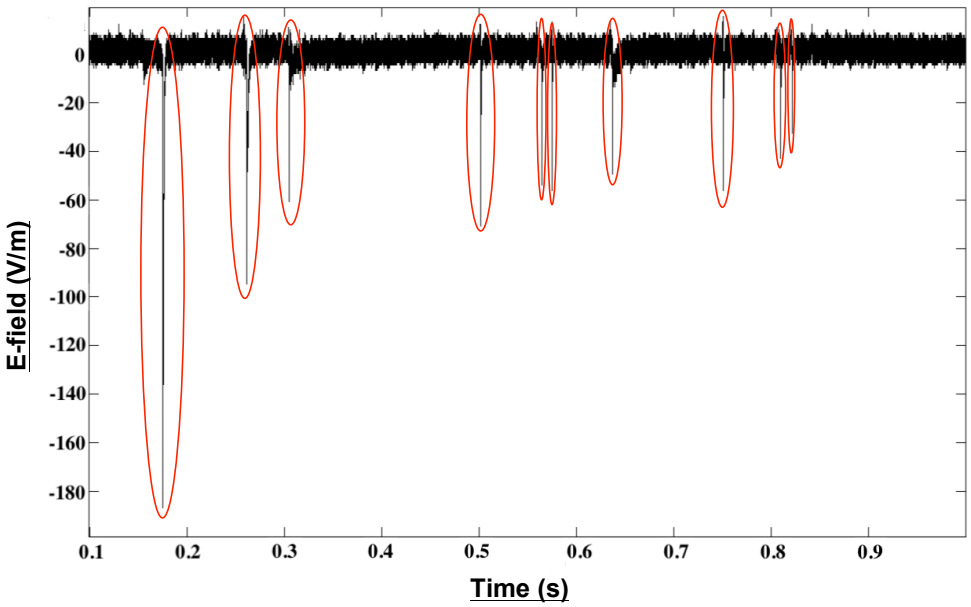

FIGURE 3.3: Changing electric field waveform with individual strokes circled in red.

Figure 3.3 is a changing electric field waveform of a negative CG lightning flash. This particular flash was recorded on 14 November 2017 in Johannesburg and

was used in this study. This waveform represents a single flash comprising of 10 strokes. In the figure, each individual stroke is circled in red. With reference to Table 3.1, this flash contributes to the 'Negative' column with 1 in the 'Number of flashes' row and 10 in the 'Number of strokes' row.

3.2 High-speed cameras

High-speed cameras are used in this study in conjunction with the changing electric field measurements. The camera footage allows for the duration of continuing current in a lightning stroke to be determined [6]. Continuing current duration is required in order to apply the charge transfer inference model to lightning strokes. This section details the specifications of the high-speed cameras used and provides the raw data that was obtained from recording lightning flashes over a period between February 2017 and November 2018.

3.2.1 Camera specifications

Two high-speed cameras were used to record lightning flashes. The cameras are positioned with a field of view bound by two towers on either side of a central business district in Johannesburg, South Africa. The two towers are named the Hillbrow tower and the Sentech tower. The cameras used are the Phantom v310 ($15,000\ fps$, exposure time 58 μs) and Phantom v7.1 ($5,000\ fps$, exposure time 990 μs). The differences in frame rate and exposure time allow for comparison of footage and hence, more accurate characterisation of flashes [6]. Each camera is triggered manually by using a push button that has variable pre-trigger and post-trigger times that are customised depending on the operator.

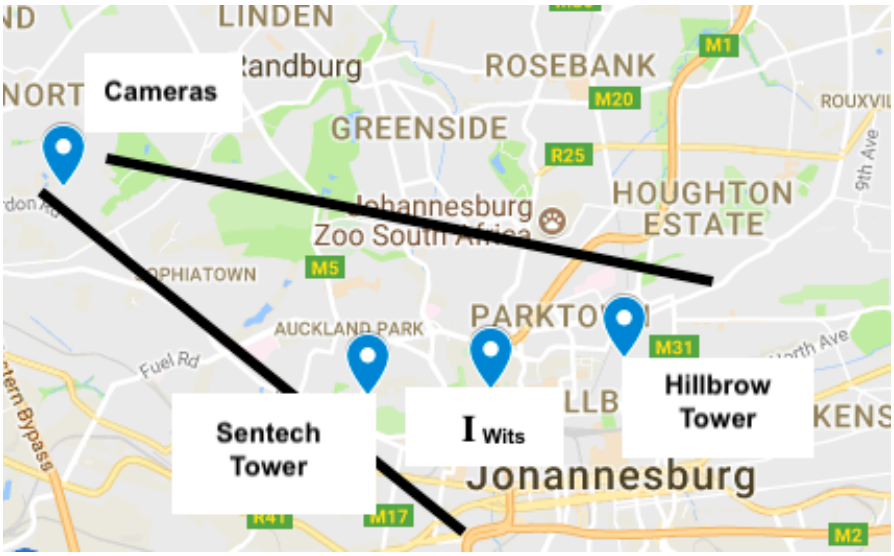

FIGURE 3.4: Field of view of the high-speed cameras.

Figure 3.4, which was constructed using Google Maps software, shows the field of view of the cameras, relative to the towers and the flat-plate antenna system (I_{Wits}).



FIGURE 3.5: The set-up of the Phantom v310 (far left) and the Phantom v7.1 (far right) high-speed cameras.

Figure 3.5 is a photograph of the cameras used and their field of view. The Phantom v310 is on the left of Figure 3.5 and the Phantom v7.1 is on the right.

3.2.2 Measured continuing current data

The quantities presented in Table 3.2 represent the details of the lightning flashes captured using the high-speed video cameras over a period from February 2017 to November 2018.

TABLE 3.2: Continuing current data obtained from high-speed camera footage.

Continuing current quantity	**Positive (N=14 strokes)**	**Negative (N=609 strokes)**
Maximum duration (ms)	567	929
Minimum duration (ms)	2	1
Mean duration (ms)	250.21	32.8
Strokes with no CC $t > 3\ ms$	2	99
Strokes with very short CC $t > 3\ ms$ but $t < 10\ ms$	1	268
Strokes with short CC $t > 10\ ms$ but $t < 40\ ms$	0	156
Strokes with long CC $t > 40\ ms$	11	86

The number of strokes with long, short and very short continuing current durations are given as well as the corresponding maximum, minimum and mean duration statistics. The data set presented in Table 3.2 comprises of 14 positive strokes and 609 negative strokes.

Presented in Table 3.2, the mean duration of continuing current in positive flashes is approximately 8 times greater than the duration of continuing current in negative flashes. From studies conducted in Brazil and USA, this factor is approximately 1.5 times [15]. From studies conducted in Austria, positive and negative strokes had similar durations [15]. The results of these studies are reviewed in more depth in Chapter 5.

One reason for the significant difference in this factor between the continuing current durations recorded in this study and the other aforementioned studies is the discrepancy in sample size between negative and positive strokes. Only 14 positive strokes were recorded compared to 609 negative strokes. It is likely that if the sample size of positive strokes was increased significantly, the results from this study would have an increased similarity to the others.

It is noted that approximately 21 % of positive strokes had short or no continuing current ($t < 10\ ms$) compared to 60 % of negative strokes. Long continuing current

($t > 40\ ms$) was present in 79 % of positive strokes compared to approximately 14 % in negative strokes. This dataset does not consider initial return strokes or subsequent return strokes separately. It is known that, on average, negative lightning flashes consist of significantly more subsequent return strokes than positive and that in general, subsequent return strokes have shorter continuing current duration than initial return strokes [5]. This compounded with the discrepancy in sample size, provides justification for the large difference of recorded continuing current durations in negative and positive strokes.



FIGURE 3.6: High-speed video frames of leader propagation (a), attachment (b) and continuing current (c) [6].

Figure 3.6 shows three high-speed video frames of a negative CG lightning process [6]. The frames consist of leader propagation, attachment and continuing current. The data presented in Table 3.2 is with reference to the duration of the continuing current phase of a lightning flash. This process is depicted in the third frame of Figure 3.6.

3.3 Auxiliary measurement equipment

The primary measurement instruments in this study are the flat-plate antenna to record changing electric field measurements and the high-speed cameras to determine the duration of continuing currents in lightning strokes. In conjunction with these measurements, two important parameters are required for the charge transfer inference model to be applied. The first of these parameters is the distance from the ground strike-point of the lightning flash to the flat-plate antenna. The second is the height of the charge centre in the cloud. These paramaters are obtained by using a lightning location system and radio sounding technology, respectively. This section details the specifications of the aforementioned aquisition methods and provides a summary of the obtained data.

3.3.1 Lightning Location System

A lightning location system is used to obtain the distance parameter required in the charge transfer inference model. This parameter represents the distance between the ground strike-point of a lightning stroke and the flat-plate antenna. The lightning location system provides the coordinates of the ground strike-point and, since the location of the flat-plate antenna is known, the distance can be calculated. The details of the specific lightning location system used are provided below, along with a summary of the calculated distance data.

3.3.1.1 Specifications

Lightning Location System (LLS) data was acquired from the South African Weather Service (SAWS). The LLS was first established in 2005 and since the most recent addition in 2014, is made up of 24 Vaisala LS7000 sensors distributed throughout South Africa [34]. The LLS is used to determine quantities such as the lightning ground flash density and lightning intensity risk [13].

The location and time stamp of all lightning strokes, within range, is recorded by this network. The coordinates of lightning flash strike-points and their associated current stroke magnitudes and polarities are studied. The strike-point coordinates are used to determine the distance parameter in the charge transfer inference model, shown in Equation 2.1 in Chapter 2.

Figure 3.7 shows the distribution of the 24 Vaisala LS7000 sensors around South Africa in 2014 [13]. The sensor located in Irene, circled in red on the figure, is the closest to Johannesburg - where this study was conducted.



FIGURE 3.7: The location of the 24 Vaisala LS7000 sensors distributed throughout South Africa, taken from 2014 [13].

3.3.1.2 Measured ground stike-point distance data

Table 3.3 presents minimum, maximum and mean ground strike-point distance values for 623 strokes recorded by the LLS. These strokes correspond to those recorded by the high-speed cameras during the period between February 2017 and November 2018.

TABLE 3.3: Ground strike-point distance data for a sample of 623 strokes.

Distance from antenna to strike-point	**Distance** (km)
Maximum	28.2
Minimum	0.8
Arithmetic mean	5.7

Distance constraints limit the data set to flashes with ground strike-point distances between 5 and 45 km away from the flat-plate antenna. Because of this, the values presented in Table 3.1 are different to the distance statistics of the flashes analysed in the charge transfer inference process. Each stroke is examined individually, therefore, if a flash consists of multiple strike-points, distances from the different

strike-points are calculated separately. Of the 623 strokes recorded by the LLS and summarised in Table 3.1, 34 negative strokes and 5 positive strokes have both long continuing current (i.e. greater than 40 ms in duration) and fall within the $5 - 45$ km distance range. These subsets have a mean distance of 13.1 km and 10.7 km, respectively. All the aformentioned distance statistics are reviewed and discussed in Chapter 5.

3.3.2 Radio sounding measurement of charge centre height

Radio sounding technology is used to determine the height of different isotherms in the atmosphere. This height parameter is required by the model used in the charge transfer inference process. As discussed in Chapter 2, the negative charge centre sits in the -10 $°C$ isotherm and the positive charge centre sits 3000 m above that [15].

3.3.2.1 Data

Table 3.4 shows the maximum, minimum and mean heights of the -10 $°C$ isotherm for 56 strokes that were recorded between February 2017 and November 2018.

TABLE 3.4: Summary of -10 $°C$ isotherm heights.

-10 $°C$ **isotherm height**	**Height** (m)
Maximum	6650
Minimum	5530
Arithmetic mean	6225

All 56 strokes were recorded by both the flat-plate antenna measurement system and the high-speed cameras and fell within the $5 - 45$ km distance constraint. Of the 56 strokes, 51 were negative and 5 were positive. All of these strokes were used in the final charge transfer inference calculations and a more comprehensive summary of the results is provided in Chapter 5.

3.4 Summary

The flat-plate antenna set-up continuously records changing electric field measurements. The integrator used in this set-up has a calibration factor of $CF = 4.34\ \frac{mV}{V/m}$ and an RC-decay time-constant of $\tau = 0.47\ ms$. The raw dataset of these electric field measurements consists of 663 negative strokes and 17 positive strokes. All the recorded data detailed in this section was obtained during the period between February 2017 and November 2018.

Two high-speed cameras, the Phantom v310 and Phantom v7.1 are used to record the luminosity persistence in lightning strokes, which allows for continuing current duration to be determined. High-speed footage of 609 negative strokes and 14 positive strokes was recorded and subsequent continuing current durations were resolved.

The South African Weather Service provided access to the LLS data and radio sounding data that is used to obtain ground strike-point distance parameters and charge centre heights for the charge transfer inference model. From 623 lightning strokes, the mean distance between the ground strike-point and the flat-plate antenna is calculated to be 5.7 km. The distance data presented in this section is raw and has not yet been filtered down by the $5 - 45\ km$ distance constraint. The mean height of the $-10\ ^{\circ}C$ isotherm for 56 strokes is calculated to be 6225 m. This mean height value was determined from only strokes that were within the $5-45\ km$ range away from the flat-plate antenna.

The following chapter details the implementation of the charge transfer inference process. The necessary filtering of the data presented in this section is explained and the methodology followed during this study is presented.

CHAPTER 4

The charge inference process

The following chapter provides the methodology applied to obtain overall charge transfer quantities. The methodology relating to the electric field measurements and the electronic decay compensation is discussed. The methods for determining charge centre heights, continuing current durations and ground strike point-distances are detailed.

The charge transfer inference process relies fundamentally on processing the changing electric field files that are recorded by the flat-plate antenna system. Since only the continuing current phase of a lightning stroke is examined, the duration of the continuing current is important to quantify. This duration is determined by the luminosity persistance of the lightning channel and requires high-speed video cameras for analysis. The charge transfer inference model requires the height of the charge centre above the ground and the distance between the ground strike-point and the flat-plate antenna. These two parameters are quantified using radio sounding technology and a lightning location system, respectively. The following section provides the methodology that is implemented in acquiring the post-processed changing electric field waveform, the continuing current durations and the distance and height parameters.

4.1 Methodology overview

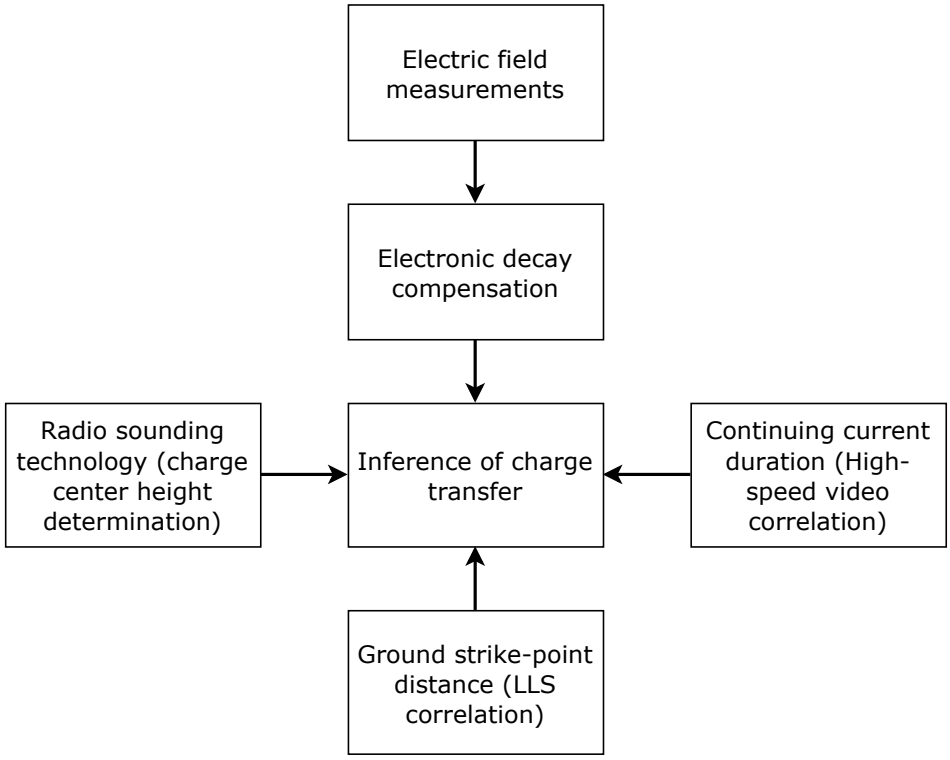

FIGURE 4.1: Methodology followed in the charge transfer inference process.

The flow diagram, presented in Figure 4.1, provides an overview of the charge transfer inference process. As seen at the top of the figure, the process begins with changing electric field measurements being recorded. Due to the short time-constant of the integrator in the flat-plate antenna set-up, the waveform requires decay compensation so that the slower changing continuing current phase of the lightning stroke can be resolved. The resultant compensated waveform forms the basis of the charge transfer inference model, which is depicted as the centre block in Figure 4.1. Other parameters required by the model are the continuing current duration, the height of the charge centre above the ground and the distance from the ground strike-point to the flat-plate antenna. These parameters are obtained by the use of high-speed cameras, radio sounding technology and a lightning location system, respectively.

For a lightning stroke to be included in the charge transfer inference process, it must be recorded by both the flat-plate antenna system and the high-speed cameras. From inspecting the camera footage, if the persistent luminosity results in the continuing current being shorter than 3 ms, the stroke is omitted. If the luminosity persistence is less than 3 ms, it is not conclusive that significant continuing current exists [15]. Using time-stamp correlation, the coordinates of the ground strike-point of the lightning stroke are extracted from the lightning location system database. From this, the distance between the ground strike-point and the antenna is calculated. If this distance is outside of a $5 - 45$ km range, the sample is omitted. This constraint was determined by Schumann, et al. [15] who determined that any error in the charge centre height becomes exacerbated for distances outside of this range and hence, would not produce accurate charge transfer results.

As originally presented in Chapter 2, the derived equation based on the point-charge model of the lightning is provided again below in Equation 2.3, for ease of reference. From this equation, the necessity of the height 'h' and distance 'd' parameters can be seen. The compensated changing electric field measurement is represented by ΔE_z. The continuing current duration is needed to determine the set of ΔQ values to sum in order to attain a final charge transfer quantity.

$$\Delta Q = -\Delta E_z \frac{2\pi\epsilon_0(h^2 + d^2)^{\frac{3}{2}}}{h} \tag{2.3}$$

4.2 Electric field measurements

As discussed in Section 3.1 in Chapter 3 the integrated changing electric field measurement is digitised. This quantisation process, which is accuratedly time-stamped from GPS correlation, results in the continuous measurement being stored in separate, $1-second$ long binary files using a datalogger software program. The data points in these files correspond to instantaneous values that are scaled representatives of the change in the vertical electric field above the flat-plate antenna.

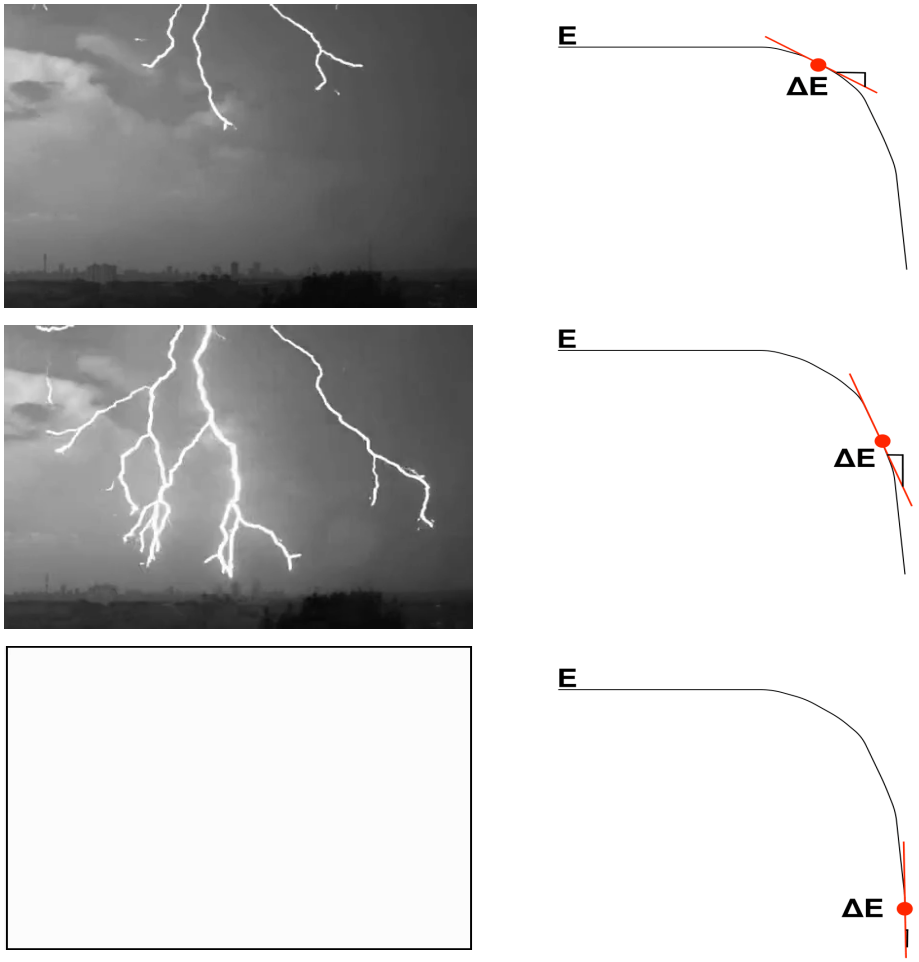

FIGURE 4.2: Depiction of electric field gradient change with reference to leader propagation.

Figure 4.2 shows how the gradient of the electric field profile changes during the processes of leader propagation and attachment. The first frame shows the stepped leaders beginning to propagate downwards. As this occurs, the electric field begins to break down. The rate at which the electric field breaks down is equivalent to the gradient of the electric field profile during this process. The second and third frames show moments before attachment and attachment, respectively. The third frame, depicting attachment, is saturated due to intense luminosity caused by the return stroke process. The gradient becomes increasingly steeper and reaches a maximum at the point of attachment. The aforementioned changing electric field waveforms represent the continuous change of this gradient during a lightning flash process.

As stated previously, the only relevant lightning strokes are those that are recorded by both the flat-plate antenna and the high-speed cameras. The time-stamps on the camera footage are correlated to the time-stamped changing electric field files. The files that correspond to the lightning flashes recorded on the cameras are stored and the rest are omitted.

4.3 Electronic decay compensation

From the changing electric field files that correspond to the lightning flashes recorded on the high-speed cameras, an electronic decay compensation algorithm is applied. The presence of the electronic decay is due to the short time-constant of the integrator subsystem that causes the waveform to become distorted in the slower-changing, low frequency ranges. This prevents the continuing current phase of the lightning flash from being realised. Once the decay is compensated for, the original changing electric field waveform is converted into a representation of the physical electric field profile. From this, the low frequency components can be realised and the continuing current phase can be resolved.

A method introduced by Rubinstein, et al. [21] and later extended by Kohlmann, et al. [14, 22], to compensate for the electronic decay of the recorded signal, is adapted for this research. The software used for data processing is MATLAB, however, the high-level application of the method will not change across any software platform.

After the quantisation of the changing electric field signal, the data is then scaled by the inverse of the calibration factor (i.e. $1/CF$) and the inverse of any enhancement factor that may be present (i.e. $1/BF$). In this case, the calibration factor is $CF = 4.34 \cdot 10^{-3}$ and the building enhancement factor is $BF = 1.55$, as mentioned in Chapter 3. The outcome of this is the same changing electric field waveform with magnitude values that correspond to the realistic conditions without any unwanted measurement scaling.

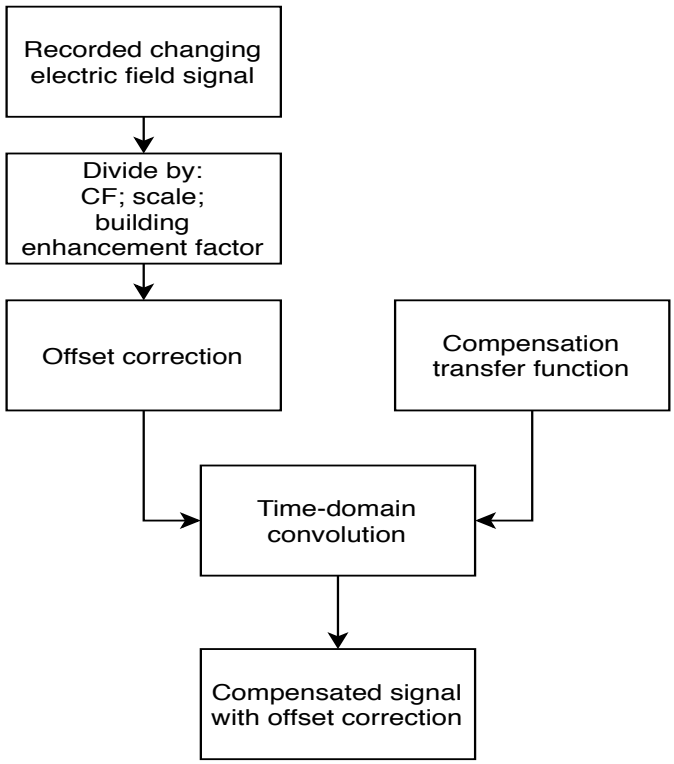

FIGURE 4.3: High-level structure of the offset correction and decay compensation algorithm.

As seen in Figure 4.3, following the calibration factor and enhancement factor normalisation, an offset correction is applied. The waveform may have a zero-bias due to offset currents and/or voltages of the operational amplifier in the integrator circuit. This bias level is determined by taking the mean value of a sample under ambient conditions (i.e. without any lightning strokes). Since the value of this bias can change over time, the average offset is calculated for each specific changing electric field file that is examined. The offset correction process consists of subtracting the mean offset value from each sample point in the digitised file. This correction is necessary as, given the convolution process shown in Figure 4.3, any offset errors will be compounded every convolution iteration and ultimately corrupt the final output [14, 22].

After offset correction is applied, the output is convolved with the aforementioned compensation transfer function that was developed by Kohlmann, et al. [14]. The impulse response of this transfer function is presented in Equation 4.1. In this equation, $\tau = 0.47\ ms$ and refers to the decay time constant of the integrator. The calibration factor is given as $CF = 4.34 \cdot 10^{-3}$. The $\delta(t)$ represents the dirac pulse and $U(t)$ represents the unit step function.

$$h(t) = \frac{1}{CF}\delta(t) + \frac{1}{\tau CF}U(t) \tag{4.1}$$

Equation 4.2 describes the convolution process between the impulse response of the compensation transfer function and the changing electric field waveform with offset correction.

$$y(t) = magnitudeCorrected(t) * h(t) \tag{4.2}$$

Convolution in the time domain can be represented by multiplication in the frequency domain, which is shown in Equation 4.3. Whether time-domain convolution or frequency-domain multiplication is implemented, the result will be the same. The outcome of this convolution process is the final compensated waveform that represents the physical vertical electric field profile seen by the antenna.

$$y(t) = \mathscr{F}^{-1}\big[\mathscr{F}\{magnitudeCorrected(t)\}.\mathscr{F}\{h(t)\}\big] \tag{4.3}$$

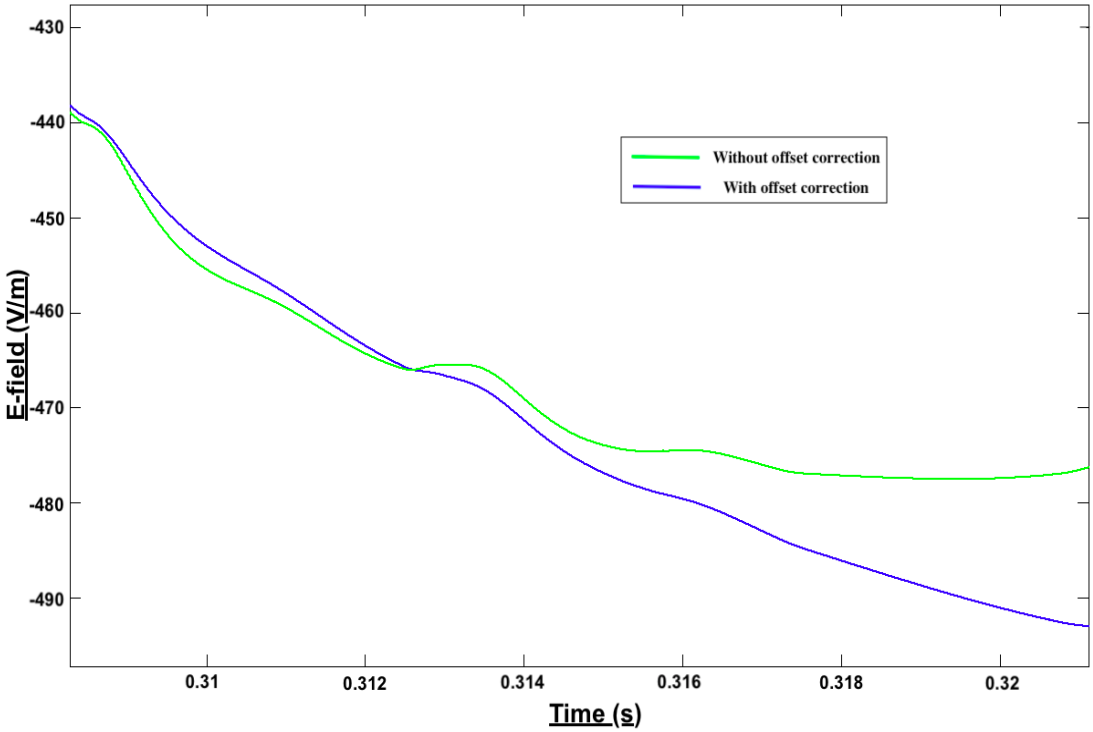

FIGURE 4.4: The effect of offset correction on the final compensated output.

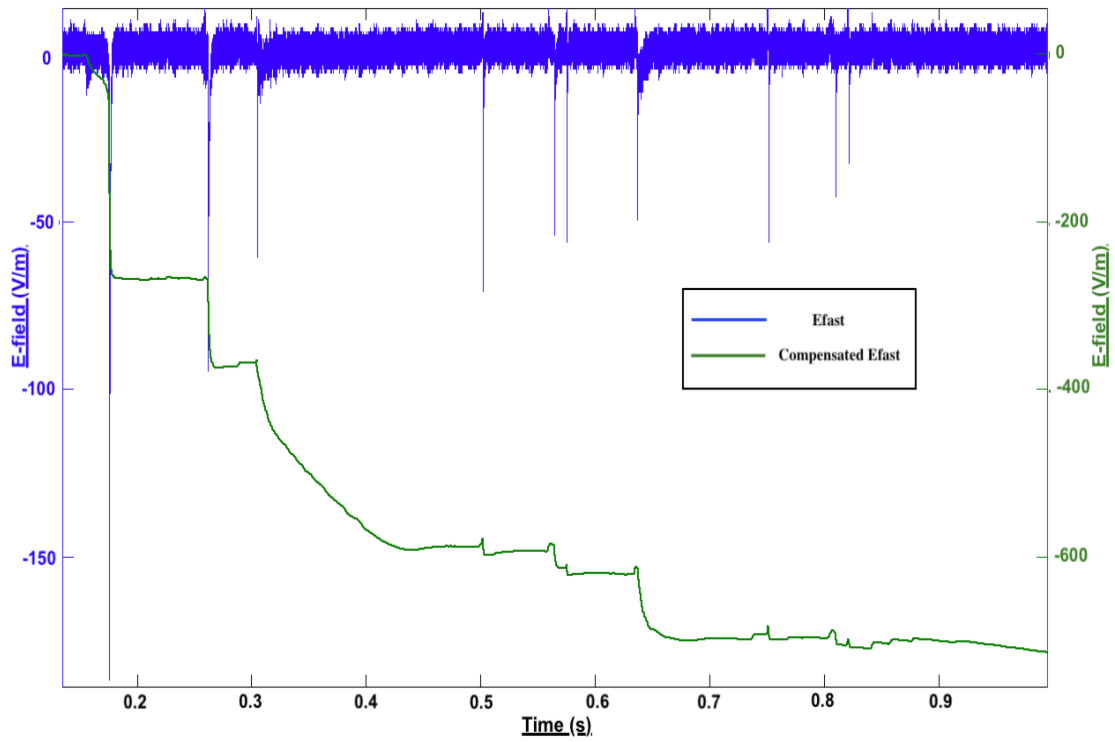

FIGURE 4.5: Uncompensated changing electric field waveform (Efast) and corresponding compensated waveform (compensated Efast).

The offset correction effect is made apparent by the illustration on the previous page in Figure 4.4. This measurement was taken from a lightning flash recorded on 14 November 2017 in Johannesburg. The blue line is the compensated waveform with offset correction applied and the green line is the output of the compensation algorithm without the application of offset correction. It is seen that due to the compounding of offset errors in the convolution process, the final result will include a distorted waveform relative to the output on which offset correction is applied.

Figure 4.5, on the previous page, shows a recorded changing electric field measurement, denoted as 'Efast' and plotted in blue. This measurement was taken from a lightning flash recorded on 14 November 2017 in Johannesburg. The corresponding compensated waveform is provided in green. This figure ultimately presents the raw recorded data and the corresponding processed data from which charge transfer can be inferred. In the blue waveform, the high frequency components are resolved with high precision, however, due to the short decay time constant of the integrator, the low frequency components are distorted. During the compensation process, the lower frequency components are amplified and the higher frequency components are attenuated. This results in the green waveform, shown in Figure 4.5, in which the slow-changing continuing current waves are not distorted and can be examined.

4.4 Continuing current duration

The following section details the methodology behind how the high-speed cameras are operated and how the video footage is examined to extract the relevant data. This section provides detail regarding the determination of continuing current durations using luminosity persistence and GPS time-stamp correlation.

4.4.1 Camera operation

High-speed cameras are set up overlooking a specific area, with a field of view that includes the surroundings of where the flat-plate antenna is set up. The cameras

are time-synchronised with a GPS for accurate time-stamping of the lightning footage. The operation of these cameras relies on manual triggering. For this triggering method, the pre-trigger and post-trigger times are set-up to the preferences of the individuals operating the cameras to ensure that the entire flash is captured and saved. In this study, two high-speed cameras are used to record lightning flashes. A manual 0.2 s pre-trigger and a 0.8 s post-trigger is used when saving footage of a lightning flash.

4.4.2 High-speed video analysis

The examination of the recorded high-speed footage of the lightning flashes is performed manually. The duration of the luminosity persistence, indicating the presence of continuing current, is determined by recording length of time between initial attachment of the leader and the time at which the ionised channel is no longer visible. The continuing current duration is an integral quantity in the application of the charge transfer inference process.

Figure 4.6 shows eight time-stamped frames obtained from the high-speed video footage of a negative CG lightning flash on April 6, 2017. The corresponding changing electric field waveform is presented next to these frames. The vertical red line on the changing electric field waveform tracks the time of each high-speed video frame that is presented. Frame 1 and 2 show the propagation of negatively charged downward stepped leaders. In frame 3, attachment occurs and causes saturation of the footage due to the intense luminosity spike that is a result of the return stroke current impulse. The time of attachment is recorded and stored. The relatively lower intensity continuing current, shown in frames 4 to 7, is seen as persistent luminosity of the ionised channel. As discussed by Schumann, et al. [15], the continuing current phase of a lightning stroke is said to begin 3 ms after the time of attachment. The end time of the continuing current is taken as the first frame where the ionised channel is no longer visible. In Figure 4.6, the end-point of the continuing current is frame 8.

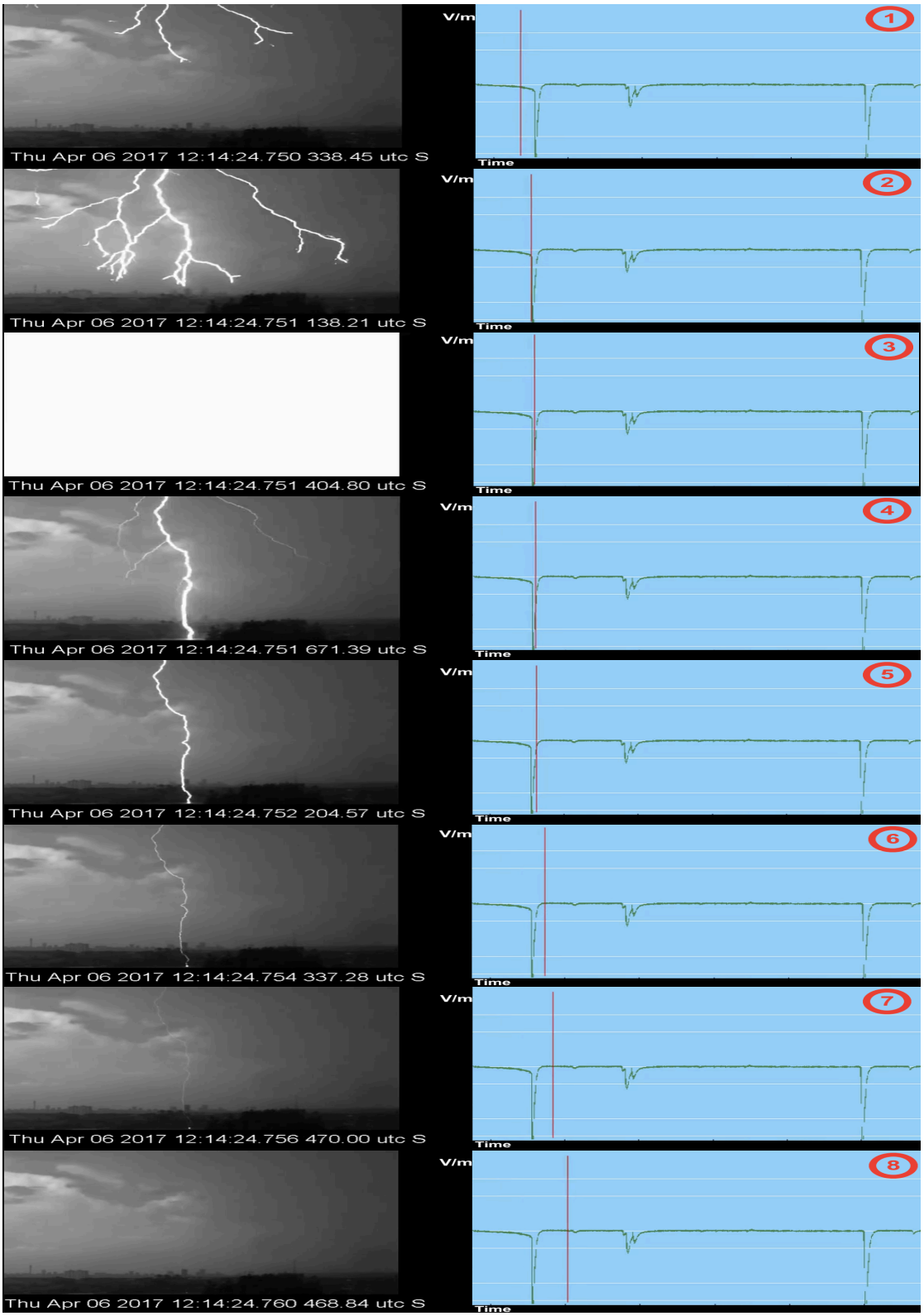

FIGURE 4.6: High-speed video frames and the corresponding changing electric field waveform and time stamps.

From the stroke shown in Figure 4.6, the continuing current duration is taken as the time between 3 ms after the point of attachment (i.e. $12:14:24.751404 + 0.003 = 12:14:24.754404$, taken from frame 3) and the time stamped on frame 8 ($12:14:24.760468$). For this example, the continuing current duration would be $CC_{duration} = 12:14:24.754404 - 12:14:24.760468 = 6.1\ ms$.

4.5 Auxiliary measurements

The following section provides the methodology behind how the height, h, and distance, d, parameters required for the charge transfer inference model, are obtained. The South African Weather Services (SAWS) provided radio-sounding plots that allow for the determination of charge centre height ('h'). The lightning location system, operated by SAWS, is used to determine the distance between the ground strike-point of a lightning stroke and the flat-plate antenna ('d').

4.5.1 Ground-strike point distance

As discussed in Chapter 2, the distance between the ground strike-point of the lightning stroke and the flat-plate antenna is significant when inferring charge transfer quantities. This parameter is required in the final charge transfer inference equation, however, is only relevant if the stroke is captured by both the high-speed cameras and the flat-plate antenna and falls within a $5 - 45\ km$ distance range.

In order to determine this distance parameter, the location coordinates of the ground strike-point of a lightning stroke are required. This data is obtained from a local weather service organisation or an independent company that has access to the necessary equipment for determining ground strike-point locations. In the case of this study, LLS data was provided by SAWS.

To find the specific lightning stroke entry in the LLS database corresponding to the recorded flash on the high-speed video, time-stamp correlation is used. After time-stamp matches are found, the coordinates are checked to confirm that the

flash occured within the field of view of the cameras and does, in fact, correspond to the recorded flash.

Once the corresponding entry is found in the LLS database, the distance between the ground strike-point and the antenna can be determined. For the most accurate results, Equation 4.4 is used.

$$d = K\left[\arccos\left(\sin(Y_{GS})\sin(Y_{Ant}) + \cos(Y_{GS})\cos(Y_{Ant})\cos(X_{GS} - X_{Ant})\right)\right] \quad (4.4)$$

This equation is derived from the law of haversines and takes the curvature of the earth into account [35]. It is more precise than a simple pythagorian distance calculation for this application. The coordinates used in the equation refer to the longitude and latitude of the ground strike-point (X_{GS},Y_{GS}) and the antenna (X_{Ant},Y_{Ant}), respectively. The trigonometric operations used in this equation are computed in radians. The constant $K = (111.3)(\frac{180}{\pi}) = 6377.02$.

If the ground strike-point of the flash is within $5 - 45$ km from the flat-plate antenna, the changing electric field measurement of that flash is used in collaboration with the corresponding high-speed footage to form a datum entry. Only flashes that satisfy this distance criteria are used in applying the decay compensation and charge transfer inference algorithms.

4.5.2 Charge centre height determination

As explained in Chapter 2, a negative charge centre is located in the $-$ 10 $^{\circ}C$ isotherm and a positive charge centre is assumed to be at 3000 m above this [15]. The polarity of the lightning stroke being examined, determines the height value that is used in the charge transfer inference calculation. This height parameter is required in the final charge transfer inference equation.

Radio sounding technology is commonly used by weather services and provides the height of different atmospheric isotherms. The height of the isotherms change and therefore, the date and time of the stroke being examined is used to extract the correct height information from the radio sounding data. In this study, the radio sounding data provided by SAWS, is updated every twelve hours.

The height of the $-10\ ^{\circ}C$ isotherm is not always explicitly given. Rakov and Uman concluded that the majority of lightning exists within the troposphere [5]. In this region, temperature linearly varies with height [36]. By applying this linearity theory, the $-10\ ^{\circ}C$ level is estimated by determining the linear relationship between temperature and height for each specific radio sounding dataset.

TABLE 4.1: An extract from the full radio sounding dataset for the hours of 24h00 - 12h00 on June 1 2018.

Height (m)	**Temperature** $(^{\circ}C)$
4572	-2.2
5182	-6.5
5830	-11.1
6401	-15.2
7010	-19.6

Table 4.1 shows an extracted sample from the full dataset of radio sounding data for the morning of June 1 2018. The temperature levels ($T_{\circ C}$) and the corresponding heights above the ground (H_m)are provided in this dataset.

$$H_m = -140.12(T_{\circ C}) + 4268.89 \tag{4.5}$$

Using Table 4.1 as an example, a straight line of best fit is determined using Equation 4.5. The $-10\ ^{\circ}C$ isotherm is therefore calculated to be at a height of $Height = 5670$.

4.6 Inference of charge transfer

For the charge transfer inference model to be applied on a lightning stroke and the total charge transferred during the continuing current phase to be calculated,

the following requirements must be met:

- Stroke must be recorded by both the flat-plate antenna system and the high-speed cameras
- Continuing current duration must be known
- Height of $-10\ ^{\circ}C$ isotherm must be known
- Distance between the flat-plate antenna and the ground strike-point of the stroke must be known

Once all of these requirements are met and the electronic decay compensation algorithm is applied on the digitised changing electric field file, the charge transfer inference model is applied. The result is the quantity of charge transferred during the continuing current phase of a lightning stroke is computed.

4.7 Charge transfer computation algorithm

Table 4.2 shows a high-level representation of the algorithms used in implementing the charge transfer inference process. The code used for this implementation is presented in Appendix B. With reference to Table 4.2, lines 1-5 are variable declarations, lines 7-14 show the offset correction algorithm, line 16 shows how the compensation transfer function vector is populated and lines 18-22 describe the implementation of the decay compensation algorithm. Lines 24-41 show the implementation of the charge transfer inference model and generate a final quantity of charge transferred in the continuing current phase of the lightning stroke being processed.

TABLE 4.2: High-level code representation for the charge transfer inference algorithm.

	Offset correction, decay compensation and charge transfer inference algorithm	**Comments**
1:	$mag \leftarrow$ recorded magnitude vector of changing electric field samples	
2:	$CF \leftarrow 4.34 \cdot 10^{-3}$	*calibration factor*
3:	$BF \leftarrow 1.55$	*building enhancement factor*
4:	$\tau \leftarrow 0.47 \cdot 10^{-3}$	*integrator decay time constant (s)*
5:	$magnitudeWithOffset \leftarrow mag \cdot \frac{CF}{BF}$	*actual magnitude vector of changing electric field*
6:		
7:	$magnitudeWithOffset \leftarrow$ normalised magnitude vector of changing electric field samples	
8:	$start \leftarrow 0.01 \cdot length(magnitudeWithOffset)$	*beginning index of* 0.1 *s sample range*
9:	$finish \leftarrow 0.11 \cdot length(magnitudeWithOffset)$	*end index of* 0.1 *s sample range*
10:	$OCsampleLength \leftarrow$ length(magnitudeWithOffset(start:finish))	*quantity of samples in* 0.1 *s range*
11:	$sortedSamples \leftarrow$ sort(magnitudeWithOffset(start:finish))	*sort the samples in ascending order*
12:	$filtered \leftarrow$ sortedSamples($0.2 \cdot OCsampleLength$:$0.8 \cdot OCsampleLength$)	*discard the top and bottom* 20 % *of sortedSamples*
13:	$meanOffset \leftarrow$ mean(filtered)	*mean value of the remaining samples post-filtering*
14:	$magnitudeCorrected \leftarrow magnitudeWithOffset$ - $meanOffset$	*subtract offset value from all samples*
15:		
16:	$compensationVector \leftarrow -CF \cdot dirac(t) - (\frac{1}{\tau \cdot CF}) \cdot heaviside(t)$	*time-domain compensation vector*
17:		
18:	$magnitudeCorrected_{FD} \leftarrow \mathscr{F}\{magnitudeCorrected\}$	*FT of offset-corrected magnitude vector*
19:	$compensationVector_{FD} \leftarrow \mathscr{F}\{magnitudeCorrected\}$	*FT of compensation vector*
20:	$compensatedOutput_{FD} \leftarrow magnitudeCorrected_{FD} \cdot compensationVector_{FD}$	*frequency-domain output with offset compensation*
21:	$\mathscr{F}^{-1}\{compensatedOutput_{FD}\} \leftarrow compensatedOutput_{TD}$	*time-domain output with offset compensation*
22:	compensatedWave $\leftarrow compensatedOutput_{TD}$	*renaming resultant compensated waveform*
23:		
24:	d $\leftarrow \ldots$	*distance from ground strike-point to sensor (m)*
25:	h $\leftarrow \ldots$	*height of charge centre above ground (m)*
26:	$\epsilon_0 \leftarrow 8.85 \cdot 10^{-12}$	*permittivity of free space (F/m)*
27:	$CC_{start} \leftarrow 0.x \cdot length(compensatedWave)$	*sample index corresponding to the start time of CC*
28:	$CC_{end} \leftarrow 0.y \cdot length(compensatedWave)$	*sample index corresponding to the end time of CC*
29:	$compensatedCC \leftarrow$ compensatedWave($CC_{start} : CC_{end}$)	*isolates segment of continuing current*
30:		
31:	FOR i $\leftarrow 1 : length(compensatedCC) - 1$	
32:	$\Delta E \leftarrow$ compensatedCC(i+1) - compensatedCC(i)	*populate vector corresponding to delta in consecutive*
33:	END FOR	*compensatedCC samples*
34:		
35:	*FOR* $i \leftarrow 0 : length(\Delta E)$	
36:	*IF* $\Delta E(x) > 0$	< 0 *for positive strokes*
37:	$\Delta E(x) = 0$	*Don't include positive* ΔE *values*
38:	END IF	
39:	END FOR	
40:	$\Delta Q \leftarrow -\Delta E \frac{2\pi\epsilon_0(h^2+d^2)^{\frac{3}{2}}}{h}$	
41:	$chargeTotal \leftarrow sum(\Delta Q)$	*total quantity of charge transferred*

The digitised changing electric field file is imported and stored in a column vector. This is scaled in line 5 of Table 4.2 so it is representative of the physical magnitudes of the change in the electric field. In order to determine the zero-bias offset, a 0.1 s sample range is taken from an ambient segment of the file before a lightning stroke. Line 8 and 9 shows how this range is isolated. This sample is then filtered and the mean value is determined. This mean value is then subtracted from all the sample values that constitute the changing electric field file. This step is executed in line 14 and the result is a changing electric field waveform with offset compensation.

In line 16 in Table 4.2, a vector is populated with the compensation impulse response that was discussed earlier in this chapter. This vector, along with the offset-corrected changing electric field vector, is then taken into the frequency domain using a fourier transform in lines 18 and 19. The frequency domain multiplication of these two vectors is performed in line 20 and the result is then transformed back into the time domain in line 21. The result of this is the decay-compensated electric field waveform.

The calculated distance and height parameters for the lightning stroke of interest are manually inserted in lines 24 and 25. Line 27 and 28 is where the start and end boundaries of the continuing current phase are defined. The sample set containing the continuing current data is then isolated in line 29. The for-loop in lines 31-33 populates a vector containing the change (delta) between samples in the isolated continuing current data set. If the lightning stroke of interest is negative in polarity, only negative changes in the electric field are included in the calculation. The opposite applies for positive lightning strokes. Lines 35-39 contain the algorithm that implements this.

The charge transfer inference model is applied in line 40 in Table 4.2. This step populates a vector of individual changes in charge (transferred charge) that correspond to each electric field delta sample. To generate the total charge transferred during the continuing current phase of the lightning stroke being examined, the individual changes in charge are summed together. This final summation is presented in line 41.

4.8 Summary

The methodology followed in the charge transfer inference process was presented in this chapter. The electric field measurements were normalised due to calibration and building enhancement factors. The resultant normalised output is then corrected for offset biases and convolved with a compensation function derived by Kohlmann, et al. [14]. Using this compensated waveform, the model presented by Jacobson and Krider [3] can be applied, along with charge height and ground strike-point distance parameters, to infer the quantity of charge transferred during the continuing current phase of a lightning stroke.

The following chapter presents a summary of the data recorded during this study and the overall charge transfer results. A discussion on the interpretation of the results is included.

CHAPTER 5

Results and discussion

This chapter presents the final charge transfer results obtained from this study. The results are compared to previously conducted studies in Brazil, USA and Austria. The results from this study fall within the range of charge transfer quantities found in the aforementioned studies.

The final results generated by this study are attained by applying the methodology presented in Chapter 4. This charge transfer inference process requires different parameters for each lightning stroke that is studied. The duration of the continuing current limits the range of samples used when applying the model. The height of the $-10\ ^{\circ}C$ isotherm is important as it provides a parameter in the model that represents the height of the charge centre above the ground. A distance parameter is also required in the model and represents the distance between the flat-plate antenna and the ground strike-point of the lightning stroke.

5.1 Summary of records

Table 5.1 provides a summary of the filtered data that represents the completed set for charge transfer inference analysis. All strokes included in the summary table were recorded by both the flat-plate antenna measurement system and the high-speed cameras. The ground strike-point distances all fell within the $5-45\ km$ distance range from the antenna. All the presented data was collected over the period between February 2017 and November 2018.

TABLE 5.1: The filtered data used in the charge transfer inference process.

Quantity		**value**
Flashes	Negative	33
	Positive	5
Strokes	Negative	51
	Positive	5
Continuing current duration	Long ($t > 40\ ms$)	34
	Short ($10 < t < 40\ ms$)	14
	Very short ($3 < t < 10\ ms$)	3
Distance (km)	Minimum	5.2
	Maximum	25.4
	Mean	12.3
Height of $-10\ ^{\circ}C$ isotherm (m)	Minimum	5530
	Maximum	6650
	Mean	6225

As seen from the data provided in Table 5.1, 51 negative strokes were recorded that satisfy the $5-45\ km$ distance constraint. Of these 51 strokes, 34 of them had a continuing current duration of greater than 40 ms, 14 of them had a continuing current duration between 10 ms and 40 ms and 3 of them had a continuing current duration between 3 ms and 10 ms. All 5 recorded positive strokes that satisfy the distance criteria had a continuing current duration greater than 40 ms. From all 56 positive and negative strokes, the mean distance from the ground strike point to the flat plate antenna was 12.3 km and the mean height of the $-10\ ^{\circ}C$ isotherm was 6225 m.

5.2 Charge transfer results

The data provided in Table 5.2 represents the final charge transfer results obtained from this study. The total quantities of charge transferred from the 51 negative strokes and 5 positive strokes, detailed in the summary of records above, are given. The results from negative strokes are segmented into three categories with reference to the continuing current duration: long ($t > 40\ ms$), short ($10 < t < 40\ ms$) and very short ($3 < t < 10\ ms$). All 5 positive strokes had continuing current durations of longer than 40 ms. Maximum, minimum and mean statistics on continuing current duration, ground strike-point distance, $-10\ ^{\circ}C$ isotherm heights and charge transfer are provided for each partitioned data set. The number of strokes recorded for each column in the table are listed in the first row.

The continuing current durations, detailed in the second row of Table 5.2, range from 4.0 ms to 926 ms for the 51 recorded negative strokes. The 34 recorded negative strokes with long continuing current have an average duration of 190.7 ms, the 14 negative strokes with short continuing current have an average duration of 21.1 ms and the 3 with very short continuing current have an average duration of 6.7 ms. The continuing current durations of the 5 recorded positive strokes range from 43 ms to 564 ms with an average of 253 ms.

The third row of Table 5.2, details the maximum, minimum and mean quantities of the distances between the ground strike-point and the flat-plate antenna of all recorded strokes. This parameter is used in the charge transfer inference model and is necessary in determining charge transfer quantities. For the 51 negative strokes, the distance ranges from 5.2 km to 25.4 km with mean distances of 13.1 km for the 34 strokes with long CC, 11.4 km for the 14 strokes with short CC and 10.0 km for the 3 strokes with very short CC. For the 5 recorded positive strokes, the distances range from 5.3 km to 15.0 km, with a mean distance of 10.7 km. As shown, all recorded strokes conform to the primary distance constraint range of $5 - 45\ km$.

TABLE 5.2: The final summarised results of the charge transfer inference process.

	Negative CG strokes			**Positive CG strokes**
	Long CC ($t > 40\ ms$)	Short ($10 < t < 40\ ms$)	Very short ($3 < t < 10\ ms$)	Long CC ($t > 40\ ms$)
Samples	34	14	3	5
Continuing current duration (ms)				
Minimum	41.0	12.0	4.0	43
Maximum	926.0	36.0	8.0	564
Mean	190.7	21.1	6.7	253
Distance (km)				
Minimum	5.2	5.7	8.0	5.3
Maximum	25.4	17.4	13.8	15.0
Mean	13.1	11.4	10.0	10.7
Height of $-10\ ^{\circ}C$ isotherm (m) (+ 3000 m for positive charge centre height)				
Minimum	5530	5850	5850	8865
Maximum	6650	6650	6650	9450
Mean	6205	6314	6133	9160
Charge transferred (C)				
Minimum	0.3	0.1	0.1	3.7
Maximum	145.5	3.0	0.3	66.6
Mean	18.3	0.7	0.2	-

The maximum, minimum and mean $-10\ ^{\circ}C$ isotherm heights are shown in row 4 in Table 5.2. This provides the height parameter required in the charge transfer inference model and physically represents the height at which the negative charge centre sits in the cloud. The height parameter used when the model is applied on positive strokes is taken as 3000 m above the $-10\ ^{\circ}C$ isotherm. For the 51 negative strokes, the height of the $-10\ ^{\circ}C$ isotherm ranges from 5530 m to 6650 m above the ground. For the 5 positive strokes, the height of the positive charge centre ranges from 8865 m to 9450 m.

Shown in the bottom row of Table 5.2 are the final calculated charge transfer quantities. For the negative polarity, 34 strokes with long continuing current were calculated to transfer an average of 18.3 C with a maximum transfer of 145.5 C and a minimum of 0.3 C. The 14 strokes with short continuing current transferred an average of 0.7 C and the 3 strokes with very short continuing current had an average charge transfer of 0.2 C. From the 5 positive strokes, the maximum charge transferred was 66.6 C and the minimum was 3.7 C. With only 5 positive strokes in the data set, the mean charge transfer is statistically insignificant and therefore, omitted from the results in Table 5.2.

5.3 Comparison of findings with similar studies

Figure 5.1 illustrates the summarised results from the charge transfer quantities for negative lightning strokes. This provides a comparison between the results obtained in this study to those obtained in studies conducted in Brazil, Austria and the USA by Schumann, et al. [15]. The data set consists of 59 samples from Brazil, 70 from Austria, 36 from the USA and 34 from this study. All of these studies make use of flat-plate antennas and high-speed cameras and perform charge transfer inference using the same methodology detailed in Chapter 4. All lightning strokes used in the aformentioned studies, including this study, consist of continuing current durations greater than 40 ms and apply the $5-45$ km distance constraint.

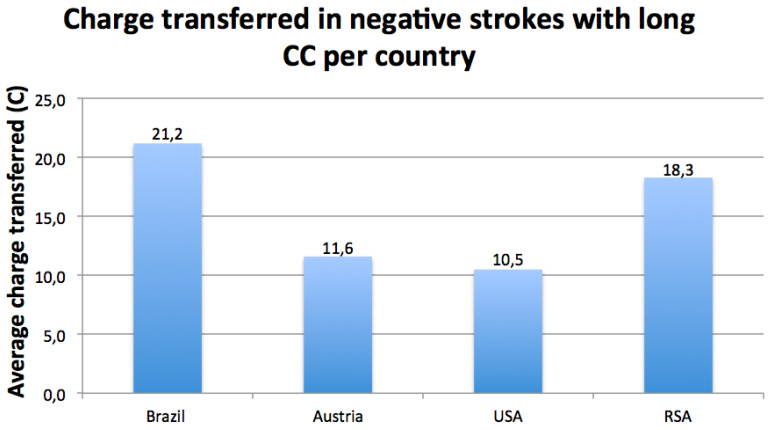

FIGURE 5.1: Average charge transfer in negative lightning strokes from this study and studies conducted in Brazil, Austria and the USA.

Figure 5.1 shows that the average charge transferred in negative lightning strokes from measurements taken in Brazil, Austria and the USA is 21.2 C, 11.6 C and 10.5 C, respectively. The results from this study, performed in South Africa (RSA), show an average charge transfer of 18.3 C. The results from Austria and the USA are similar, however, the South Africa shows significantly larger magnitudes of charge transfer. The quantities from Brazil are slightly larger than those from RSA and approximately twice the quantity of charge transferred in negative strokes as compared with Austria and the USA.

Table 5.3 shows the fully detailed comparison between this study and those conducted in Brazil, Austria and the USA. The primary limiting factor on the number of samples from which charge transfer can be inferred is the $5-45\ km$ constraint. As discussed by Schumann, et al. [15], the reason this $5-45\ km$ ground strike-point distance constraint is implemented is to minimise errors in final charge transfer results. It was explained that any error in the $-10\ ^{\circ}C$ isotherm height parameter, which is already fundamentally a coarse measurement, will result in significant charge quantity errors for ground strike-point distances less than $5\ km$ and greater than $45\ km$. This is an underlying characteristic of the model used in this study. By applying the ground strike-point distance constraint, errors are not eradicated however, they are minimised to a degree that has been accepted in the consulted literature [3, 7, 15].

Also shown in Table 5.3, the continuing current durations for the data set of negative strokes from Brazil, Austria, USA and this study (RSA) are all greater than $40\ ms$ and have mean values of $185.1\ ms$, $133.0\ ms$, $197.1\ ms$ and $190.7\ ms$, respectively. The mean heights of the $-10\ ^{\circ}C$ isotherm are $6501\ m$, $5702\ m$, $5848\ m$ and $6205\ m$, respectively. The mean charge transfers are $21.2\ C$, $11.6\ C$, $10.5\ C$ and $18.3\ C$, respectively. It is concluded that the charge transfer results obtained in this study are consistent with the results from the three other studies.

There is a clear discrepancy in the charge transfer values between the two countries in the northern hemisphere (USA and Austria) and the two countries in the southern hemisphere (South Africa and Brazil). From these results, lightning strokes recorded in countries in the southern hemisphere transfer considerably more charge than strokes recorded from countries in the northern hemisphere. Although these observations could be attributed to the specific atmospheric conditions of each location, there is the possibility that hemespheric geography is influential on charge transfer quantities. The average air temperature in the northern hemisphere is approximately $1-2\ ^{\circ}C$ warmer than the southern hemisphere [37]. This temperature difference could be a contributing factor to the difference in charge transfer quantities during lightning events. It is documented that approximately 87.5 % of the total human population lives in the northern hemisphere [38]. This population

density likely contributes to a higher average pollution level, which too could affect the charge transfer quantities in lightning flashes.

As seen in Table 5.3, the data set of positive strokes consists of 20 samples from Brazil, 35 from Austria, 45 from the USA and 5 from this study (RSA). In comparison to the number of samples from Brazil, Austria and the USA, the mean charge transfer obtained in this study is statistically insignificant. However, looking at the range of charge transfer quantities, a comparison can be drawn. The ranges from the studies conducted in Brazil, Austria and the USA are $2.5-1329\ C$, $2.9-434\ C$ and $1.7-358\ C$, respectively. From the 5 positive samples in this study, the quantity of charge transferred ranges from $3.7\ C$ to $66.6\ C$. It is deduced that, even though the mean charge transfer values from this study are essentially not comparable to the other studies, the range is congruous.

TABLE 5.3: Results of this study (RSA) compared to similar studies conducted in Brazil, Austria and the United States [15].

	Negative CG strokes (long CC)				**Positive CG strokes (long CC)**			
	Brazil	Austria	USA	RSA	Brazil	Austria	USA	RSA
Number of case samples	59	70	36	34	20	35	45	5
Continuing current duration (ms)								
Minimum	42.0	40.0	41.0	**41.0**	40.0	40.0	43.0	**43.0**
Maximum	570.0	580.0	527.0	**926.0**	800.0	355.0	689.0	**564.0**
Mean	185.1	133.0	197.1	**190.7**	262.0	124.0	290.6	**253.0**
Distance (km)								
Minimum	5.0	5.5	5.0	**5.2**	6.9	6.5	9.8	**5.3**
Maximum	35.0	34.1	35.4	**25.4**	44.1	32.8	35.5	**15.0**
Height of $-10\ ^{\circ}C$ isotherm (m) (+ 3000 m for positive charge centre height)								
Minimum	6120	4564	5182	**5530**	8683	7970	8182	**8865**
Maximum	7043	5906	6809	**6650**	9896	9115	9618	**9450**
Mean	6501	5702	5848	**6205**	9266	8818	8683	**9160**
Charge transferred (C)								
Minimum	0.6	0.4	0.2	**0.3**	2.5	2.9	1.7	**3.7**
Maximum	127	115	46	**145.5**	1329	434	358	**66.6**
Mean	21.2	11.6	10.5	**18.3**	255.4	50.1	74.9	**-**

5.4 Summary

From this study, it was determined that the quantity of charge transferred from 34 negative lightning strokes with long continuing current (i.e. $t > 40\ ms$) ranges from 0.3 C to 145.5 C and has an mean value of 18.3 C. For positive strokes, the relatively small sample size rendered the mean quantity insignificant, however, the results range from 3.7 C to 66.6 C. Both the mean charge transfer in negative strokes and the range of charge transferred in positive strokes are congruous with similar studies conducted in Brazil, Austria and the USA. The mean charge transfer values of negative strokes attained from this study are approximately 60 % greater than values calculated in Austria and the USA and are approximately 15 % less than the negative charge transfer quantities calculated in Brazil.

Errors in the final result are minimised to an acceptable level by implementing the ground strike-point distance constraint of only applying the charge transfer inference model on flashes with ground strike-points in the $5 - 45\ km$ range away from the sensor.

CHAPTER 6

Conclusion and future work

A flat-plate antenna with an integrator and amplifier is used to measure the changing vertical electric field and infer the charge transferred during the continuing current phase of lightning flashes over an area in Johannesburg, South Africa. High-speed video cameras are used to record the same lightning flashes measured by the antenna to determine the time-stamps and hence, duration of the continuing current. The integrator subsystem introduces an electronic decay into the changing electric field signal. This decay is compensated for in software and a reconstruction of the physical vertical electric field profile is produced. Along with data representing distances from ground strike-points to the antenna and heights of the charge centres in the cloud, this waveform is used to infer the quantity of charge transferred during the continuing current phase of a lightning stroke.

The study presented in this dissertation makes use of an electromagnetic charge transfer inference model developed by Jacobson and Krider [3]. The methodology used to record the lightning strokes, apply the changing electric field compensation algorithm and ultimately infer the quantity of charge transfer is discussed in detail. Using a database of lightning flashes recorded in the period of time between February 2017 and November 2018, this model is applied and charge transfer quantities are determined. For long continuing current (i.e. with durations lasting longer than 40 ms), the charge transferred from 34 negative strokes range from 0.3 C to 145.5 C and have a mean quantity of 18.3 C. From 5 positive strokes, the charge transfer quantity ranges from 3.7 C to 66.6 C. These values are concluded to be congruous with studies conducted in Brazil, Austria and the USA that use the same equipment and the same charge transfer inference model as this study.

In order to ensure the most accurate charge transfer results, flashes that occurred outside a $5 - 45\ km$ range were excluded from the study.

6.1 Future work

The charge transfer results determined in this study contribute to the greater body of knowledge in the field of lightning research. On top of this and in a more general sense, charge transfer quantities can be useful in a variety of industries. For example, from an actuarial standpoint, charge transfer quantities can be used to develop more accurate models to determine insurance premiums, improve surge protective equipment or assist in general lightning protection design.

Based on the results of this study, it has been decided that a second antenna will be placed at a location, approximately 40 km away from the current antenna set-up. With both of these antennas set-up at different distances, different components of the propagated electromagnetic field can be analysed for the same flash. Charge inference can also be performed using both antennas, if the flash is within the constrained distance range for both, which will provide an extra level of accuracy with regards to the final results obtained. The intention is to extend the work in this paper by adding samples to the current dataset, which will provide results that may be more comparable to the aforementioned studies performed in Brazil, Austria and the USA.

References

[1] M. G. Ballarotti, M. M. F. Saba, and O. P. Jr. "High-speed camera observations of negative ground flashes on a millisecond-scale." *Geophysical Research Letters*, vol. 32, December 2005.

[2] T. A. Warner, K. L. Cummins, and R. E. Orville. "Upward lightning observations from towers in Rapid City, South Dakota and comparison with National Lightning Detection Network data, 2004-2010." *Journal of Geophysical Research*, vol. 117, no. D19109, 2012.

[3] E. A. Jacobsen and E. P. Krider. "Electrostatic Field Changes Produced by Florida Lightning." *Journal of the atmospheric sciences*, vol. 33, pp. 103–117, January 1976.

[4] V. Cooray. *An Introduction to Lightning*. Springer Netherlands, 1st ed., 2015.

[5] V. A. Rakov and M. A. Uman. *Lightning Physics and Effects*. Cambridge University Press, 1st ed., 2003.

[6] C. Schumann, H. G. P. Hunt, J. Tasman, H. Fensham, K. J. Nixon, T. A. Warner, and M. M. F. Saba. "High-speed video observation of lightning flashes over Johannesburg, South Africa 2017-2018." *34th International Conference on Lightning Protection (ICLP)*, September 2018.

[7] C. Schumann and M. M. F. Saba. "Continuing Current Intensity in Positive Ground Flashes." *International Conference on Lightning Protection (ICLP)*, September 2012.

[8] H. Pichler, G. Diendorfer, and M. Mair. "Some Parameters of Correlated Current and Radiated Field Pulses from Lightning to the Gaisberg Tower."

IEEJ Transactions on Electrical and Electronic Engineering, vol. 5, pp. 8–13, 2010.

[9] G. Diendorfer, W. Schulz, and M. Mair. "Evaluation of a LLS based on lightning strikes to an instrumented tower." *International Lightning Detection Conference (ILDC), Tucson, Arizona*, 2000.

[10] G. Diendorfer, W. Schulz, and C. Scherney. "Area of increased lightning flash density on mountain tops." *Lightning and Mountains, Charmonix, France*, June 1997.

[11] A. Smorgonsky, F. Rachidi, M. Rubinstein, G. Diendorfer, and W. Schulz. "On the Proportion of Upward Flashes to Lightning Research Towers." *7th Asia-Pacific International Conference on Lightning, Chengdu, China*, pp. 858–862, November 2011.

[12] E. P. Krider, R. C. Noggle, and M. A. Uman. "A Gated, Wideband Magnetic Direction Finder for Lightning Return Strokes." *Journal of Applied Meteorology*, vol. 15, no. 3, pp. 301–306, March 1976.

[13] H. G. P. Hunt, Y. C. Liu, and K. J. Nixon. "Evaluation of the South African Lightning Detection Network using Photographed Tall Tower Lightning Events from 2009 - 2013." *International Conference on Lightning Protection (ICLP), Shanghai, China*, pp. 1746–1751, 2014.

[14] H. Kohlmann, W. Schulz, and H. Pichler. "Compensation of integrator time constants for electric field measurements." *Electric Power Systems Research*, vol. 153, pp. 38–45, 2017.

[15] C. Schumann, M. M. F. Saba, A. R. de Paiva, H. Kohlmann, W. Schulz, G. Diendorfer, M. A. da Silva Ferro, T. A. Warner, and J. H. Jr. "Charge transfer in natural negative and positive downward flashes." *International Conference on Lightning Protection (ICLP), Estoril, Portugal*, September 2016.

[16] E. de C. Ferraz, M. M. F. Saba, and O. P. Jr. "First measurements of continuing current intensity in Brazil." *International Symposium on Lightning Protection, Curitiba, Brazil*, November 2009.

[17] M. Brook, N. Kitagawa, and E. J. Workman. "Quantitative study of strokes and continuing currents in lightning discharges to ground." *Journal of Geophysical Research*, vol. 67, no. 2, pp. 649–659, February 1962.

[18] N. Kitagawa, M. Brook, and E. J. Workman. "Continuing currents in cloud-to-ground lightning discharges." *Journal of Geophysical Research*, vol. 67, no. 2, pp. 637–647, February 1962.

[19] M. M. F. Saba, C. Schumann, T. A. Warner, J. H. H. Jr., W. Schulz, and R. E. Orville. "Bipolar cloud-to-ground lightning flash observations." *Journal of Geophysical Research: Atmospheres*, vol. 118, pp. 11098–11106, October 2013.

[20] T. Gill. "A lightning climatology of South Africa for the first two years of operation of the South African Lightning Detection Network: 2006-2007." *2nd International Lightning Meteorology Conference, Tucson, Arizona, USA*, pp. 1–12, 2008.

[21] M. Rubinstein, J. Bermudez, V. Rakov, F. Rachidi, and A. Hussein. "Compensation of the Instrumental Decay in Measured Lightning Electric Field Waveforms." *IEEE Transactions on Electromagnetic Compatibility*, vol. 54, no. 3, pp. 685–688, June 2012.

[22] H. Kohlmann, W. Schulz, and H. Pichler. "Compensation of Integrator Time Constants for Electric Field Measurements." *International Symposium on Lightning Protection, Balneario Camboriu, Brazil*, October 2015.

[23] E. de C. Ferraz. "Measuring of Continuing Currents in Natural Negative Cloud-to-Ground Lightning on Brasil: Development of Equipment and First Results." *PhD Thesis, INPE*, 2009.

[24] C. T. R. Wilson. "Investigations on Lightning Discharges and on the Electric Field of Thunderstorms." *Philosophical Transactions of the Royal Society of London*, vol. 221, pp. 73–115, 1920.

[25] T. W. Wormell. "The effects of thunderstorms and lightning discharges on the earth's electric field." *Philosophical Transactions of the Royal Society of London*, vol. 238, pp. 249–303, 1939.

[26] E. T. Pierce. "Electrostatic field-changes due to lightning discharges." *Quarterly Journal of the Royal Meteorological Society*, vol. 81, pp. 211–228, 1955.

[27] E. R. Williams. "The tripole structure of thunderstorms." *Journal of Geophysical Research: Atmospheres*, vol. 94, pp. 13151 – 13167, September 1989.

[28] R. Zandbergen and J. M. Dow. "Sounding the Atmosphere Ground Support for GNSS Radio-Occultation Processing." *ESA bulletin 126*, pp. 48–53, May 2006.

[29] Y. H. Kuo, W. S. Schreiner, J. Wang, and D. L. Rossiter. "Comparison of GPS radio occultation soundings with radiosondes." *Geophysical Research Letters*, vol. 32, no. 5, March 2005.

[30] J. Wickert, C. Reigber, G. Beyerle, and R. Konig. "Atmosphere sounding by GPS radio occultation: First results from CHAMP." *Goephysical Research Letters*, vol. 28, no. 17, September 2001.

[31] L. Lin, X. Zou, R. Anthes, and Y.-H. Kuo. "COSMIC GPS radio occultation temperature profiles in clouds." *Monthly Weather Review*, vol. 147, no. 2, February 2019.

[32] V. Kan, M. E. Gorbunov, and V. F. Sofieva. "Fluctuations of radio occultation signals in sounding the Earth's atmosphere." *Atmospheric Measurement Techniques*, vol. 11, pp. 663–680, February 2018.

[33] R. A. Anthes. "Exploring Earth's atmosphere with radio occultation: contributions to weather, climate and space weather." *Atmospherics Measurement Techniques*, vol. 4, pp. 1077–1103, June 2011.

[34] M. Gijben. "The lightning climatology of South Africa." *South African Journal of Science*, vol. 108, no. 3-4, March 2012.

[35] H. Mahmoud and N. Akkari. "Shortest Path Calculation: A Comparative Study for Location-Based Recommender System." *2016 World Symposium on Computer Applications Research*, March 2016.

[36] C. Braak. "The vertical temperature distribution in the atmosphere." *International Journal of Science*, vol. 93, March 1914.

[37] G. Feulner, S. Rahmstorf, A. Levermann, and S. Volkwardt. "On the Origin of the Surface Air Temperature Difference between the Hemispheres in Earth?s Present-Day Climate." *Journal of Climate*, vol. 26, March 2013.

[38] M. Kummu and A. Varis. "The world by latitudes: A global analysis of human population, development level and environment across the north-south axis over the past half century." *Applied Geography*, vol. 31, pp. 495–507, 2010.

Appendix A

Antenna calibration

A.1 Content discussion

The following two subsections provide the measurement methodology and results obtained in quantifying the enhancement effect that the building, on which the antenna used in this study (I_{wits}), is placed. In order to determine the enhancement factor, a second integrator $I_{calibration}$ was used. From placing $I_{calibration}$ and I_{wits} next to each other during a thunderstorm, a relative amplification factor α between the two integrators was observed. After the determination of α, $I_{calibration}$ was placed at the closest point to I_{Wits} that was not affected by significant electric field enhancements. Further measurements were then taken. Using these measurements, while taking into account α, the building enhancement factor was calculated to be $BF = 1.55$.

A.2 Relative antenna gain

An initial calibration process was performed for both integrators. The integrator gains were determined by exposing the sensor plate on the antenna to a known electric field and measuring the output. Furthermore, the frequency response of each integrator was used to quantify the measurement bandwidths.

$$\alpha I_{wits} = I_{calibration} \tag{A.1}$$

For data retrieved from both antenna set-ups to be comparable, a purely scalar amplification factor, α, was determined experimentally for Equation A.1 to hold true. With the physical geometry of both antennas being identical, the α factor disparity between the two integrators is attributed to a difference in signal gain. The methodology followed for this calibration process is listed below.

- Ensure both antennas are set-up identically, use the same digitiser and are time-synced.
- During a thunderstorm, record the continuous measurements of both integrators.
- Compare the peak digitised voltage reading, for each channel, that corresponds to the peak electric field change during a return stroke.
- Calculate errors and determine the mean of recorded α factors.

A total of 19 lightning strokes were measured by both antennas and integrators. An α factor was calculated for each lightning stroke sample. The mean α factor was determined to be $\alpha = 1.04$. The scatter plot in Figure A.1 represents the calculated α factors.

As seen in Equation A.2, a relationship between I_{wits} and $I_{calibration}$ is derived from the average of the above samples.

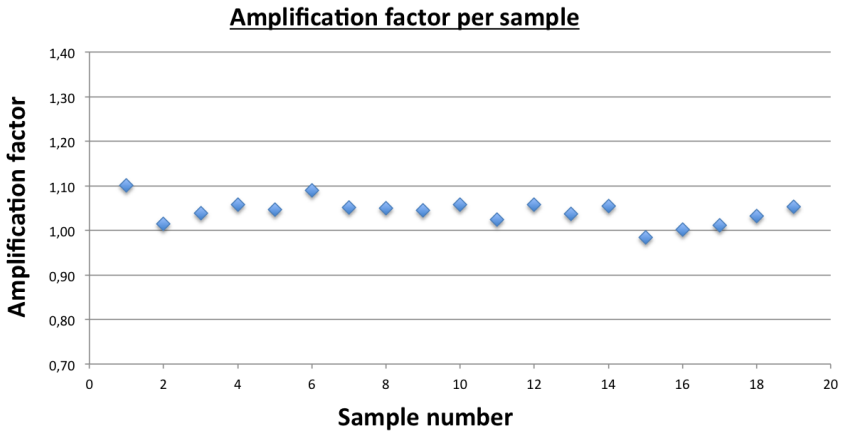

FIGURE A.1: Scatter plot of the I_{wits} and $I_{calibration}$ amplification factor, α

$$1.04 * I_{wits} = I_{calibration} \tag{A.2}$$

A.3 Overall building enhancement factor

As depicted in Figure A.2, the electric field measured by the antenna with I_{wits} on top of the building will be enhanced due to the steeper voltage gradient. The concept of electric field enhancement is commonly quantified when a measurement system is placed on a structure that is elevated above the surrounding area, such as an antenna placed on a building or tower. Schumann, et al. [15] provides enhancement correction factors for all the relevant locations included in the studies presented by the authors.

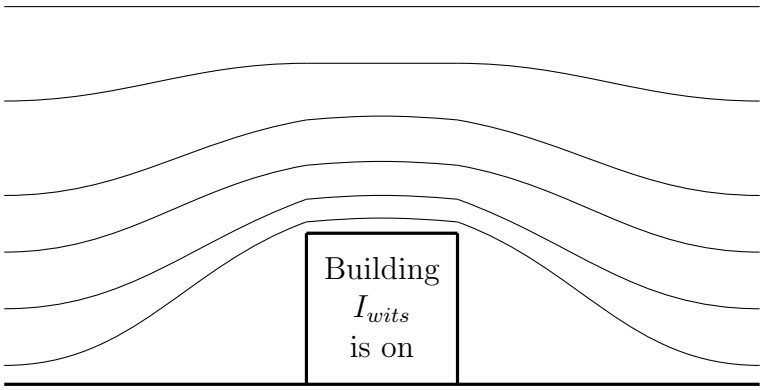

FIGURE A.2: The enhancement effect of a building on equipotential field lines

$$\alpha I_{wits} = BF * I_{calibration} \tag{A.3}$$

With this factor, the measurements from I_{wits} can be directly compared to measurements taken on an empty, flat surface with no enhancements of the electric field. With α accounted for, a building enhancement factor BF was calculated using the following methodology. The mathematical relationship between α and BF is presented in Equation A.3.

- Antenna with I_{wits} is set-up on the roof. Set up antenna with $I_{calibration}$ in the closest, feasible area to the building with no nearby electric field enhancements.
- Ensure both integrators are time synced and their measurements digitised with identical sampling characteristics.
- During a thunderstorm, record the continuous measurements of both integrators.
- Compare the peak digitised voltage reading for each channel, accounting for α, that corresponds to the peak electric field change during a return stroke.
- Calculate errors and determine the arithmetic mean of all recorded BF factors.

Figure A.3 presents the building enhancement factors calculated for 40 different lightning stroke samples. The amplification factor of $\alpha = 1.04$ was taken into account before the enhancement factor was definitively calculated.

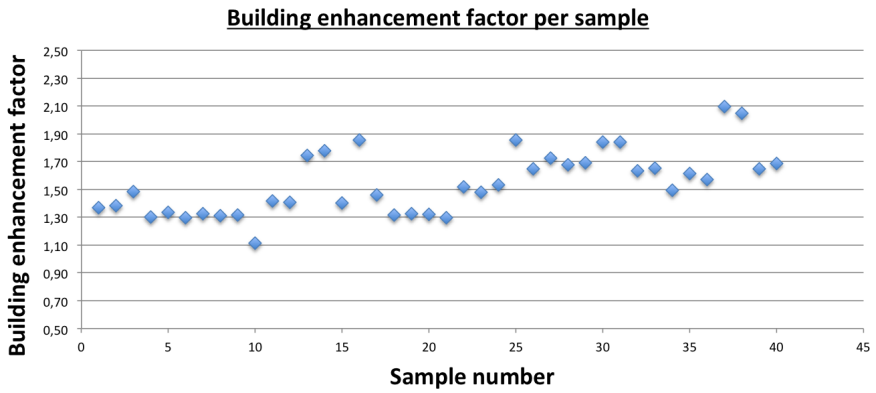

FIGURE A.3: Scatter plot of the building enhancement factor after taking the amplification factor α into account

The result was a building enhancement factor of $BF = 1.55$. Equation A.4, presented below, highlights the effect of the building enhancement. In this equation, I_{flat} would be the equivalent normalised changing electric field measurement with no enhancement present.

$$I_{wits} = 1.55 * I_{flat} \tag{A.4}$$

Appendix B

The complete code used in the charge inference process

B.1 Content description

The following appendix presents the code that was implemented to compute charge inference calculations on the recorded changing electric field measurements used in this study. Every line of code is commented for ease of understanding. Both the offset correction and decay compensation code is presented along with the charge inference calculation and all subsequent functions used within these main algorithms. A high-level representation of this code can be found in the main body of the dissertation.

The following pages include the algorithms for data normalisation and decay compensation, offset correction and charge transfer inference. This is followed by the vector population functions for the compensation transfer function and the delta of the compensated field measurements.

```
%Calibration factor
CF = 4.34*10^-3; %(Epsilon0*A/C2)

%Building enhancement factor
BF = 1.55;

%Electronic decay time constant
tau = 0.47*10^-3; %(C2R2)

%Measurement scaling
scale = 1;


%Efast with "REAL" magnitudes
offsetMag = mag./(CF.*BF.*scale);


%newMag is now the Efast with offset correction
newMag = offset(offsetMag);


%creating a linear time scale relative to the number of samples
newtime = linspace(1/length(newMag),1,length(newMag)+(1/length(newMag)));


%FUNCTION DEFINED IN populate.m - used to populate compensation vector
He = populate(newtime,CF,tau);



%Plots the measured Efast graph before normalisation (scaled and with CF)
plot(newtime,mag,'k');
hold on


%FFT, multiplication, IFFT
Fsample = length( newMag ); %Define sampling frequency
dt = 1/Fsample; %Define sampling period
Ly=length( newMag ) + length( He ) -1;
newMagFFT=dt.*fft( newMag, Ly);        % Fast Fourier transform
HeFFT=dt.*fft(He, Ly);             % Fast Fourier transform
compensatedOut_FD= newMagFFT.*HeFFT';
compensatedOut_TD=( Fsample.*( ifft(compensatedOut_FD, Ly) ) );
compensatedOut_TD=compensatedOut_TD(1:1:length(newtime)); % Take just the
    first length(newtime) elements


%Plot the compensated waveform with 'REAL' magnitudes
plot(newtime,(compensatedOut_TD), 'b');
```

```
%FUNCTION USED TO offset the Efast
function myOutput = offset(newmag)

%set start and end points of ambient noise in Efast file
start = round(  0.01*length(newmag)  );
finish = round(  0.06*length(newmag)  );

%determine the amount of datapoints in the sample
OC_SampleLength = length( newmag(start:finish) );

%Sorts the values of ambient noise in ascending order
sorted = sort( ( newmag(start:finish) ) );

%Filters out the top and bottom 20% of the sorted vector and takes the mean
y = mean(  sorted(  round(0.2.*OC_SampleLength) : round(0.8.*OC_SampleLength)
    ) );

%Output the normalised Efast that is now corrected for its offset error
myOutput = newmag - y;


end
```

```
%example Negative CG
d = 11.9 .*10^3; % distance to strike-point in meters
h = 6650; % charge center height in meters
epsilon = 8.85*10^-12; % permitivity of free space in Farads/meter

%Start of CC relative to index in compensated waveform vector
CCstart = round(0.665 .* length(compensatedOut_TD));

%End of CC relative to index in compensated waveform vector
CCend = round(0.920 .* length(compensatedOut_TD));

%Extract only the section of CC needed for analysis
compOutput = ((compensatedOut_TD(CCstart:CCend)));

%deltaHe takes the delta between each datapoint in the CC section
dE = deltaHe(compOutput);

% dE must be <0 for a negative stroke -> make positive values = 0
for k = 1:1:length(dE)
    if (dE(k) > 0)
        dE(k) = 0;
    end
end


%Charge inference equation
dQ = -dE.*((2*pi*epsilon*(h^2 + d^2)^(3/2))/h);

%Sum the charge deltas to get the total charge transferred
sumCharge = sum(dQ);
```

```
%FUNCTION USED TO POPULATE COMPENSATION VECTOR
function myOutput = populate(t,CF,tau)


   myOutput = - CF.*dirac(t) - (1./tau.*CF).*heaviside(t);


end
```

```
%FUNCTION USED TO OBTAIN deltaHe for charge inference equation
function myOutput = deltaHe(t)

for x=1:(length(t)-1)

    myOutput(x) = (t(x+1)-t(x));

end

end
```

Appendix C

Characterisation of lightning flashes from changing electric field measurements in Johannesburg, South Africa

C.1 Paper description

The following paper was published and presented at the 34th Internationcal Conference on Lightning Protection (ICLP) in September 2018 in Rzeszow, Poland. The primary measurement intrument used in this study is the same flat-plate antenna measurement system that has been detailed in the main body of this dissertation. The results from these changing electric field measurements were analysed and the rise times, durations and peak intensities of the waveforms are presented. A comparison of these results to similar studies conducted around the world is presented and conclusions are drawn.

34th International Conference on Lightning Protection
02-07 September 2018
Rzeszow, Poland

Characterisation of lightning flashes from changing electric field measurements in Johannesburg, South Africa

J. D. Tasman, C. Schumann,
H. G. P. Hunt , H. G. Fensham,
K. J. Nixon
School of Electrical and Information Engineering
University of the Witwatersrand
Johannesburg, South Africa
jesstasman@gmail.com

M. M. F. Saba
Atmospheric Electricity Group
Brazilian National Institute for Space Research
São José dos Campos, Brazil
marcelo.saba@inpe.br

T. A. Warner
ZT Research
Rapid City, South Dakota, USA
tom.warner@ztresearch.com

***Abstract*—Presented are results obtained from changing electric field measurements and high-speed video analysis on lightning flashes over Johannesburg, South Africa. A flat-plate antenna and integrator were used to record changing electric fields and the high-speed footage was recorded using Phantom v310 and v7.1 (15,000 fps and 5,000 fps respectively) cameras. A total of 34 negative strokes and 3 positive strokes were analysed. The recorded negative strokes presented an average peak intensity of 8.0 V/m, 0 - 100 % rise time of 3.3 µs, 10 - 90 % rise time of 1.8 µs and pulse duration of 6.4 µs. The positive strokes presented an average peak intensity of 36.7 V/m, 0 - 100 % rise time of 22.9 µs, 10 - 90 % rise time of 7.4 µs and pulse duration of 33.4 µs. The average continuing current durations, determined using high-speed videos, was 6.3 ms for the negative strokes and 81.5 ms for the positive strokes.**

Keywords—changing E-field; flat-plate antenna; high-speed video; rise time

I. INTRODUCTION

Previous studies have been performed using changing electric field (E-field) measurements to characterise and record data from cloud-to-ground (CG) lightning flashes. These include studies performed in Brazil, Austria, Malaysia and Florida (USA), among others [1-4]. The common parameters recorded from the changing electric field profiles measured in these studies include rise times, intensities and durations. These parameters correspond to the attachment of a leader and the magnitude and duration of the current impulse. If the strike-point is too close to the measurement device, the electronics could be driven into saturation and an accurate profile may not be obtainable. The ideal setup would have sensors installed at a range of distances. The presence of a near and far E-field measurement sensor ensures that all recorded strokes can be analysed.

High-speed videos and changing electric field measurements are two accurate ways in which lightning flashes can be characterised and analysed. From 10 February 2017 to 6 February 2018, both methods were applied in assessing lightning flashes that occurred in Johannesburg, South Africa. For the changing electric field data to be viewed, the E-field files were analysed using the Dataviewer 1.4 software.

A flat-plate antenna is set up to perform changing electric field measurements and is detailed in Section II. The high-speed video and changing E-field measurement studies are presented in Section III and IV. These sections include a detailed methodology on the extraction of the aforementioned parameters from the recorded measurements. Comparisons between previous studies and the results from this study are presented in Section V.

II. CHANGING ELECTRIC FIELD MEASUREMENTS

Measuring a change in the electric field between a thundercloud and the ground is a highly effective way of characterising lightning flashes. In this study, a flat-plate antenna was used to perform these changing electric field measurements. Using the assumption of an infinite ground plane, justified by Cooray [5], the flat-plate antenna measures a change in the vertical electric field by using a capacitive antenna. The output signal from the antenna is then integrated and amplified, which allows for a waveform to be resolved that is proportional to the time derivative of the measured electric field.

A flat-plate antenna and integrator system was installed at coordinates 26.19134° S, 28.02712° E, on the roof of a four-story building in Johannesburg, South Africa. The integrator has a decay time-constant of 0.47 s and operates at a bandwidth between 300 Hz and 1.5 MHz. The measurement system comprises of a 12-bit, 5 MS/s PCI N-6110 National Instruments digitiser, which allows for continuous recording. An external antenna and a Meinberg PCI-170GPS board is integrated into the system to ensure accurate time stamping of recordings. This allows for time correlation with other measurement equipment, such as high-speed cameras. The process that the changing E-field measurement equipment follows is presented in Fig. 1.

The flat-plate antenna set-up is shown in Fig. 2. A PV panel is utilised to ensure the battery used to power the integrator is always sufficiently charged.

978-1-5386-6635-7/18/$31.00 ©2018 IEEE

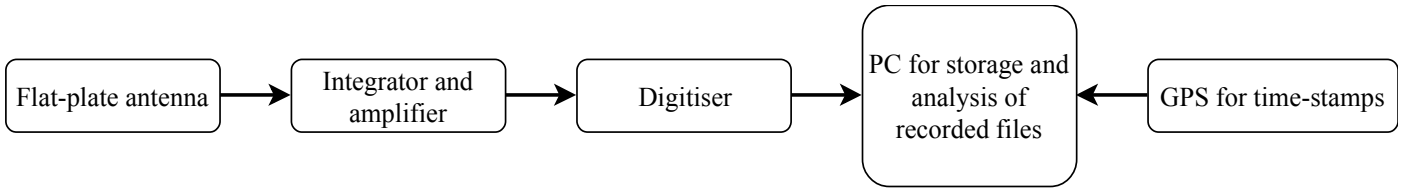

Fig. 1. High-level flow diagram of changing electric field measurement process

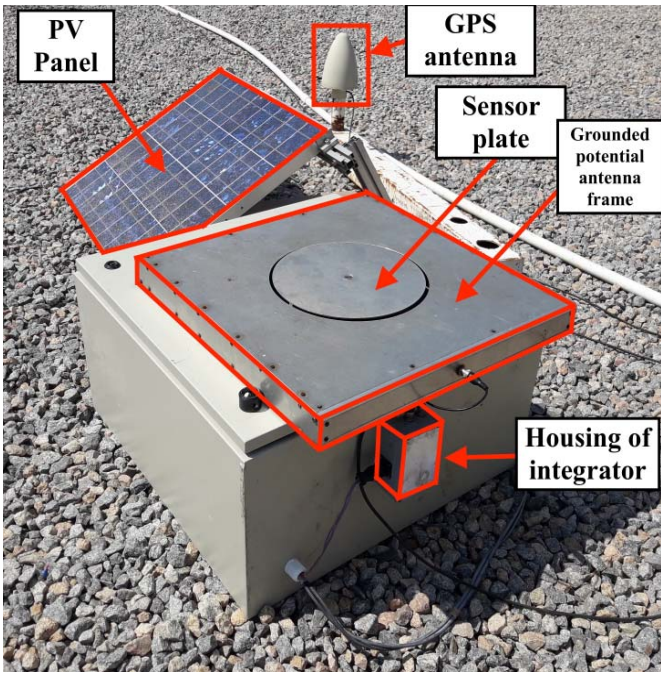

Fig. 2. Flat-plate antenna set-up

III. HIGH-SPEED VIDEO CAMERAS

The high-speed cameras used in this study are the Phantom v310 (15,000 fps, exposure time 58 µs) and the Phantom v7.1 (5,000 fps, exposure time 990 µs). The difference in frame rate and exposure time of each camera allows for the footage to be compared and ultimately, more accurate characterisation of lightning flashes.

The cameras are installed at coordinates 26.1614° S, 27.957° E. This is approximately 8 km Northwest of central Johannesburg. The field of view of the cameras relative to the Brixton and Hillbrow towers and the changing E-field measurement set-up is shown in Fig. 3.

IV. ANALYSIS

The following section presents an analysis of the changing electric field data. This includes a detailed methodology on the characterisation process of the recorded changing E-field data and the overall results. Previous studies were consulted to ensure the analysis procedure produced comparable results [6 – 8].

A. Data

The changing electric field data consists of lightning flashes occurring between 10 February 2017 and 6 February 2018. A sample waveform of a negative flash registered by the flat-plate antenna system is presented in Fig. 4. Peak intensity magnitudes, rise times (0 - 100 % and

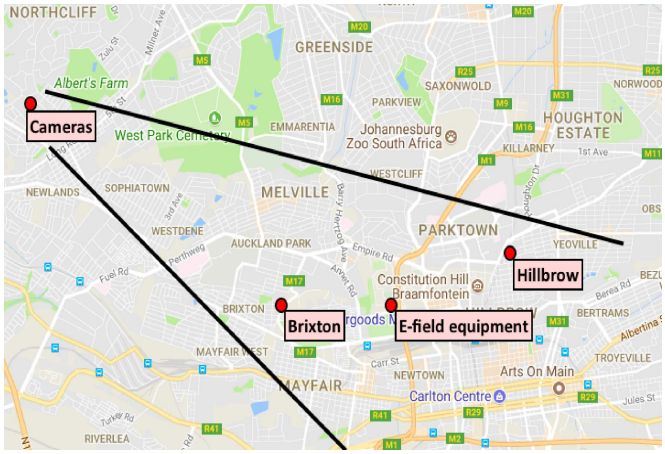

Fig. 3. Map illustrating field of view of high-speed cameras (developed using Google Maps software)

10 – 90 %) and pulse durations were obtained from the waveforms.

In this study, the distance from the sensor to the strike-point of the flashes ranged from 5.7 km to 28.2 km. In this distance range, the radiation field component of the propagated electromagnetic field is prominent. Distances were claculated using the strike-point coordinates obtained from the South African Lightning Detection Network (SALDN). The recorded intensity of the change in the electric field is dependent on the distance the strike-point was relative to the flat-plate antenna. To allow for this parameter to be compared objectively with other studies, the recorded peak intensities were normalised to 100 km.

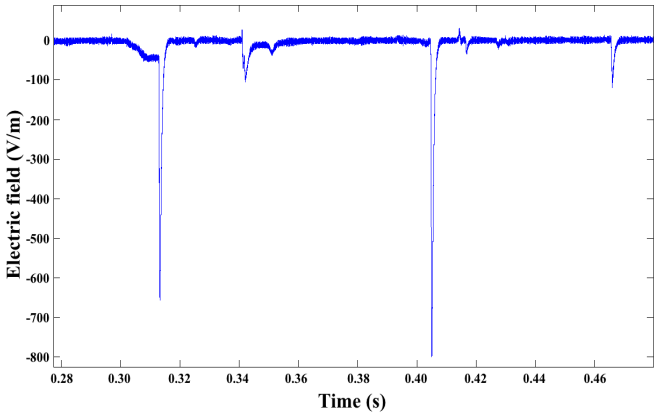

Fig. 4. Sample of a negative flash waveform

B. Methodology

The waveform of a negative stroke is shown in Fig. 5. The slow front (SF) and fast transition (FT) phases

associated with this stroke is discussed by Tran and Rakov [9] and illustrated on Fig. 5. With reference to the time (T) and intensity (i) parameters used in this section, the points indicated in Fig. 5 are defined by the following parameters:

- A: (T_0, i_0)
- B: (T_{100}, i_{100})
- C: (T_{end}, i_{50})

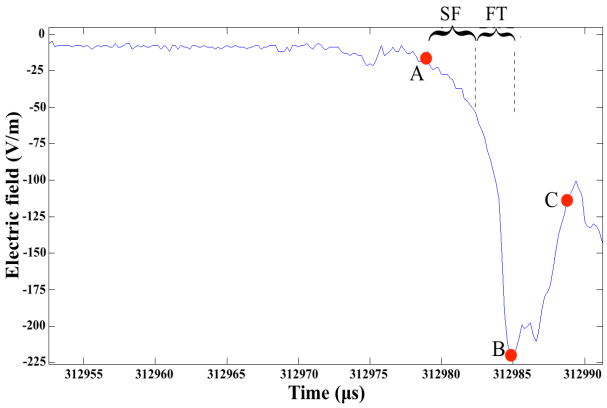

Fig. 5. Slow front (SF) and fast transition (FT) of a changing electric field waveform of a negative return stroke

Determination of changing E-field parameters:

1) Changing E-field intensity

- Take point A as the intensity where the waveform gradient begins its decay to infinity.
- Take point B as the intensity at the peak of the stroke.
- $i_{max} = i_{100} - i_0$

2) Normalised peak intensity

- Determine distance between strike-point and changing E-field measurement device using SALDN coordinates of strike-point.
- Normalise peak intensity to 100 km.

3) 0 % - 100 % rise time ($T_{0\text{-}100}$)

- T_0 is the time at i_0
- T_{100} is the time at i_{100}
- $T_{0\text{-}100} = T_{100} - T_0$

4) 10 % - 90 % rise time ($T_{10\text{-}90}$)

- T_{10} is the time corresponding to i_{10}
  - $i_{10} = i_0 + 0.1(i_{100} - i_0)$
- T_{90} is the time corresponding to i_{90}
  - $i_{90} = i_0 + 0.9(i_{100} - i_0)$
- $T_{10\text{-}90} = T_{90} - T_{10}$

5) Pulse duration ($T_{duration}$)

- T_{end} at point C on Fig. 5 is the time taken for the intensity to return to 50 % of i_{100} from point A (T_0).
- $T_{duration} = T_{end} - T_0$

6) Polarity

- Classified as positive if $i_{100} > i_0$
- Classified as negative if $i_{100} < i_0$

C. Results

From a total of 18 recorded flashes, 15 were classified as negative CG and 3 as positive CG. From the 15 negative flashes, a total of 34 strokes were observed and only two consisted of more than 3 strokes (6 strokes and 9 strokes). All three positive flashes consisted of only one stroke. The arithmetic means (AM) and geometric means (GM) of the data obtained from the positive strokes and negative strokes are presented in Table I and Table II, respectively.

TABLE I. POSITIVE STROKES (3 SAMPLES)

Parameter	AM	GM	Unit
Normalised peak intensity	40.5	36.7	V/m
$T_{0\text{-}100}$	23.7	22.9	µs
$T_{10\text{-}90}$	7.8	7.4	µs
$T_{duration}$	34.5	33.4	µs

TABLE II. NEGATIVE STROKES

Samples		Parameter	AM	GM	Unit
1st RS	12	Normalised peak intensity	9.4	8.6	V/m
		$T_{0\text{-}100}$	4.6	4.5	µs
		$T_{10\text{-}90}$	2.8	2.5	µs
		$T_{duration}$	9.3	8.5	µs
2nd RS	9	Normalised peak intensity	7.5	6.3	V/m
		$T_{0\text{-}100}$	4.0	3.5	µs
		$T_{10\text{-}90}$	2.6	2.3	µs
		$T_{duration}$	5.8	5.3	µs
3rd RS	5	Normalised peak intensity	8.1	7.7	V/m
		$T_{0\text{-}100}$	2.4	2.3	µs
		$T_{10\text{-}90}$	1.0	0.9	µs
		$T_{duration}$	7.0	6.4	µs
All	34	Normalised peak intensity	9.5	8.0	V/m
		$T_{0\text{-}100}$	3.9	3.3	µs
		$T_{10\text{-}90}$	2.2	1.8	µs
		$T_{duration}$	7.4	6.4	µs

V. DISCUSSION

The results of the changing E-field measurements are discussed below and are compared with other studies. The durations measured from the changing electric field waveforms correspond to the pulse duration of the impulse phase of the lightning flash. The duration parameter attained from the high-speed videos represents the duration of the continuing current phase of the lightning flash.

A. Changing electric field

The Geometric mean (GM) of changing E-field peak intensities, normalised to 100 km, for South Africa and Austria are provided in Table III. The Austrian data set used is made up of 31 return strokes. The integrator used for the flat-plate antenna in the Austrian study has a decay time-constant of 0.5 s resulting in a similar bandwidth to the equipment used in this study, hence, ensuring comparable peak intensities.

TABLE III. GEOMETRIC MEAN OF NORMALISED CHANGING ELECTRIC FIELD INTENSITIES

RS	SA	Austria [1]	Units
All	9.5*	8.6	V/m

* TAKEN FROM NEGATIVE STROKE DATA ONLY

The Austrian data used in Table III lists a 0-100 % rise time of 7.4 µs (GM) for all return strokes. For comparison, the GM for the same parameter from the data obtained in this study is 3.3 µs. A comparison of 0 – 100 % and 10 – 90 % rise times with studies conducted in Malaysia and Florida is presented in Table IV. A possible reason for the discrepancies in these rise-times could be due to the measurement equipment operating in different bandwidths.

TABLE IV. GEOMETRIC MEANS OF RISE TIMES FOR NEGATIVE FIRST RETURN STROKES

RS	%	SA	Malaysia [3]	Florida [2]
1st	0 - 100	4.5 µs	9.1 µs	6.5 µs
	10 - 90	2.5 µs	5.0 µs	3.6 µs

The data obtained from the positive flashes is compared with other studies and presented in Table V. The data collected in this study along with the study performed by Schumann, et al. [4] are tabulated in bold text as the antenna and integrator used were the same. This means the frequency content in both measurements are similar and, therefore, allow for accurate rise time comparisons. With the flat-plate antenna being placed on the roof of a building, a significant local, vertical electric field enhancement occurs. This effect will be accounted for by determining a scalar factor that will normalise the results.

B. High-speed video correlation

A set of data was compiled from high-speed video footage of all flashes corresponding to those recorded by the changing electric field measurement system. From these recordings, the luminosity persistence in the lightning channel after attachment had been made was used as an indicator for continuing current duration. A statistical summary of the continuing current durations for both negative and positive flashes is presented in Table VI. From the videos, the end of the continuing current was determined by when the channel disappeared. Visibility of the channel can vary based on the lighting environment and the computer monitor that was used for analysis and, therefore, could account for possible inaccuracies in recorded duration times.

TABLE V. COMPARISON OF CHANGING ELECTRIC FIELD PARAMETERS FOR POSITIVE STROKES

Parameter	Studies	Samples	AM
Peak instensities (V/m)	**This study**	**3**	**40.5**
	Schumann, et al. [4]	**66**	**17.0**
	Cooray, et al. [10]	46	11.5
Rise time (0 – 100 %, µs)	**This study**	**3**	**23.7**
	Schumann, et al. [4]	**72**	**9.5**
	Hojo, et al. [11]	32	22.3
	Cooray [12]	20	8.9
	Ushio, et al. [13]	19	18.0
Rise time (10 – 90 %, µs)	**This work**	**3**	**7.8**
	Schumann, et al. [4]	**72**	**5.7**
	Hojo, et al. [11]	32	6.7
	Cooray [12]	15	6.2

TABLE VI. RECORDED CONTINUING CURRENT DURATIONS FROM LUMINOSITY PERSISTENCE IN HIGH-SPEED VIDEO FOOTAGE

Polarity	Samples	Duration AM	Duration GM	Max	Min	Units
Negative	34	21.4	6.3	271	1	ms
Positive	3	348.7	81.5	567	2	ms

C. Notable points

Throughout this study, certain constraints existed due to the equipment used and the data acquisition methodology. These, along with other noteworthy observations, are presented below:

- The peak changing E-field intensities could only be normalised if there was corresponding SALDN coordinate data on the strike-point locations of the recorded flashes.
- The changing E-field stroke data that could be correlated to the videos was limited to flashes with strike-points in the field of view of the cameras (illustrated in Fig. 3).
- The beginning stages of the electric field collapse are observable before T_0. This information, if studied further, could have significant practical applications,

such as improving the response time of certain lightning protection systems.

- An advantage of using both changing E-field measurements in collaboration with high-speed videos is that if unfamiliar anomalies occur in the electric field, the videos can be used to provide clarity. The converse also applies.
- A disadvantage of using both analysis techniques is that the field of view of the cameras is the limiting factor in the number of strokes that can be correlated to the changing E-field data. The antenna sensors register more flashes than the high-speed cameras can capture.
- The localised enhancement of the vertical electric field on the building that the antenna was placed has been noted. An enhancement factor is yet to be developed and as such, the presented electric field peaks are assumed to be marginally higher than the true values.

VI. CONCLUSION

Presented in this paper are the results obtained from analysing the data obtained from 18 separate lightning flashes over Johannesburg, South Africa. A flat-plate antenna with an integrator was used to record the peak intensity, rise times and pulse duration parameters of the propagated vertical electric field from lightning flashes. The normalised peak intensities for the 34 recorded negative strokes and 3 positive strokes were 8.0 V/m and 36.7 V/m, respectively. The pulse durations for the negative and positive stroke samples were 6.4 μs and 33.4 μs, respectively. From high-speed video recordings of the corresponding flashes, the negative and positive strokes presented an average continuing current duration of 6.3 ms and 81.5 ms, respectively.

ACKNOWLEDGEMENTS

The authors would like to thank the South African Weather Service (SAWS) for their support and for providing the SALDN data used in this paper. They would also like to thank Eskom for the support of the Lightning/EMC Research Group through the TESP programme. Thanks are extended to the Department of Trade and Industry (DTI) for THRIP funding as well as to the National Research Fund (NRF) for direct funding of the Research Group.

REFERENCES

[1] H. Pichler, G. Diendorfer and M. Mair. “Some Parameters of Correlated and Radiated Field Pulses from Lightning to the Gaisberg Tower” IEEJ Transactions on Electrical and Electronic Engineering, 2010.

[2] A. Nag, V. A. Rakow, D. Tsalikis, J. S. Howard, C. J. Biagi, J. D. Hill, M. A. Uman and D. M. Jordan. “Characteristics of the initial rising portion of near and far lightning return stroke electric field waveforms” ICLP, 2010.

[3] M. N. Hamzah, M. Z. A. Ab Kadir, C. Gomes and S. N. M. Arshad. “Unusually Long Duration Lightning Electric Field Return Strokes in Malaysia” ICLP, 2014.

[4] C. Schumann, M. M. F. Saba, R. B. G. Da Silva and W. Schulz. “Electric fields changes produced by positive cloud-to-ground lightning flashes” Journal of Atmospheric and Solar-Terrestrial Physics, Volume 92, 2012.

[5] V. Cooray. An Introduction to Lightning. Springer Netherlands, 1st ed., 2015. □

[6] S. N. M. Arshad, M. Z. A. Ab Kadir, M. Izadi, M. N. Hamzah, C. Gomes and J. Jasni. “Characterization of Measured Lightning Electric Fields Observed in Malaysia” ICLP, 2014.

[7] M. A. Haddad, V. A. Rakov, S. A. Cummer. “New measurements of lightning electric fields in Florida: Waveform characteristics, interaction with the ionosphere, and peak current estimates” Journal of Geophysical Research, Volume 117, 2012.

[8] A. D. Watt. “ELF Electric Fields From Thunderstorms” Journal of Research of the National Bureau of Standards, Volume 64D, 1960.

[9] M. D. Tran and V. A. Rakov. “A study of the ground-attachment process in natural lightning with emphasis on its breakthrough phase” Scientific Reports, 2017.

[10] V. Cooray, M. Fernando, C. Gomes, and T. Sorenssen. “The fine structure of positive lightning return-stroke radiation fields” IEEE Transactions on Electromagnetic Compatibility, Volume 46 (1), pp. 87–95, 2004.

[11] J. Hojo, M. Ishii, T. Kawamura, F. Suzuki and R. Funayama. “The fine structure in the field change produced by positve ground strokes” Journal of Geophysical Research, Volume 90, pp. 6139–6143, 1985.

[12] V. Cooray. “A novel method to identify the radiation fields produced by positive return strokes and their submicrosecond structure” Journal of Geophysical Research 91 (D7), pp. 7907–7911, 1986.

[13] T. Ushio, Z. Kawasaki, K. Matsu-ura and D. Wang. “Electric fields of initial breakdown in positive ground flash” American Geophysical Union. Paper no. 97d01975–0148-0227/97/97JD-01975, 1998.

Appendix D

Performance evaluation of the SALDN using high-speed camera footage of ground truth lightning events over Johannesburg, South Africa

D.1 Paper description

The following paper was published and presented at the 34th Internationcal Conference on Lightning Protection (ICLP) in September 2018 in Rzeszow, Poland. Presented in this paper are the preliminary results of a performance evaluation performed on the South African Lightning Detection Network (SALDN). The lightning flash and stroke detection efficiency and location accuracy is quantified and certain interesting cases are discussed. The methodology behind this analysis is also explained in detail.

34th International Conference on Lightning Protection
02-07 September 2018
Rzeszow, Poland

Performance evaluation of the SALDN using high-speed camera footage of ground truth lightning events over Johannesburg, South Africa

H.G. Fensham, C. Schumann, H.G.P. Hunt, J.D. Tasman, K.J. Nixon
School of Electrical & Information Engineering
University of the Witwatersrand
Johannesburg, South Africa
hgfensham@gmail.com

T.A. Warner
ZT Research
Rapid City-SD-USA
Tom.Warner@ztresearch.com

M. Gijben
South Africa Weather Service
Pretoria, South Africa
Morne.Gijben@weathersa.co.za

***Abstract*— The performance of the South African Lightning Detection Network (SALDN) with regards to detection efficiency and location accuracy is presented in this paper. The performance is evaluated over a region in South Africa by using high-speed camera footage of ground truth lightning events, time-correlated with data from the SALDN. The data set contains 128 flashes which were recorded with high-speed cameras. The flash detection efficiency of the network is 88.3 % and the stroke detection efficiency is 72.1 %. The location accuracy has a median location error of 67.7 m based on 71 events which attached to the Hillbrow and Sentech Towers.**

Keywords- Detection efficiency, Location accuracy, SALDN

I. INTRODUCTION

Lightning Detection Networks (LDNs) consist of sensors which measure magnetic and/or electric fields propagated from lightning events. These lightning events are time-correlated and in certain instances, given a geographical location [1]. However, there are errors in these measurements, whether the LDN detected a lightning event and if the location given for a lightning event is correct. The performance of LDNs can be evaluated by determining the detection efficiency (DE) and the location accuracy (LA) of the system.

Around the world many LDNs have been evaluated with regards to their DE and LA. These include: the Guangdong-Hongkong-Macau Lightning Location System (GHMLLS), U.S. National Lightning Detection Network (NLDN), the European Lightning Location System (EUCLID) and the Austrian Lightning Detection and Information System (ALDIS) [2-5]. There are different ways to collect ground truth lightning event data to evaluate an LDN, to list a few: rocket triggered lightning events, high-speed camera footage and E-field measurements and natural lightning events on tall towers [4].

This paper aims to determine the DE, with regards to flash and stroke detection, and LA of the South African Lightning Detection Network (SALDN) over Johannesburg, South Africa, using high-speed camera footage of ground truth lightning events.

II. SALDN

The SALDN was established in 2005, consisting of 19 sensors throughout the country. Since 2009 there have been 2 upgrades to the system. In the early part of 2010 the systems number of sensors increased to 22 and in 2011 sensors were relocated and a further 2 sensors were added. As of 2014, the SALDN contains 24 Vaisala LS7000 sensors positioned throughout South Africa as seen in Fig. 1 [6]. The SALDN has a self-evaluated performance of 90 % for flash DE and a median location error of 0.5 km for LA [7].

The flash DE and LA of the SALDN was determined previously in 2014. This was done by using low speed cameras which meant the stroke DE could not be determined. Additionally, the camera was only recording lightning events which took place on the Sentech Tower. Therefore, the flash DE was calculated for one specific location, nonetheless it was found to be 76 %. The LA of the system was found to have a median location error of 290 m since the lightning events had a known geographical location from the tower [6].

The data provided by the SALDN was cloud-to-ground stroke data for the whole of South Africa which needed to be time-correlated with the high-speed camera footage.

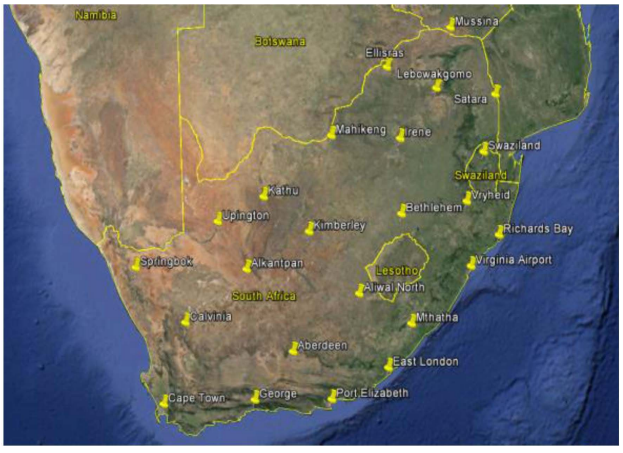

Fig. 1. Location of the 24 Vaisala sensors in South Africa as of 2014 [6].

978-1-5386-6635-7/18/$31.00 ©2018 IEEE

III. HIGH-SPEED CAMERA FOOTAGE

The high-speed cameras used were the Phantom v310 and the Phantom v7.1. The camera footage was collected between the 5th of February 2017 and the 6th of February 2018. Table I, gives a summary of the data collected by the cameras, this data set was used in finding the DE and LA of the SALDN.

This data was found by positioning the cameras where the blue pin is situated (26.16283°S, 27.95986°E) in Fig. 2. From this location the cameras looked over Johannesburg, South Africa. The field of view which is illustrated by the black lines, encloses the Hillbrow (26.18696°S, 28.04948°E) and Sentech (26.1925°S, 28.00666°E) Towers illustrated by the black pins. The red pins illustrate the region that was focused on for the SALDN data. The respective decimal coordinates are given with each red pin.

TABLE I. HIGH-SPEED CAMERA DATA

Lightning events	High-speed camera events
Thunderstorms	22
Flashes	128
Downward flashes	101
Strokes	431
M-components	82
Upward flashes	27
Upward leaders	34
ICC pulses	246
Subsequent return strokes	30
M-components	8

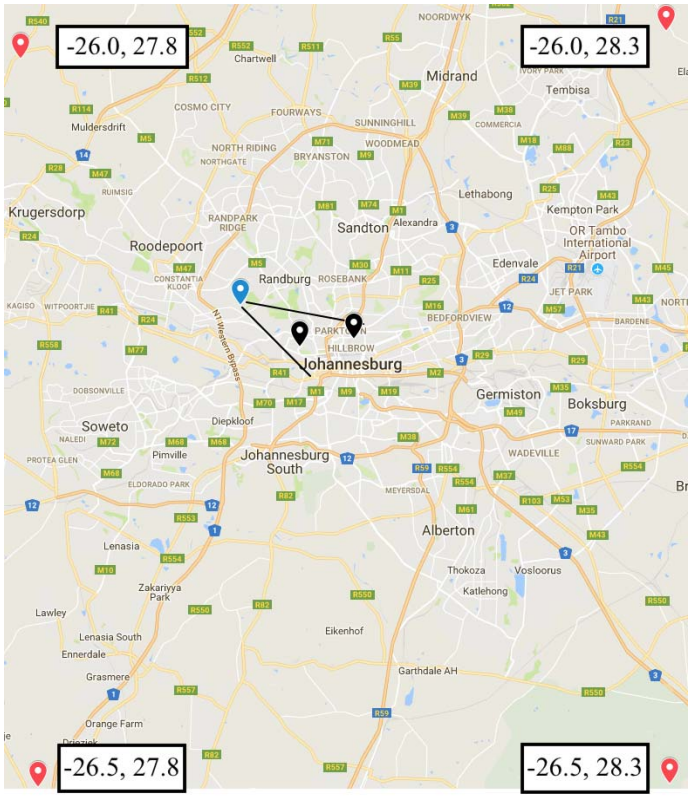

Fig. 2. Map of region which SALDN data is filtered by, camera location and Hillbrow and Sentech Tower

IV. METHODOLOGY

In order to evaluate the performance of the SALDN, the two data sets needed to be time-correlated. From this time-correlation the DE and LA methodology can be applied.

A. Time-correlation between SALDN data and high-speed camera footage

- Filter the cloud-to-ground SALDN stroke data to only contain strokes between the red pins illustrated in Fig. 2 in order to find the localized SALDN data.
- Time-correlate the lightning events seen in the high-speed camera data with the localized SALDN data.
- Determine if the SALDN detected the events.

B. Detection Efficiency

The DE of the SALDN is comprised of the flash DE and the stroke DE.

1) Flash Detection Efficiency

- Find the number of flashes captured with the high-speed cameras.
- Determine if the SALDN stroke data detected any strokes (return strokes and subsequent return strokes), upward leaders, M-components or ICC pulses in the time-correlated data.
- If the SALDN detected any one of the above-mentioned lightning events, then a flash has been detected by the SALDN.
- Calculate the percentage of flashes detected by the SALDN compared to the total number of high-speed camera flashes.

2) Stroke Detection Efficiency

- Find the number of strokes for downward and upward flashes captured with the high speed cameras.
- Calculate the number of strokes that were detected by the SALDN, in the time-correlated data.
- Calculate the percentage of SALDN strokes that were detected compared to the number of strokes in the high-speed camera footage.

C. Location accuracy

- Create a subset of the data from the high-speed camera footage with the lightning events that occurred on the Hillbrow and Sentech Tower.
- Calculate the distance between the coordinates of the towers and the coordinates given by the SALDN data for the events which were detected on these towers.

- Determine the number of samples, maximum, minimum, median, standard deviation, mode and arithmetic mean of the distances calculated.

V. RESULTS

The following section will provide the results obtained from applying the methodology in section IV as well as interesting cases which were found throughout the evaluation of the performance of the SALDN.

A. Time-correlation Results

Table II is the summarized results of the time-correlation between the high-speed camera footage and the SALDN data.

TABLE II. TIME-CORRELATED DATA OF THE HIGH-SPEED CAMERA DATA AND THE SALDN DATA

Lightning events	High-speed camera events	SALDN events
Flashes	128	113
Downward flashes	101	95
Strokes	431	311
M-components	82	9
Upward flashes	27	18
Upward leaders	34	0
ICC pulses	246	45
Subsequent return strokes	35	25
M-components	8	2

B. Detection Efficiency

The DE has been defined for both flash and stroke levels. Naturally, a network will have a greater chance of detecting a flash compared to a stroke. This is because a single detected stroke, within a flash, will constitute a flash [8].

1) Flash Detection Efficiency

The SALDN was found to have detected 113 flashes as seen in table II. This was found by using section IV. With the camera footage recording 128 flashes, this meant the SALDN has a flash DE of 88.3 % as seen in table III.

TABLE III. FLASH DETECTION EFFICIENCY

Number of flashes recorded by high-speed camera	128
Number of flashes detected by SALDN	113
Flash Detection Efficiency	**88.3 %**

This compared with the self-evaluation value DE of 90 %, shows that the system is performing close to its expectation. Additionally, the flash DE for downward flashes is 94 %. This is greater than the flash DE for upward flashes which is 66.7 %.

2) Stroke Detection Efficiency

The high-speed camera data had a total of 466 strokes for downward and upward flashes. Of this, the SALDN detected a total of 336, equating to a stroke DE of 72.1 %. This can be seen in table IV.

TABLE IV. STROKE DETECTION EFFICIECNY

Number of strokes recorded by high-speed camera	466
Number of strokes detected by SALDN	336
Stroke Detection Efficiency	**72.1 %**

It must be noted that in upward lightning, the upward leader is generally not detected and sometimes the superimposed ICC pulses can be classified as intra-cloud (IC) discharges [9, 10]. Unfortunately, the IC SALDN data was not obtainable for this dataset.

C. Location Accuracy

The high-speed camera footage is crucial for determining the LA of the SALDN. The high-speed cameras allow the lightning events on the Hillbrow and Sentech Tower to be viewed, meaning the true location of the event is known. As described above in section IV, the coordinates for the events which made attachment with the two towers in the video footage and were detected by the SALDN were used to form a subset of the data set. The coordinates given by the SALDN could then be compared to the true coordinates of the Hillbrow and Sentech Tower. From this the distance between the towers and the SALDN detection coordinates could be calculated.

The amount of events which occurred on both of the towers totals to 71. The SALDN has a LA with a median location error of 68.5 m. This value is well within the self-performance evaluation for the LA which has a 0.5 km median location error. The results of this data for both towers together and each tower separately can be seen in table V. The following two subsections will discuss the LA on each tower.

1) Sentech Tower

Of the 71 events which took place on the towers, 36 of them took place on the Sentech Tower. However, one of the events which took place on the tower was an outlier. This event was calculated to be 1.7 km away from the tower. In Fig. 3 a) one can see this outlier and in Fig. 3 b) this outlier has been excluded to get a better view of the SALDN locations detected around the Sentech Tower. Table V shows the results of the LA on the Sentech Tower, having a median location error of 80.5 m.

2) Hillbrow Tower

Of the 71 events, 35 occurred on the Hillbrow Tower. Two of these events were found to be outliers as the one event had a distance of 11.65 km and the other event having a distance of 3.85 km from the tower. This can be seen in Fig. 3 c). In Fig. 3 d) the two events were excluded to give a closer view on the distribution around the Hillbrow Tower.

Table V gives the results of the LA on the Hillbrow Tower with all the events taken into account. It shows that the median location error is 60.1 m.

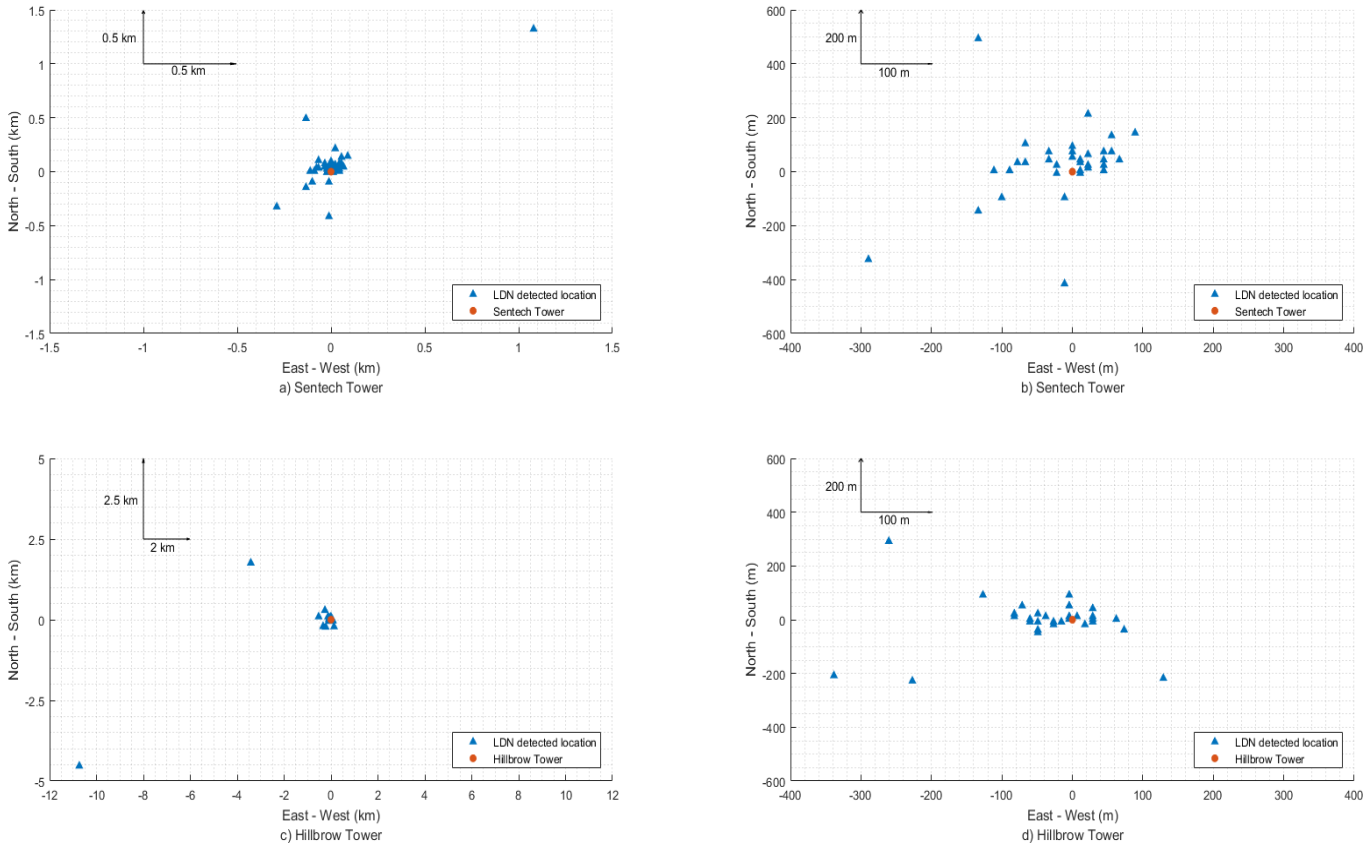

Fig. 3. Detected locations of the SALDN data which has been time-correlated with the high-speed video footage for the Sentech and Hillbrow Towers

TABLE V. LOCATION ACCURACY OF TOWER EVENTS

Tower	N	Max	Min	Median	σ	Mode	Mean
Both Towers	71	11650.7 m	4.9 m	68.5 m	1501.0 m	4.9 m	363.0 m
Sentech Tower	36	1707.1 m	11.8 m	80.5 m	285.5 m	53.9 m	156.4 m
Hillbrow Tower	35	11650.7 m	4.9 m	60.1 m	2009.5 m	4.9 m	536.5 m

D. Interesting Cases

In the process of evaluating the performance of the SALDN, it was seen that there were upward triggering events, M-components and ICC pulses which were detected as strokes by the SALDN and the odd case where two strokes would be detected at the same time and geographical location by the SALDN.

1) Upward triggering event

Of the 18 detected upward flashes in the high-speed camera footage, approximately 8 upward flashes had a positive lightning stroke before the upward flash was initiated and then seen on camera. These positive lightning strokes were detected by the SALDN with positive current and would initiate an upward leader within 100 ms.

2) Detected M-components and ICC pulses

In the comparison between the high-speed camera footage and the SALDN data, it was noticed that strokes were detected by the SALDN which were actually M-components or ICC pulses as observed in the high-speed camera footage.

From table II, the number of M-components and ICC pulses detected by the SALDN equate to 56. The total number of ICC pulses and M-components in the high-speed camera data equates to 336. This means that 16.6 % of M-components and ICC pulses were classified as a stroke by the SALDN. It must be noted that of this percentage, ICC pulses are responsible for 13.4 %.

3) SALDN dual stroke entry

During the time-correlation between the high-speed camera data and the SALDN data, it was noticed that a small amount of strokes in the SALDN data were detected twice. Meaning the SALDN data detected two strokes at the same time, down to the millisecond, with a similar geographical location. These strokes were all downward negatives within a downward or upward flash. The strokes were also given current estimates which were similar if not the exact same.

In the high-speed video footage these dual entry strokes did not have any substantial differences to other strokes which were analyzed. These entries can be seen in table VI.

TABLE VI. DUAL STROKE ENTRIES BY SALDN

Dual stroke entry	Time	Latitude	Longitude	Current (kA)
1				
	20:05:13.575	-26.2071	28.0791	-16
	20:05:13.575	-26.2073	28.0800	-16
2				
	20:28:35.709	-26.2339	28.1945	-17
	20:28:35.709	-26.2349	28.1947	-16
3				
	15:46:51.678	-26.1863	28.0491	-27
	15:46:51.678	-26.1867	28.0494	-24

VI. CONCLUSION

The South African Lightning Detection Network is still a relatively new LDN which has a self-evaluated performance of 90 % for flash detection efficiency and a location accuracy with a median location error of 0.5 km. Using high-speed camera footage over Johannesburg, South Africa, time-correlated with cloud-to-ground SALDN stroke data, the flash detection efficiency and stroke detection efficiency was calculated to be 88.3 % and 72.1 % respectively. Additionally, the SALDN was found to have a flash detection efficiency of 94 % for downward flashes and a flash detection efficiency of 66.7 % for upward flashes. The location accuracy had an overall median location error of 68.5 m with 71 events in total making attachment on the Sentech and Hillbrow Tower. The Sentech Tower had a location accuracy with a median location error of 80.5 m and the Hillbrow Tower had a location accuracy with a median location error of 60.1 m.

ACKNOWLEGDMENTS

The authors would like to thank the South African Weather Service (SAWS) for their support and for providing the SALDN data used in this paper. They would also like to thank Eskom for the support of the Lightning/EMCResearch Group through the TESP programme. Thanks are extended to the Department of Trade and Industry (DTI) for THRIP funding as well as to the National Research Foundation (NRF) for direct funding of the Research Group.

REFERENCES

[1] H. G. P. Hunt, K. J. Nixon and I. R. Jandrell, "Establishing a methodology to investigate LDN median error ellipses used as corroborating evidence for a lightning event at a specific geographic location," Electric Power Systems Research, vol. 113, 2014.

[2] Y. Zhang, W. Lu, Y. Zhang, D. Zheng, L. Chen, S. Chen, and X. Yan, "Evaluation for the performance of the Guangdong-Hongkong-Macau Lightning Location System," 23rd International Lightning Detection Conference, March 2014.

[3] S. Mallick, V. A. Rakov, T. Ngin, W. R. Gamerota, J. T. Pilkey, J. D. Hill, M. A. Uman, D. M. Jordan, J. A. Cramer and A. Nag, "An update on the performance characteristics of the NLDN," 23rd International Lightning Detection Conference, March 2014.

[4] W. Schulz, G. Diendorfer, S. Pedeboy, and D. R. Poelman, "The European Lightning Location System EUCLID – Part 1: Performance analysis and validation," Natural Hazards and Earth System Sciences, March 2016.

[5] C. Vergeiner, W. Schulz and S. Pack, "On the performance of the Austrian Lightning Detection and Information System (ALDIS)," Institute of High Voltage Engineering and System Management, Graz University of Technology, Graz, Austria, November 2013.

[6] H. G. P. Hunt, Y. C. Liu, and K. J. Nixon, "Evaluation of the South African Lightning Detection Network using photographed tall tower lightning events from 2009 – 2013," 2014 International Conference on Lightning Protection (ICLP), 2014.

[7] M. Gijben, "The lightning climatology of South Africa," South African Journal of Science, vol. 108, 2012.

[8] H. G. P. Hunt, K. J. Nixon and I. R. Jandrell, "Comparison between South African Lightning Detection Network interpretation of single-channel and branched upward lightning flashes to a tall structure," 2013 International Symposium on Lightning Protection (XII SIPDA), Belo Horizonte, Brazil, October 2013.

[9] T. A. Warner, K. L. Cummins and R. E. Orville, "Upward lightning observations from towers in Rapid City, South Dakota and comparison with National Lightning Detection Network data, 2004-2010," Journal of Geophysical Research, 2012.

[10] G. Diendorfer, H. Pichler and W. Schulz, "LLS detection of upward initiated lightning flashes," 2015 Asia-Pacific International Conference on Lightning (APL), Nagoya, Japan, 2015.

Appendix E

High-speed video observation of lightning flashes over Johannesburg, South Africa 2017 - 2018

E.1 Paper description

The following paper was published and presented at the 34th Internationcal Conference on Lightning Protection (ICLP) in September 2018 in Rzeszow, Poland. The primary measurement instruments used for this study were two Phantom high-speed cameras. The dataset consisted of 168 lightning flashes, which were subsequently categorised and being either upward or downward and either negative, positive or bipolar. Strike-point location, interstroke interval and continuing current duration are paramters used to characterise the recorded flashes in more detail.

34th International Conference on Lightning Protection
02-07 September 2018
Rzeszow, Poland

High-speed video observation of lightning flashes over Johannesburg, South Africa 2017 - 2018

Carina Schumann
School of Electrical and Information Engineering
University of the Witwatersrand
Johannesburg, South Africa
Email: carina.schumann@wits.ac.za

Hugh.G.P. Hunt
School of Electrical and Information Engineering
University of the Witwatersrand
Johannesburg, South Africa
Email: hugh.hunt@wits.ac.za

Jesse Tasman
School of Electrical and Information Engineering
University of the Witwatersrand
Johannesburg, South Africa

Haydn Fensham
School of Electrical and Information Engineering
University of the Witwatersrand
Johannesburg, South Africa

Ken J. Nixon
School of Electrical and Information Engineering
University of the Witwatersrand
Johannesburg, South Africa
Email: ken.nixon@wits.ac.za

Tom A. Warner
ZT Research,
Rapid City, USA
Email: tom.warner@ztresearch.com

Marcelo M.F. Saba
Atmospheric Electricity Group
Brazilian National Institute for Space Research
São José dos Campos, Brazil
Email: marcelo.saba@inpe.br

Abstract— **South Africa has a long history of lightning research. Tall towers provide a useful tool for investigating lightning as they generally have a high repeatability of events. The Johannesburg region in the Gauteng province has two tall towers, the Brixton tower and the Hillbrow tower, with a high frequency of lightning events. This paper presents a project beginning in January 2017 and aims to study the physics of lightning through high-speed video observation and fast electric field measurements. Thunderstorms over Johannesburg have a high cloud base which allows for visible channels from the tall towers. More than 200 videos of downward and upward flashes were observed since the project started. Also, 6 flashes to a 53 m tall building were observed. The project also aims to raise awareness around lightning dangers in Africa.**

Keywords- South African lightning; high-speed camera; upward lightning; downward lightning

I. INTRODUCTION

South Africa has a long history of research into lightning to tall structures [1,2]. The purpose of this paper is to present a project that is to be undertaken in 2017-2018. This is a scientific project that aims to investigate the physics of lightning by high-speed video observation along with electric field measurements and potential current measurements as well in Johannesburg, South Africa. It is part of an international collaboration between Brazil, USA, Austria and Sweden. Historically, these are all locations where tall tower investigations of lightning have been performed (using high-speed camera observations, electric field measurements, current measurements or a combination of these). Tall towers provide a useful tool for investigating lightning as they generally have a high repeatability of events. The Johannesburg region has two tall towers, the Brixton tower and the Hillbrow tower, with a high frequency of lightning events. However, these events are usually upward in nature, and an investigation of the density of lightning over Johannesburg to determine other, less tall locations is considered.

II. JOHANNESBURG, SOUTH AFRICA

Johannesburg is the main economic city in South Africa and can be found in the north-east of the country. It is the location of much of the industry in South Africa. It is also notable for its altitude – approximately 1600 m above sea level. Figure 1 shows the skyline of Johannesburg.

Claude Leon Post-doctoral fellowship, Eskom TESP Programme

978-1-5386-6635-7/18/$31.00 ©2018 IEEE



Figure 1. The skyline of Johannesburg city, view from the north looking south through the city.

This photograph is taken from the north facing south through the city. Two tall towers on either ends of the skyline can be seen. These are the Brixton (right) and Hillbrow (left) tower. The Brixton tower is west of the city and Hillbrow tower is east. Figure 2 is a sketch of the height, and distance between the towers.

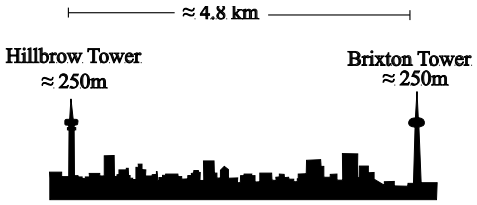

Figure 2. The two tall towers in Johannesburg city, Brixton (right) and Hillbrow (left) tower.

While these are the two tallest buildings, a number of other locations and buildings of interest fall within the city. The University of the Witwatersrand is located approximately halfway between the Brixton and Hillbrow tower.

Figure 3 shows the lightning flash density map of South Africa as of 2014. This map was created by the South African Weather Service (SAWS) utilizing data from the South African Lightning Detection Network (SALDN) – the lightning location system in operation in South Africa.

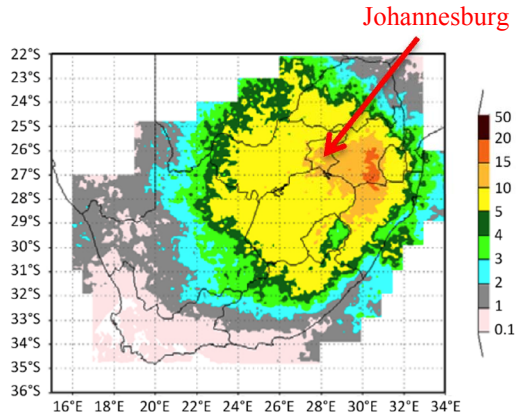

Figure 3. Lightning flash density over South Africa. Image used with permission, courtesy Morné Gijben [3]. The location of Johannesburg is indicated.

The SALDN consists of 25 Vaisala LS7000 sensors located across the country (with one sensor located in Swaziland) and has been operational since 2006. SAWS has collected more than 10 years worth of lightning data over the whole country. The network has an estimated average detection efficiency of 90% and approximately 500 m median location accuracy.

As can be seen in figure 3, the areas of highest lightning flash density are to the north-east of the country, in region known as the Mpumalanga province. Johannesburg is located close to this region (indicated in the figure), not quite in the highest flash density region but still high with approximately 10-15 *flashes/km^2/year*. The combination of the tall towers, altitude, cloud base and high flash density make Johannesburg a unique and relevant choice for lightning studies.

A. Lightning Occurrence over Johannesburg

Utilizing Gaussian smoothing techniques, lightning location system data can be further interrogated for more detail. Gaussian smoothing techniques utilize the confidence ellipses of stroke reports to represent a stroke as a distribution rather than a single point. In this way, it is possible to create flash density maps that are independent of resolution - ideal for looking at areas smaller than 10×10 km. Given that each attachment point has been "spread out" and is rather represented as a fraction over the grid, no actual values can be attributed to the values but visual density trends are clearly displayed.

Figure 4 shows a Gaussian smoothed map over Johannesburg city. The map utilizes data from the SALDN from 2007 – 2015. The locations of the Brixton tower and the Hillbrow tower are shown. As is clear in the figure, there is a high density around the location of the two towers indicating that they are regularly struck – and much more than other locations within the city.

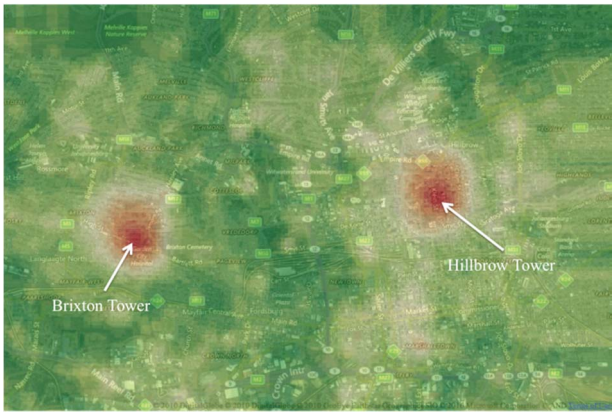

Figure 4. Gaussian smoothed lightning density map based on SALDN data from 2007 - 2015. The Brixton and Hillbrow towers are indicated in the image and can be distinguished by the "hotspots".

Gaussian smoothed maps can be used to investigate even further – figure 5 shows a similar image but only over the University of the Witwatersrand campus, located roughly in the city center about half-way between the Brixton and the Hillbrow tower.

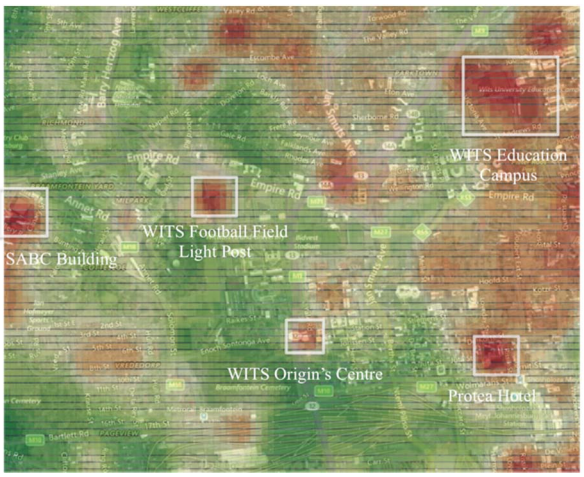

Figure 5. Gaussian smoothed lightning density map over Johannesburg, WITS University campus.

By examining the smaller area and excluding the Brixton and Hillbrow tower, more detail can be gained on specific locations around the city center and campus. It can be seen in the Figure 5 that there are a number of locations that seem to have been struck multiple times in the last 10 years. Five locations are identified on the map:

- The SABC broadcasting buildings
- A light post on a WITS football field
- The Origins Centre building on WITS campus
- The Protea Hotel in Braamfontein, Johannesburg
- The WITS Education Campus

None of these locations are significantly tall towers and it is very likely that the events they have endured are downward lightning events. The SABC broadcasting buildings, while close to the Brixton tower is sufficiently far away (1 km) so as not to be protected by the Brixton tower. Also of interest, is the Protea hotel in the Braamfontein area, a dense city area and yet, the Protea hotel clearly is struck fairly regularly, likely due to its height.

B. Previous Photographic Studies

Since 2009, a simple surveillance system to photograph lightning attachments to the Brixton tower was in operation. The system was initially installed to capture lightning images for 3-dimensional modeling of the lightning channel but was later used as a ground-truth location for comparison with the SALDN. The system consisted of a simple motion-triggered camera located at the University of the Witwatersrand and looking east towards the Brixton tower with an approximate field of view of 55° [4]

The system initially operated from 2009-2013 but was shutdown in 2014. It was reinitiated in 2015 with a second camera added looking at the tower from a different perspective. Figure 6(a) and (b) shows an example of the type of images captured by the system – a lightning flash attaching to the Brixton tower on Friday, 20 November 2015 at 22:24:48 SAST.



(a) (b)

Figure 6. A lightning strike to the Brixton tower on the 20 November 2015 at 22:24:48 SAST. Two cameras observe the Brixton tower – (a) one situated at WITS university and facing east, (b) the other situated 1 km north of the tower and facing south.

Table 1 shows the number of flashes to the Brixton tower photographed by the camera for each season since 2009. The cases are separated between upward flashes and downward flashes and, as expected, the majority of flashes to the tower are upward. However, some downward events do also attach to the tower.

TABLE I. PHOTOGRAPHED FLASHES TO BRIXTON TOWER

Season	***Number Upward Flashes***	***Number Downward Flashes***	***Total Number Flashes***
2009-2010	12	0	12
2010-2011	24	2	26
2011-2012	6	1	7
2012-2013	17	4	21
2015-2016	46	9	55
Total	105	16	121

Also notable in the photographs is the clarity of the channel – the cloud base is far above the top of the tower allowing for a complete view of the channel, unlike many other tall towers in the world, which find themselves reaching into the clouds and therefore obscuring the visibility of any lightning events that may attach to them.

III. HIGH-SPEED VIDEO STUDY

Before Abbreviations and Acronyms

A. Collaborators

The project has a number of collaborators who assist both with equipment and experience: ZT Research in South Dakota, USA and INPE in São Paulo, Brazil have performed similar studies in their respective countries and SAWS and EarthNetworks operate lightning location systems. This section details the nature of the projects performed by these collaborators and highlights how their knowledge and results feed into the South African project.

1) ZT Research

Tom Warner, of ZT Research, has worked with high-speed cameras since 2010 in Rapid City, USA. The city has 10 towers that produce upward lightning [5]. Figure 7 shows a frame from a high-speed video, which captured upward

lightning events from towers in Rapid City. The researchers spent four summers recording flashes in Rapid City along with electric field measurements provided the Brazilian National Institute for Space Research (INPE). Tom Warner lent two high-speed cameras (10,000 and 1,000 frames per second) to the project in South Africa and is involved in all research analysis.



Figure 7. Upward lightning from towers in Rapid City, South Dakota.

2) Brazilian National Institute of Space Research (INPE)

The INPE team has experience with high-speed cameras and flat plate electric field measurements since 2003, and are pioneers on the characterization of the different polarities of flashes by images [6-7]. The team are have lent a flat plate electric field sensor, able to record data continuously at 5 MSamples/s to the South African project. Collaboration and comparison with ongoing research in São Paulo, Brazil (upward lightning to Jaraguá peak and downward lightning to normal apartment buildings) allows for comparison between data sets.

3) SAWS

SAWS has a long-standing agreement with the research group regarding the use of the SALDN data. The data provides insight into the filmed high-speed cases and simultaneously the video observation provide and ideal ground-truth data set for comparison with SALDN stroke detections and reports.

4) EarthNetworks

EarthNetworks have recently begun implementing a lightning location system in South Africa and similarly, there is value in comparing high-speed video observations with reports from such a network.

B. Equipment and Experimental Setup

The two high-speed cameras provided by ZT Research and being used for the study are the Phantom v310, Phantom v7.1. In general, the v310 records at approximately 15000 fps with an exposure time of 58µs and the v7.1 at 5000 fps with an exposure time of 990µs. The different frame rates of the cameras and their subsequent exposure times and resolution allow for each recorded flash to be separately analysed. analysed separately - optimising the accuracy of the characterization process.

Figure 8 shows where the two high-speed cameras are located – an area north-west of the Johannesburg city center on a ridge known as Northcliff hill – along with the locations of the Brixton and the Hillbrow tower, and the city center between them. The camera view over the city is therefore the same as shown in figure 1, the skyline of Johannesburg.

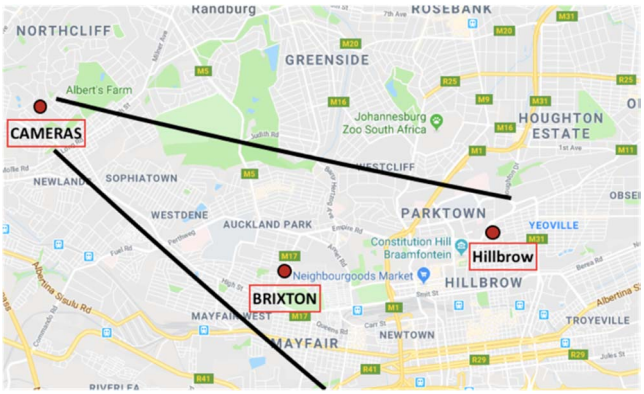

Figure 8. Location of high-speed cameras and the Brixton and Hillbrow towers, indicating Johannesburg city.

Also shown in figure 8 the locations of a number of simple surveillance camera setups similar to those used in the previous photographic study. However, here cameras located at the University of the Witwatersrand look not only to the Brixton tower but also at the Hillbrow tower and the city centre. Another on of these camera setups is located on the 52nd floor of a building known as Ponte, a tall apartment building in the city not far from the Hillbrow tower. Figure 9 shows a photograph of a lightning event to the Hillbrow tower taken by the South African photographer Jonathan Wood.



Figure 9. Photograph lightning event to Hillbrow tower taken from the Ponte building. Courtesy Jonathan Wood.

These simple surveillance camera setups provide additional information to the high-speed video observations, giving a different perspective on the channel and allowing for identification of strike-points that may not have been visible from the high-speed footage.

C. Methodology

For the end of the season (January – May 2017) and the following season (October 2017 – May 2018), the high-speed camera setup and surveillance camera setup were activated and capturing video footage of lightning during thunderstorm over South Africa.

For each filmed lightning flash, the following categorizations were performed based on the video:

- Downward flashes
  - Continuing current duration
  - Polarity
  - Multiplicity
  - Multiple strike points
  - Total flash duration
- Upward flashes
  - Triggering events
  - Duration and continuing current
  - Polarity
  - Subsequent return strokes
  - ICC pulses
  - Tall towers involved

Also discussed in the analysis are a number of bipolar events observed by the camera. Upward and downward events are categorized based on the direction of propagation of the leader. Polarity is determined based on the presence of branching and recoil leaders.

IV. First Results: 2017 - 2018

During this first year of high-speed video recording in Johannesburg, 168 downward flashes were recorded. Upward flashes also were observed from Johannesburg towers and tall buildings. A total of 45 upward flashes were registered. Table 2 shows a summary of the lightning events captured by high-speed video over Johannesburg from February 2017 to February 2018.

TABLE II. Number of Flashes Recorded Feb 2017-2018

Type		***Quantity***
Downward	Negative	155
	Positive	6
Upward	Negative	43
	Positive	2
Triggering events		6
Bi-polar		1
Total		262

A. Downward flashes

A total of 155 negative downward flashes, 6 positive downward flashes and 1 bipolar downward flash were recorded. A bipolar flashes was considered only when a channel was used to transfer different polarities of charge. In addition to this amount, 6 downward flashes were classified as triggering flashes due to the occurrence at the same time and framed in the same camera view of upward flashes. These triggering flashes were observed to be 5 positive downward flashes and 1 bipolar flash.

The number of strokes and statistics for the duration of each flash consider all registered downward strokes, including triggering events. A total of 605 negative strokes and 13 positive strokes were recorded. Figure 10 shows a frame taken for a high-speed video of a downward flash over Johannesburg. Table III summarizes the characteristics of the downward flashes recorded over Johannesburg.



Figure 10. Frame taken from high-speed video of downward lightning over Johannesburg, South Africa.

The two bipolar flashes began with a single positive stroke followed by 2 and 3 negative strokes respectively. The strokes followed the same channel and attached to the same strike point. The bipolar flash that had 4 strokes, triggered an upward leader from the Brixton tower 2 kilometers from the downward strike point. The upward leader started after the positive stroke and the following 3 negative strokes happened during the continuous current of the upward leader. Both bipolar flashes follow the same structure as that seen by Saba et al. [8].



Figure 11. Downward bipolar flash struck the building and triggered an upward leader from a 250 meter-tower 2 kilometer away.

TABLE III. Downward Flash Strokes

	N	**AM**	**Min**	**Max**
NEGATIVE FLASHES	155			
Max Number of Strike Points	3			
Multiplicity - Average of Strokes per flash		3,1	1	26

Max Duration Negative strokes	605	28,7	1	929
Time between Strokes (ms)	460	66,5	6	546
Time with no current (ms)	425	43,3	2	360
Total duration (ms)	206	320,4	2	1162

POSITIVE FLASHES	**N**	**AM**	**Min**	**Max**
Positive strokes	6			
Max Duration Positive strokes* (*Including bipolar and triggering events)	13	230	2	567

As presented by Kitagawa et al. [9], Brook et al. [10] Shindo and Uman [11], Ballarotti et al. [12] the continuous current can be defined by the duration and the terms are "*very short*" for durations from 3 ms up to 10 ms, "*short*" for durations between 10ms up and 40 ms and "*long*" for cases where the duration is more than 40 ms. The continuous current duration for negative and positive strokes is presented in Table IV.

TABLE IV. CONTINUOUS CURRENT DURATION

	Negative Strokes	Positive Strokes
	605	13
Number of strokes without CC	108	1
CC Very short 3>CC>10	264	1
CC Short 10>CC>40ms	160	0
CC Long more than 40ms	73	11

B. Upward Flashes

From a total of 43 upward flashes that were recorded, 41 were negative upward flashes and 2 were positive upward flashes. Negative upward flashes are the flashes that transfer negative charge to the ground, i.e. the upward positive leader propagates toward to the cloud. The image obtained from the high-speed camera shows a leader with no branches. On the other hand, positive upward flashes have branched negative upward leaders propagating towards the cloud. Figure 12 shows the two types of upward leader: a) positive and no-branched upward leader and b) negative and branched upward leader.

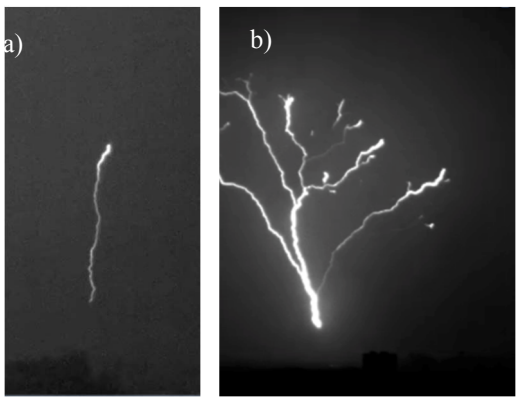

Figure 12. Frames taken from high-speed video of (a) positive upward leader (negative upward flash) and (b) negative upward leader (Positive upward flash)

Upward flashes were recorded mainly from the Brixton and Hillbrow tower. For the multiple tower-involved cases, 10 out of 11 had both towers producing upward leaders (4.8 km from each other), one case had three upward leaders from both towers and also the SABC building (115-meter building). One other case involved a 90 m tall tower 2.5 km from the Hillbrow tower and the Hillbrow tower.

Upward flashes start with an upward leader propagation that is known in the literature as a Initial Continuous Current (ICC), any fluctuation of luminosity in this stage are designated as ICC pulses. After this stage the upward flash can end or, after some tens of milliseconds, a downward leader can use the ionized channel to transfer charge to the ground (Return Stroke). These return strokes can then be followed by continuous current. The luminosity of upward flashes can be summarized as in the figure 13.

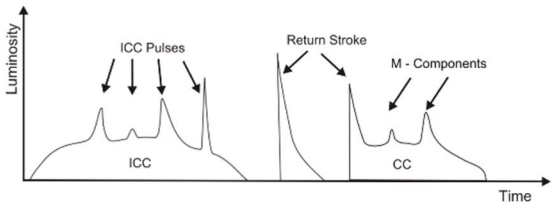

Figure 13. Upward flash luminosity profile (Saba et al. 2016)

The average and maximum duration of upward initial continuous current stages were 405ms and 990ms respectively. 398 pulses were registered in the 41 negative upward flashes. Table V shows some of the characteristics of the upward flashes filmed over Johannesburg.

TABLE V. NEGATIVE UPWARD FLASH

Negative upward flashes	41
Negative Leaders	53
w/ multiple tower involved	11
Max duration ICC	990 ms (AM=405ms)
ICC Pulses (N)	398
RS in negative upward flash (N)	38
Max Duration RS	269 (AM=28ms)
Triggering event:	
w/ triggering event visible:	6
Positive Flashes	5
Bipolar flashes (+CG > UP > -CG)	1

C. Potential current measurement:

A number of lightning events were observed attaching to a 53 m tall apartment building (Figure 14). From the SALDN and videos, this building was struck by positive, negative and bipolar downward flashes.

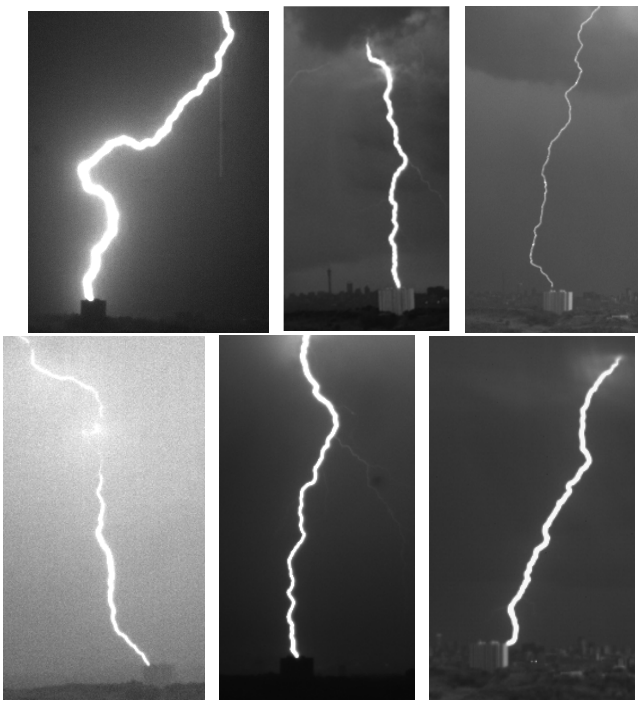

V. SUMMARY

The Johannesburg scientific project aims to investigate the physics of lightning by high-speed video observation along with electric field measurements. All equipment and collaborations available were presented. Previous studies about the location were also provided.

A total of 168 downward flashes and 43 upward flashes were characterized. Characteristics of 13 positive and 605 negative strokes and 41 negative upward flashes were presented. Flashes with almost 1 second connected to ground: negative downward flash (929ms) and upward flash (990ms).

One building in particular presented an ideal location to install a current system for natural downward flash measurement. Towers approximately 250 meters-tall and 4.8 km from each also are potential locations for the installation of a current measurement system due to number of upward flashes. The current system combined with high-speed video and the high cloud base in Johannesburg would provide more information about the initiation of flashes.

ACKNOWLEDGMENT

The author Carina Schumann would like to thank the Claude Leon Foundation for the Post-doctoral fellowship. The authors also like to thank South African Weather Service (SAWS) for their support and for providing the SALDN data used in this paper. They would also like to thank Eskom for the support of the Lightning/EMC Research Group through the TESP programme. Thanks are extended to the Department of Trade and Industry (DTI) for THRIP funding as well as to the National Research Foundation (NRF) for direct funding of the Research Group.

REFERENCES

[1] Eriksson, A.J. (1978), Lightning and tall structures, Transactions: The SA Institute of Electrical Engineering, pp. 238-252.

[2] Anderson, R.B. and A. J. Eriksson (1980), Lightning parameters for engineering application.Electra Vol.69, 65–102, 1980.

[3] Gijben M. The lightning climatology of South Africa. S Afr J Sci. 2012;108(3/4), Art. #740, 10 pages.

[4] H.G.P Hunt, K.J. Nixon and I.R. Jandrell: "Establishing a methodology to investigate LDN median error ellipses used as corroborating evidence for a lightning event at a specific geographic locations." *Electric Power Systems Research Journal*, 2014.

[5] T.A. Warner, K.L. Cummins and R.E. Orville: "Upward lightning observations from towers in Rapid City, South Dakota and comparison with National Lightning Detection Network data, 2004–2010", Journal of Geophysical Research, Res. 117, D19109, doi:10.1029/2012JD018346

[6] M.M.F. Saba, M.G. Ballarotti, O. Pinto, Jr: "Negative cloud-to-ground lightning properties from high-speed video observations." Journal of Geophysical Research, vol. 111, p. D03101, 2006.

[7] M.M.F. Saba, W. Schulz, T.A. Warner, L.Z.S. Campos, K.L. Cummins, R.E. Orville: "High-speed video observations of positive lightning flashes to ground." Journal of Geophysical Research: Atmospheres, vol. 115, p. D24201, 2010.

[8] M.M.F. Saba, C. Schumann, T.A Warner, J.H. Helsdon, W. Schulz, R.E Orville: "Bipolar cloud-to-ground lightning flash oberservations." Journal of Geophysical Research: Atmospheres, vol. 118, p. 1-9, 2013.

[9] N. Kitagawa, M. Brook, E.J. Workman, ―Continuing currents in cloud-to-ground lightning discharges, J. Geophys. Res. 67, pp. 637–647, 1962.

[10] M. Brook, N. Kitagawa, E.J. Workman, ―Quantitative study of strokes and continuing currents in lightning discharges to ground, J. Geophys. Res. 67, pp. 649‑659, 1962.

[11] T. Shindo, M.A. Uman, ―Continuing current in negative cloud- to-ground lightning, J. Geophys. Res. 94, pp. 5189‑5198, 1989.

[12] M.G. Ballarotti, M.M.F. Saba, O. Pinto Jr., ―High-speed camera observations of negative ground flashes on a millisecond-scale. Geophys. Res. Lett. 32, L23802.doi:10.1029/2005GL023889, 2005.

Appendix F

High-speed video analysis of lightning flashes over Johannesburg, South Africa

F.1 Paper description

The following paper was published and presented at the 26th Southern African Universities Power Engineering Conference in January 2018. This conference took place at the University of the Witwatersrand in Johannesburg, South Africa. This paper presents the findings from analysing 100 lightning flashes using high-speed video equipment. The parameters of stroke multiplicity, continuing current duration and interstroke interval are quantified. A detailed methodology behind the analysis process is also included.

HIGH-SPEED VIDEO ANALYSIS OF LIGHTNING FLASHES OVER JOHANNESBURG, SOUTH AFRICA

J. Tasman*, H. Fensham*, C. Schumann*, H. G.P. Hunt*, K.J.Nixon*, T.A.Warner †

* *School of Electrical & Information Engineering, University of the Witwatersrand, Private Bag 3, 2050, Johannesburg, South Africa.*

† *ZT Research, Rapid City-SD-USA.*

Abstract: A discussion based on data attained from analysing high-speed footage of lightning flashes in Johannesburg, South Africa, is presented. A total of 100 lightning flashes, comprising of 346 visible strokes and 57 M-components, were analysed. The high-speed cameras used to attain the data were the Phantom v310, Phantom v7.1 and the MIRO4. From the data attained, a multiplicity of 3.6 strokes-per-flash was calculated and the arithmetic mean of 62.3 *ms* and 29.8 *ms* was calculated for the interstroke intervals and the stroke durations, respectively. Long continuous current (> 40 *ms*) was seen the most in negative upward flashes, with it being present in 47.5% of all its strokes.

Key words: Continuing current, flash, high-speed camera, lightning characteristics, M-component, stroke

1. INTRODUCTION

Fundamentally, lightning flashes can be categorised into three types; cloud-to-ground (CG), ground-to-cloud (GC) and intra/inter-cloud (IC) [1]. These labels classify the lightning's direction of propagation from its start to termination point. The research and data collected was focused on CG and GC flashes only. Each flash is made up of a certain number of strokes. Once initial attachment has been made, a return stroke will deliver current through the channel. This will cause the channel to emit a large amount of luminosity. The first return stroke will have the greatest current magnitude and luminosity and when completed, will leave behind a channel of ionised air. IC discharges will re-establish the electric field (E-field) and the channel provides an easy path for subsequent return strokes to travel through. If the channel has not disappeared completely and the E-field has not been re-established before the occurrence of another current impulse, an M-component, as opposed to a return stroke, has occurred [2].

Due to the microphysics and other conditions inside the cloud such as: wind, dust particles, temperature among others; the particles separate themselves in positive or negative, creating large charge centers.

Both CG and GC flashes can be classified as either positive or negative. Due to the microphysics involved, as well as many other physical conditions such as temperature and wind, particles within the cloud separate themselves into positive and negative - this creates large charge centers. These most commonly separate with the positive charge centers at the top of the cloud and the negative at the bottom. The strong E-fields within the clouds are the cause of IC flashes. The difference in potential between the cloud and the ground also causes an E-field to develop. In the negative CG case (nCG), this enhanced E-field causes a downward propagation of negative charge (a stepped leader) from a charge center in the cloud toward the ground. This causes a further enhancement of the field and can result in this stepped leader attaching to a point on the ground [2]. From consulting similar discussion papers and studies, it can be concluded that nGC is the most common type of lightning throughout the regions of São Paulo in Brazil, New Mexico and Arizona in the United States and the eastern Mediterranean [3–6].

Depending on the charge magnitude and density in the cloud and on the ground, it is possible for a stepped leader to originate from the ground and propagate towards the cloud. Due to how charge is most commonly separated in the cloud, the ground is generally dense with positive charge. If this charge causes a sufficient enhancement of the E-field, positive streamers can develop and begin propagating upwards. Once these streamers have attached to either a charge center in the cloud or to downward propagating negative stepped leaders, return strokes consisting of negative current impulses will be initiated - this is negative GC (nGC) [2, 7].

Depending on the type of thunderstorm or the stage of the thunderstorm, the positive charge centers can be situated at the bottom of the cloud with the negative charges at the top. This would cause the ground underneath the cloud to be dense with negative charge. Once again, if the enhancement of the E-field is strong enough, this can cause a downward propagating positive CG flash (pCG). Alternatively, upward propagating negative streamers can occur. If these find a point of termination in the cloud, return strokes consisting of positive current impulses would be initiated - this is positive GC (pGC) [2, 8].

The human eye is not able to detect, in real time, individual strokes within a flash. Therefore, in order to analyse and capture flash data, specialised high-speed cameras were used. These were set up in different locations and primarily focused on flashes occurring in the Johannesburg central

business district (CBD). The high frame rate and resolution capabilities of the cameras allowed the behaviour of each individual stroke within a flash to be independently analysed and recorded.

Many studies have been performed that discuss the behaviour of lightning flashes in different geographical locations, such as São Paulo, New Mexico, Arizona and the eastern Mediterranean. The Johannesburg CBD has not yet been focused on in this line of research and the data attained and presented in this report aims to contribute to furthering the communal understanding of lightning processes.

2. EQUIPMENT

In order to attain footage that would enable the characterisation of lightning flashes, three high-speed cameras were used. These were the Phantom v310, Phantom v7.1 and the MIRO4. For the v310 and v7.1, the Phantom Camera Control Software version 2.8 was used to run the cameras and analyse the footage [9].

The v310 recorded at 15000 fps and had an exposure time of 58 μs. The Phantom v7.1 recorded at 5000 fps and had an exposure time of 990 μs. The different frame rates of the cameras and their subsequent exposure times and resolution allowed for each flash to be analysed separately - this optimised the accuracy of the characterisation process.

The Phantom v310 has internal memory of 32 *GB* which is split into 2 individual memory partitions (2 of 16 *GB* each). A 512 *GB* CINEMAG external hard drive is attached to the camera, which allows it to save all 16 *GB* in about 2-3 seconds. Since it has two memory banks, this means another flashed can be saved in those 2-3 seconds. After completion of the thunderstorm, this footage could then be transferred onto a computer from the CINEMAG and analysed using the above mentioned software.

Initially, the v7.1 had a 16 GB internal memory capacity that was split into 10 individual memory partitions of 1.6 GB each. After filming, each partition was saved. The current settings include the memory being split into two 8 GB partitions that are set to save automatically to the computer after each trigger.

The physical setup of the camera allowed for them to be orientated at any angle or position. This allowed for different, more specific areas to be focused on.

3. METHODOLOGY

Between the dates February to December 2017, the high speed cameras (Phantom v310 and Phantom v7.1) were positioned 6 *km* away from the CBD to capture CG and GC lightning in the Johannesburg CBD (Braamfontein CBD), centered at $26°11'28''S$ $28°02'16''E$. Within the area, is the Hillbrow tower at a height of 270 m with coordinates $26°18'70''S$ $28°04'95''E$ and the Brixton tower at a height of 232 m and with coordinates $26°19'25''S$ $28°00'67''E$ [10].

Before a storm, the cameras were switched on and setup to ensure that the correct amount of light was able to pass through the cameras.

Personal were required to sit and watch the lightning storm and press the trigger once a lightning flash was completed. The trigger was a single trigger system, which triggered the Phantom v310 and the Phantom v7.1 with a single press of the button. Each camera was running off a laptop of its own, with the above mentioned program, and had pre-trigger time of 1.6 s and post-trigger time of 0.2 s.

Videos were analysed and summarised and the results will be present in the Section 4 on data analysis. Using the two different cameras for the same lightning flash allowed a more precise visual analysis as each camera has benefits with regards to their fps and exposure time. Figure 1, below, shows an example of the high-speed camera's videos captured over Johannesburg. The figure contains two nGC flashes from both the Hillbrow tower (pictured left) and the Brixton tower (pictured right). A nCG flash is also present and can be identified as the channel to the right of the Brixton tower (making attachment with the ground).



Figure 1: Frame taken from high-speed camera footage

4. DATA ANALYSIS

One hundred lightning flashes were analysed and characterised in a database. As mentioned in the introduction, IC was not a focus for this research. The database has 100 flashes that were recorded during 14 days with thunderstorms. Of these, 81 were downward flashes and 19 were upward flashes. It was observed that there were 346 strokes and 57 M-components in these flashes. Strokes that made attachment out of the camera's field of view were classified as 'non-visible' and not included. Accompanying the figures in this section are quantities N, AM and GM. These refer to the number of samples, the arithmetic mean and the geometric mean, respectively. Table 1 presents the summary of the collected data.

Of the 100 classified flashes, 79 were nCG, 2 were pCG, 17

Table 1: Summarised results of collected lightning flash data

Classification	Quantity
Thunderstorms	14
Flashes	100
Visible strokes	346
M-component	57

were nGC and 2 were pGC. Table 2 provides a percentage summary on the polarity of the lightning flashes relative to all of the collected lightning flash data.

Table 2: Summarised results of the polarity of the collected lightning flash data

Type	Polarity	Percentage
CG	Negative	79%
	Positive	2%
GC	Negative	17%
	Positive	2%

4.1 Multiplicity

The multiplicity is defined as the number of strokes in a flash. This is generally represented as a strokes-per-flash average taken from the full data set [2]. From Table 2, it is noted that nGC flashes occurred considerably more often than other types.

An M-component is defined as a return stroke with the occurrence of subsequent strokes before the ionised channel disappears [2]. The luminosity of the channel increases as discharge occurs. If the channel has not disappeared and there is an increase in luminosity after the original attachment and the return stroke, then the time stamps need to be analysed to determine if it is due to residual charge from the return stroke of if it is an M-component. If a luminosity variation occurs within the μs range after the return stroke's variation, then it is classified as residual charge and caution was taken as to not confuse the two and incorrectly classify the flash. The way in which the flashes were analysed excluded M-components in the sense that they did not contribute to the strokes per flash statistic.

Figure 2 is a bar graph plotting the number of strokes per flash against the number of flashes. This graph is representative of the entire data set. It was seen that 21% of all recorded flashes had two strokes and along with the outlying flash that had 27 strokes, a multiplicity of 3.6 was calculated for the entirety of the flash data.

4.2 Number of strike points

In order to say that a lightning flash has multiple strike points, return strokes need to have multiple points of attachment. This means that different strokes in the same

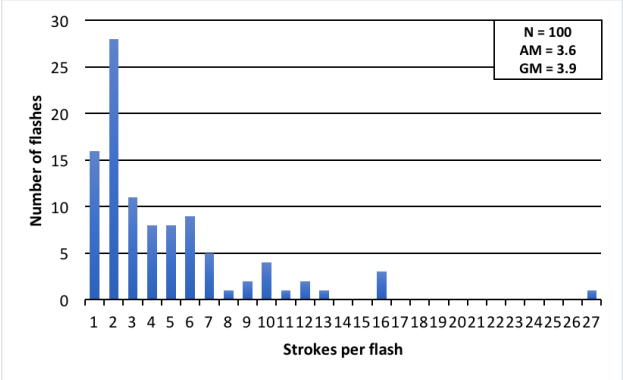

Figure 2: Bar graph showing the number of strokes per flash

flash should terminate at different or alternating points [2]. From the 100 recorded flashes, nine were found to have multiple strike points, however, none more than two. All of these were from nCG flashes.

4.3 Interstroke interval

According to the way in which the data was recorded, the interstroke interval can be defined as the time between the attachment of subsequent return strokes within the same flash. As previously discussed, an M-component is different to a single stroke and therefore, an interstroke interval was not computed if a return stroke was followed by an M-component. It is difficult to accurately determine, from visual analysis, the exact point at which the stroke's continuing current has concluded and the channel disappears. The interstroke interval was therefore taken between times of attachment as this can be determined with significantly less of an error. The accuracy of this method would come down to the frame rate of the camera - the higher the frame rate, the more precise one can be when determining the time of attachment.

Table 3: Overall interstroke interval results

Interval information	time (ms)
Arithmetic mean	62.3
Minimum	6
Maximum	546

Table 3 presents the minimum, maximum and arithmetic mean of all recorded interstroke intervals. Table 4 presents the number of interstroke intervals that fall within specific time ranges. It is seen that 57.8% of recorded interstroke intervals lasted less than 50 *ms*.

4.4 Continuing current

Continuing current (CC) is the continuous flow of charge through the ionised channel after initial attachment of the stroke [2]. There are three different ways to characterise CC. A "long" CC is a CC with a duration greater than 40 *ms* whereas a "short" CC has a duration between 10 *ms* and

Table 4: Summarised results of the number of interstroke intervals that fell within different time ranges

Intervals (*ms*)	**Number**
0<x⩽50	134
50<x⩽100	64
100<x⩽150	17
150<x⩽200	10
200<x⩽250	2
250<x⩽300	1
300<x⩽350	1
350<x⩽400	1
400<x⩽450	1
450<x⩽500	0
500<x⩽550	1
Total	232

40 *ms*. Additionally, a ”questionable” CC has a duration between 1 and 10 *ms* [11].

The results were based off the data were the initial attachment of the strike was noted and then when the channel was seen to disappear. Using the software for the cameras, the brightness of the video was changed to ensure that the channel had disappeared meaning that the CC had stopped. The flashes were recorded by two different cameras to ensure that the channel had legitimately ceased.

It was found that 40 strokes had long CC with 31 occurring from nCG flashes, 8 from nGC and 1 from pGC. Table 5 below shows the results of how many strokes had long CC in each data set. The table shows that nCG has the greatest amount of long CC, this however could be skewed due to the amount of nCG which has been captured in the results in comparison to the other types of lightning. Relative to the specific type of lightning, 39.3% percent of nCG has long CC as opposed to 47.5% percent of nGC. This shows that nGC might be more prone the having long CC.

Table 5: Summarised results of continuing current

Data set	**Long CC**
nCG	31
pCG	0
nGC	8
pGC	1
All	40

4.5 Stroke Duration

The stroke duration in the context of this investigation, was defined as the amount of time taken from attachment until the ionised channel of the stroke on the high-speed footage had completely disappeared. The arithmetically calculated mean stroke duration of all recorded strokes was calculated to be 29.8 *ms*. The maximum stroke duration was found to be 619 *ms*. Figure 3 below shows the number of strokes in a flash that are between 1 and 40 *ms*. It can be seen that the majority of strokes have a duration between 1 and 15 *ms*. This accounts for 265 of the 346 strokes, that is 76.6% of all recorded strokes lay in this time duration region.

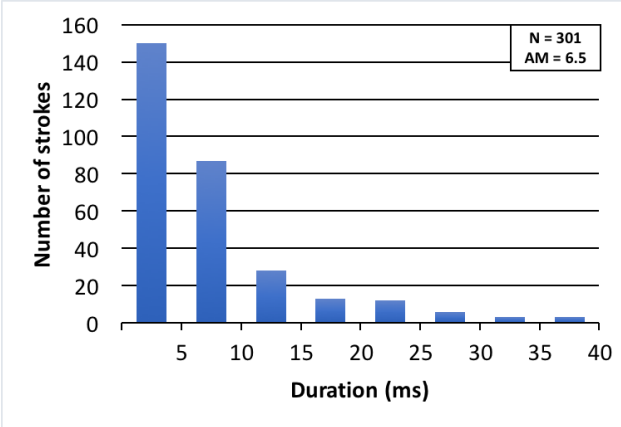

Figure 3: Bar graph showing the duration of strokes between 1 and 40 *ms*

The number of strokes with larger durations steadily decrease as seen in Figure 4 below which accounts for strokes that have a duration of greater than 40 *ms*.

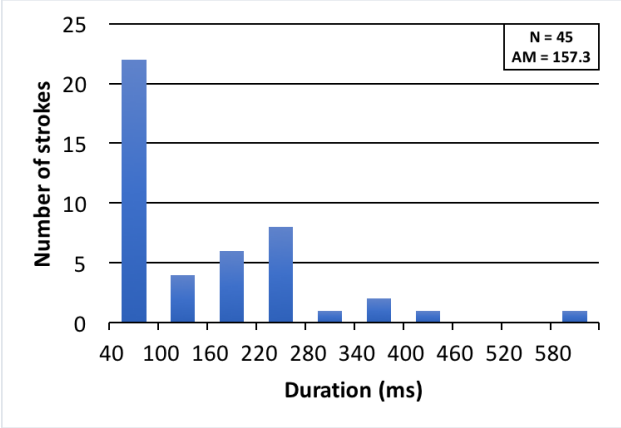

Figure 4: Bar graph showing the duration of strokes greater than 40 *ms* (Long CC)

Table 6 below shows the mean stroke duration for the different types of lightning that has been characterised in the dataset.

Table 6: Summarised results of mean stroke duration

Data set	**Mean duration** (*ms*)
nCG	23.1
pCG	97.5
nGC	437.7
pGC	256.0
All	29.8

5. SUMMARY

Of the 100 flashes which were analysed, each flash had arithmetic mean of 3.6 strokes. Strokes within a flash

ranged from 1 to 27. Within the data it was seen that 9 of the 100 flashes had two strike points, there were no cases were a flash had more than 2 strike points. The interstroke intervals in the data had an arithmetic mean of 62.3 *ms* with a range of 6 to 546 *ms*. 134 out of 232 interstroke intervals were found to have a duration of 0-50 *ms*. With regards to long CC, it was seen nGC has 47.5% long CC which is the highest in this dataset in comparison to the other lightning types. The stroke duration in the entire dataset had an arithmetic mean 29.8 *ms*. It was seen that nGC had the longest mean stroke duration with 437.7 *ms*.

REFERENCES

[1] V. A. Rakov. "Fundamentals of Lightning." *International Symposium on Lightning Protection*, October 2011.

[2] V. A. Rakov. "The Physics of Lightning." *Surveys in Geophysics - Springer*, pp. 701–729, April 2013.

[3] M. M. F. Saba, M. G. Ballarotti, and O. Pinto Jr. "Negative cloud-to-ground lightning properties from high-speed video observations." *Journal of Geophysical Research*, vol. 111, no. D3, February 2006.

[4] A. C. V. Saraiva, M. M. F. Saba, O. Pinto Jr., K. L. Cummins, E. P. Krider, and L. Z. S. Campos. "A comparative study of negative cloud?to?ground lightning characteristics in So Paulo (Brazil) and Arizona (United States) based on high?speed video observations." *Journal of Geophysical Research*, vol. 115, no. D11, June 2010.

[5] Y. Yair, S. Shalev, Z. Erlich, A. Agrachov, E. Katz, H. Saaroni, C. Price, and B. Ziv. "Lightning flash multiplicity in eastern Mediterranean thunderstorms." *Natural Hazards and Earth System Sciences*, vol. 14, no. 165, February 2014.

[6] M. M. F. Saba, T. A. Warner, and C. Schumann. "Features of lightning flashes obtained from high-speed video recordings." *The Lightning Flash*, pp. 231–266, February 2014.

[7] M. M. F. Saba, C. Schumann, T. A. Warner, M. A. S. Ferro, A. R. de Paiva, J. Helsdon Jr., and R. E. Orville. "Upward lightning flashes characteristics from high-speed videos." *Journal of Geophysical Research: Atmospheres*, vol. 121, no. 14, pp. 8493–8505, July 2016.

[8] M. M. F. Saba, W. Schulz, T. A. Warner, L. Z. S. Campos, C. Schumann, E. P. Krider, K. L. Cummins, and R. E. Orville. "Negative cloud-to-ground lightning properties from high-speed video observations." *Journal of Geophysical Research*, vol. 115, no. D24, December 2010.

[9] "PCC Software version 2.8.", October 2016. URL `http://www.phantomhighspeed.com/`. Last accessed: 11 December 2017.

[10] "GOOGLE Maps.", December 2017. URL `https://www.google.co.za/maps/place/Johannesburg/`. Last accessed: 13 December 2017.

[11] M. M. F. Saba, W. Schulz, T. A. Warner, L. Z. S. Campos, C. Schumann, E. P. Krider, K. L. Cummins, and R. E. Orville. "High?speed video observations of positive lightning flashes to ground." *Journal of Geophysical Research:*, vol. 115, no. D24, December 2010.